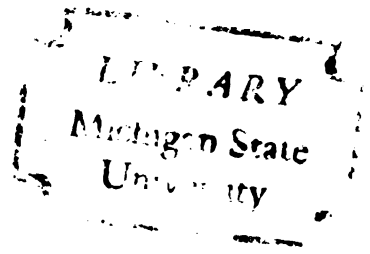


AN ANALYSIS OF HEAT AND MASS
TRANSFER IN ATMOSPHERIC
FREEZE-DRYING

Thesis for the Degree of Ph. D.
MICHIGAN STATE UNIVERSITY
GARY ARLYN HOHNER
1970



This is to certify that the

thesis entitled

AN ANALYSIS OF HEAT AND MASS
TRANSFER IN ATMOSPHERIC
FREEZE-DRYING

presented by

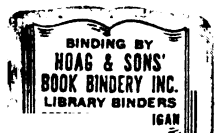
Gary Arlyn Hohner

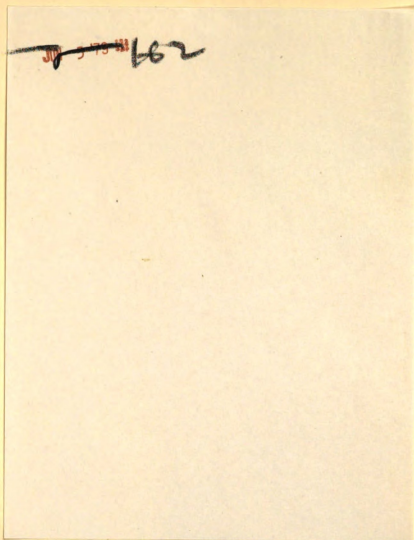
has been accepted towards fulfillment
of the requirements for

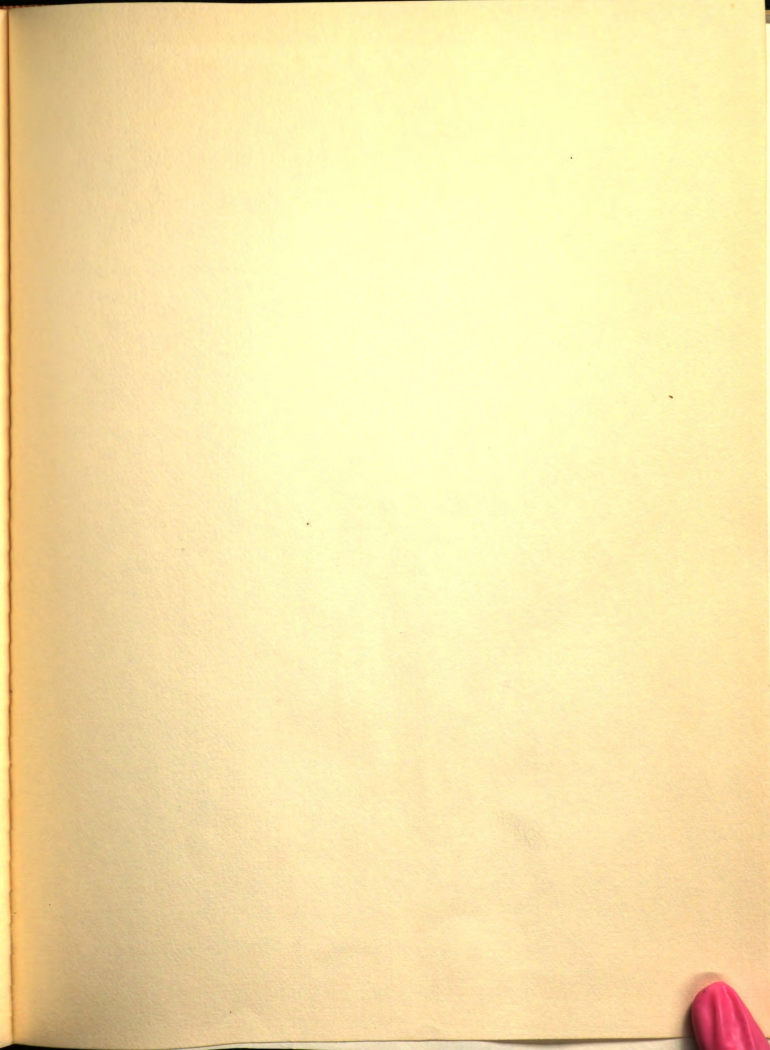
Ph.D. degree in Agr. Eng.

D. R. Heldman
Major professor

Date March 31, 1970







ABSTRACT

AN ANALYSIS OF HEAT AND MASS TRANSFER IN
ATMOSPHERIC FREEZE-DRYING

by

Gary Arvid Robert

Atmospheric freeze-drying is the process of dehydration by sublimation conducted at atmospheric pressure. The conventional sublimation dehydration process used to food and other biological products is conducted at very low pressures, usually below the triple point of water (4.28 mm Hg). Widespread application of the conventional process to convenience foods is limited by economic factors. Several investigators have noted that if sublimation could be conducted at atmospheric pressure expensive vacuum equipment would be eliminated and the process could be wide ranging.

The objective of the research conducted was to analyze the rate-limiting process in atmospheric freeze-drying of ground beef by deriving and solving a mathematical model of the process and evaluating the internal heat and mass transfer coefficients of the product. The computed values of the transfer coefficients were used to study the mechanism of heat and mass transfer in atmospheric freeze-drying.

The mathematical model involved simultaneous solution of the partial differential equations of energy and water vapor transport through the semi-dry, porous layer formed on the surface of

ABSTRACT

AN ANALYSIS OF HEAT AND MASS TRANSFER IN
ATMOSPHERIC FREEZE-DRYING

By

Gary Arlyn Hohner

Atmospheric freeze-drying is the process of dehydration by sublimation conducted at atmospheric pressure. The conventional sublimation dehydration process used in food and other biological products is conducted at very low pressures, usually below the triple point of water (4.58 mm Hg). Widespread application of the conventional process to convenience foods is limited by economic factors. Several investigators have noted that if sublimation could be conducted at atmospheric pressure expensive vacuum equipment could be eliminated and the process could be made continuous.

The objective of the research conducted was to analyze the rate-limiting process in atmospheric freeze-drying of precooked beef by deriving and solving a mathematical model of the process and evaluating the internal heat and mass transfer coefficients of the product. The computed values of the transport coefficients were used to study the mechanisms of heat and mass transfer in atmospheric freeze-drying.

The mathematical model involved simultaneous solution of the partial differential equations of energy and water vapor transport through the semi-dry, porous layer formed on the surface of

the product. The mechanism of mass transport was assumed to be water vapor diffusion through the air-filled, porous layer. Heat transfer through the porous layer was assumed to be by conduction. Complexity of the model precluded a closed form integration, so the techniques of numerical analysis were used to obtain a solution.

Three transport parameters of the numerical solution were evaluated using the statistical technique of nonlinear estimation. These parameters were the effective thermal conductivity, the structural constant of the internal mass transfer coefficient, and the surface mass transfer coefficient. The effect of air temperature, system pressure and orientation of the fiber structure on each estimated parameter was analyzed statistically from results of experimental tests. Only the effect of fiber orientation on the structural constant was significant at the 90% confidence level. The effective conductivity was found to have a mean value of $.0001 \text{ cal/cm-sec-}^{\circ}\text{C}$. The structural constant had a mean value of .81 for transport parallel to the fiber structure and .62 perpendicular to the fibers.

Analysis of the practical operating space of the process variables for atmospheric freeze-drying was accomplished by transforming the proven, one-dimensional, numerical solution into an approximate three-dimensional solution. The rate of atmospheric freeze-drying in cubical samples of precooked beef was found to be directly and strongly dependent on air temperature. When the dimensionless ratio of surface to internal mass transfer coefficients exceeded 100, the rate of drying was confirmed to be inversely related to the square of the sample thickness.

Gary Arlyn Hohner

Predicted maximum rate drying time for one centimeter cubes of beef was 30 hours. The practical range of operating variables is limited to small particle size and high air flow rates. Fluidized-bed or spray dryers are possible equipment configurations for atmospheric freeze-drying.

Approved:

D. R. Heldman 2/20/70
Major Professor

Carl W. Lee 2/20
Department Chairman

A THESIS

Submitted to
Michigan State University
in partial fulfillment of the requirements
for the degree of

DOCTOR OF PHILOSOPHY

Department of Agricultural Engineering

1970

AN ANALYSIS OF HEAT AND MASS TRANSFER IN
ATMOSPHERIC FREEZE-DRYING

By

Gary Arlyn Hohner

To: Gay, Carl and Douglas

A THESIS

Submitted to
Michigan State University
in partial fulfillment of the requirements
for the degree of

DOCTOR OF PHILOSOPHY

Department of Agricultural Engineering

1970

G-64218
10-9-70

ACKNOWLEDGMENTS

The author wishes to express appreciation to Dr. D. E. Beldman, Associate Professor, Agricultural Engineering and Food Science Departments, and Chairman of the guidance committee, for his continuous guidance and assistance throughout planning and execution of the graduate program represented by this thesis. Gratitude is also extended to Dr. F. W. Bakker-Arkema, Associate Professor, Agricultural Engineering, and Dr. W. H. Urbein, Professor of Food Science, for serving on the guidance committee.

A special expression of appreciation is due Dr. J. V. Beck, Associate Professor, Mechanical Engineering, for exemplary teaching and numerous consultations in the areas of numerical solution of mathematical models and parameter estimation on which this thesis is so heavily based.

Appreciation is also expressed to Dr. C. W. Bell, Chairman and Professor, Agricultural Engineering, and Dr. E. B. Schweigert, Chairman and Professor, Food Science, for resources and facilities with which to conduct the research program and more important for fostering the type of cooperation where meaningful interdisciplinary graduate programs can be conducted.

Finally, the author wishes to thank Dr. W. H. Hunt, Professor D. E. Brooker, Mr. M. K. Gould, Mr. G. A. Cook, and Dr. W. L. Clark who, over the past several years, have expressed encouragement and support for completion of this graduate program.

ACKNOWLEDGMENTS

The author wishes to express appreciation to Dr. D. R. Heldman, Associate Professor, Agricultural Engineering and Food Science Departments, and Chairman of the guidance committee, for his continuous guidance and assistance throughout planning and execution of the graduate program represented by this thesis. Gratitude is also extended to Dr. F. W. Bakker-Arkema, Associate Professor, Agricultural Engineering, and Dr. W. M. Urbain, Professor of Food Science, for serving on the guidance committee.

A special expression of appreciation is due Dr. J. V. Beck, Associate Professor, Mechanical Engineering, for exemplary teaching and numerous consultations in the areas of numerical solution of mathematical models and parameter estimation on which this thesis is so heavily based.

Appreciation is also expressed to Dr. C. W. Hall, Chairman and Professor, Agricultural Engineering, and Dr. B. S. Schweigert, Chairman and Professor, Food Science, for resources and facilities with which to conduct the research program and more important for fostering the type of cooperation where meaningful interdisciplinary graduate programs can be conducted.

Finally, the author wishes to thank Dr. H. B. Pfof, Professor D. B. Brooker, Mr. M. R. Gould, Mr. E. G. Rupp and Dr. W. L. Clark who, over the past several years, have expressed encouragement and support for completion of this academic endeavor.

Chapter	Page
VI. RESULTS AND DISCUSSION	73
The Parameter	73
Accuracy of	83
Simulation of Atmospheric Freeze-Drying in Three Dimensions	Page
ACKNOWLEDGMENTS	iii
LIST OF TABLES	vi
LIST OF FIGURES	vii
LIST OF APPENDICES	ix
NOMENCLATURE	x
Chapter	
I. INTRODUCTION	1
II. REVIEW OF LITERATURE	6
Atmospheric Freeze-Drying	6
Mechanisms and Parameters of Heat and Mass Transfer in Freeze-Dried Foods	9
Freeze-Drying Rate	13
III. THEORY	17
The Mathematical Model	17
The Mass Transfer Coefficient	24
The Finite-Difference Model	27
Sensitivity Analysis and Estimation of Model Parameters	33
IV. EXPERIMENTAL DESIGN AND PROCEDURES	39
Experimental Design: Sensitivity Analysis	40
Preparation and Assignment of Samples	48
Selection of Test Conditions	48
Experimental Apparatus and Procedures: Equilibrium Studies	50
Experimental Apparatus and Procedures: Rate Studies	54
V. THE NUMERICAL SOLUTION	60

Chapter	Page
VI. RESULTS AND DISCUSSION	73
The Parameter Estimates	73
Accuracy of the Model	83
Simulation of Atmospheric Freeze-Drying in Three Dimensions	87
Analysis of Atmospheric Freeze-Drying in Cubical Samples	90
VII. CONCLUSIONS	99
BIBLIOGRAPHY	101
APPENDICES	105

LIST OF TABLES

Table		Page
5.1	Numerical Values of Physical Constants Used in the Mathematical Model	64
6.1	Summary of Parameter Estimates and Variance of the Residuals	76
4.1A	Dimensionless Sensitivity Coefficients of Known Parameters for Freeze-Drying at .58 Atmosphere Pressure	43
6.2	Summary of Analysis of Variance in the Parameter Estimates	77
4.1B	Contours of the Risk-Function Surface in the Vicinity of the Computed Minimum	46
4.2	Contours of the Risk-Function Surface in the Vicinity of the Computed Minimum	46
4.3	Schematic Drawing of Experimental Apparatus for Equilibrium Moisture Content Studies .	51
4.4	Schematic Drawing of Experimental Apparatus for Atmospheric Freeze-Drying Rate Studies	55
4.5	Sample Holders, Spring and Thermocouple Assembly for Drying Rate Studies	57
5.1	Equilibrium Moisture Isotherms of Freeze-Dried Beef Below Zero °C	77
5.2	Computed Profiles of Vapor Pressure and Temperature for Typical Conditions of Atmospheric Freeze-Drying	82
5.3	Comparison of Predicted Drying Curves of the Proposed Model and the Pseudo Steady-State Model in One-Dimensional Samples	85
6.1	Comparison of the Proposed Model to Experimental Results at .97 and .58 Atmosphere Pressure	89
6.2	Comparison of Solutions of the Three-Dimensional Model to Experimental Results in Cylindrical Samples	94

Figure	Page
4.3	Predicted Effect of Air Temperature on Atmospheric Freeze-Drying Rates in One-Dimensional Samples of Cooked Beef ... 92
LIST OF FIGURES	
Figure	Predicted Effect of System Pressure on Atmospheric Freeze-Drying Rate in One-Dimensional Samples of Cooked Beef ... 92
3.1	Schematic Diagram of Atmospheric Freeze-Drying 18
3.2	Geometric Basis for the Numerical Solution 28
4.1A	Dimensionless Sensitivity Coefficients of Unknown Parameters for Freeze-Drying at .97 Atmosphere Pressure 42
4.1B	Dimensionless Sensitivity Coefficients of Unknown Parameters for Freeze-Drying at .58 Atmosphere Pressure 43
4.2	Contours of the Risk-Function Surface in the Vicinity of the Computed Minimum 46
4.3	Schematic Drawing of Experimental Apparatus for Equilibrium Moisture Content Studies . 51
4.4	Schematic Drawing of Experimental Apparatus for Atmospheric Freeze-Drying Rate Studies 55
4.5	Sample Holders, Spring and Thermocouple Assembly for Drying Rate Studies 57
5.1	Equilibrium Moisture Isotherms of Freeze-Dried Beef Below Zero °C 62
5.2	Computed Profiles of Vapor Pressure and Temperature for Typical Conditions of Atmospheric Freeze-Drying 69
5.3	Comparison of Predicted Drying Curves of the Proposed Model and the Pseudo Steady-State Model in One-Dimensional Samples 71
6.1	Comparison of the Proposed Model to Experimental Results at .97 and .58 Atmosphere Pressure 85
6.2	Comparison of Solutions of the Three-Dimensional Model to Experimental Results in Cubical Samples 89

Figure	Page
6.3 Predicted Effect of Air Temperature on Atmospheric Freeze-Drying Rates in One-Centimeter Cubes of Precooked Beef ...	92
6.4 Predicted Effect of System Pressure on Atmospheric Freeze-Drying Rate in One-Centimeter Cubes of Precooked Beef	93
6.5 Predicted Effect of Sample Size on Atmospheric Freeze-Drying Rate in Cubes of Precooked Beef	95
6.6 Dimensionless Time Elapsed at $\bar{M} = .1$ in Cubes of Precooked Beef as a Function of \bar{H} Under Atmospheric Freeze-Drying ...	96
6.7 Predicted Maximum-Rate Drying Curve for Atmospheric Freeze-Drying of Cubical Samples of Precooked Beef	98
	116

LIST OF APPENDICES

Appendix		Page
I.	Derivation of the Energy Equation, Equation (3.1)	105
II.	Derivation of the Mass Transfer Equation, Equation (3.2)	107
III.	Derivation of Finite-Difference Approxima- tions of the Heat and Mass Transfer Equations, Equations (3.18) and (3.19) .	108
IV.	Computer Program MAIN and Subroutine MODEL .	110
V.	Summary of Results from Parameter Estima- tion Tests	116
c_{pd}	Specific heat of dry product, constant pressure, calorie/gm-°C.	
c_{pw}	Specific heat of water, constant pressure, calorie/ gm-°C.	
D	Mutual ice-gas diffusivity, air and water vapor, cm ² /sec.	
DF	DF, cm ² -atm/sec.	
h_e	Effective water vapor transfer coefficient in the porous zone, defined by equation (3.18), cm- cm-atm.	
ϵ	Porosity of the porous zone, dimensionless.	
z	Position of ice-vapor interface, dimensionless.	
$F(\cdot)$	Function of \cdot	
g	Defined by equation (3.23).	
h	Defined by equation (6.2).	
h_s	Surface heat transfer coefficient, calorie/cm ² - sec-°C.	
h_m	Surface mass transfer coefficient, gm/cm ² - sec-atm.	
I	Identity matrix	

Index.

Index.

Knudsen diffusivity for air, equation (3.10).

NOMENCLATURE

Defined by equation (3.10).

Knudsen diffusivity for water vapor, equation (3.10).

- A Area, cm^2 .
- A Tridiagonal matrix, equation (3.21).
- B Tridiagonal matrix, equation (3.21).
- C Column matrix, equation (3.21).
- C_0 Constant, equation (2.1), cm^2 .
- C_1 Constant, equation (2.1), cm .
- C_2 Constant, equation (2.2), dimensionless.
- C_{pd} Specific heat of dry product, constant pressure, $\text{calorie/gm}^\circ\text{C}$.
- C_{pw} Specific heat of water, constant pressure, $\text{calorie/gm}^\circ\text{C}$.
- D Mutual free-gas diffusivity, air and water vapor, cm^2/sec .
- \bar{D} DP, $\text{cm}^2\text{-atm}/\text{sec}$.
- D_e Effective water vapor transfer coefficient in the porous zone, defined by equation (3.15), $\text{gm}/\text{sec-cm-atm}$.
- e Porosity of the porous zone, dimensionless.
- f Position of ice-vapor interface, dimensionless.
- $F(\cdot)$ Function of \cdot .
- H Defined by equation (3.23).
- \bar{H} Defined by equation (6.2).
- h Surface heat transfer coefficient, $\text{calorie}/\text{cm}^2\text{-sec}^\circ\text{C}$.
- h_D Surface mass transfer coefficient, $\text{gm}/\text{cm}^2\text{-sec-atm}$.
- I Identity matrix

i	Index.
j	Index.
K_a	Knudsen diffusivity for air, equation (3.10).
K_m	Defined by equation (3.10).
K_w	Knudsen diffusivity for water vapor, equation (3.10).
k	Effective thermal conductivity, porous zone, cal/cm-sec-°C.
k_c	Effective thermal conductivity, frozen core, cal/cm-sec-°C.
L	Number of experimental points in a test.
M	Moisture content, dry basis.
\bar{M}	Dimensionless mean moisture content.
M_a	Molecular weight, air, gm/gm-mole.
M_w	Molecular weight, water, gm/gm-mole.
M_f	Adsorbed moisture content in equilibrium with saturated water vapor, dry basis.
M_0	Initial moisture content, dry basis.
M_i^n	Moisture content at the ith node and nth time frame in the numerical solution.
m	Total number of space nodes in the numerical solution.
m_f	Space node nearest the ice-vapor interface in the numerical solution.
\dot{m}	Mass flux rate, gm/cm ² -sec.
\underline{N}	Matrix, defined by equation (3.32).
n	Index.
$O(\cdot)$	Order of .
P	Total pressure, atmosphere.
P_a	Partial pressure of air, atmosphere.
P_i^n	Partial pressure of water vapor at the ith node and nth time frame in the numerical solution, atmosphere.

P_{sat}	Saturated vapor pressure, atmosphere.
P_v	Partial pressure of water vapor, atmosphere.
P_{va}	Partial pressure of water vapor in the air stream, atm.
P_v^n	Column matrix of water vapor pressures in the nth time frame.
ρ	Bulk density of porous medium, gm/cm ³ .
q	Heat flux rate, calorie/cm ² -sec.
R	Universal gas constant, cm ³ -atm/mole-°C.
$R(\cdot)$	Risk function of \cdot .
r	Relative humidity, dimensionless.
S	Column matrix of sensitivity coefficients.
S_i^*	Dimensionless sensitivity coefficient of parameter (i), defined in Figures 4.1 and 4.2.
s	Half-thickness of the sample, cm.
T	Temperature in the porous zone, °C.
T_a	Temperature of the air stream, °C.
T_c	Temperature of the frozen core, °C.
T_i^n	Temperature at the ith node and nth time frame in the numerical solution, °C.
t	Time, sec.
x	Distance, cm.
Y	Column matrix of experimental observations.
Z	$D_e(\Delta\theta)/D(\Delta\phi)^2$, gm/cm ³ -atm.
ZZ	$k(\Delta\theta)/D(\Delta\phi)^2$, cal/cm ³ -°C.
β	Column matrix of parameters.
Δ	Incremental operator.
ΔH_s	Heat of sublimation, cal/gm.
ΔH_v	Heat of vaporization, cal/gm.
σ^2	Variance of the experimental observations.

δ	Constant, equation (3.33).
ϵ	Column matrix of experimental error.
θ	Dt/s^2 , dimensionless time.
μ	Viscosity of the gas mixture in the porous zone, gm-sec/cm ² .
ρ	Bulk density of porous zone, gm/cm ³ .
τ	Tortuosity factor of the porous media, dimensionless.
ϕ	x/s , dimensionless distance.
Ψ	Covariance matrix.
∇_p	Matrix partial derivative operator.

Freeze-dehydration is preferred from a product quality standpoint over other dehydration methods for many biological products because sublimation of water vapor from the intercellular spaces at low temperatures causes a minimum of undesirable biochemical changes. Many products can be rehydrated easily and rapidly to the original state with little or no nutritional modification. Vacuum freeze-drying has been used as a laboratory technique to include many commercial products. However, only relatively high unit cost food items such as strawberries and coffee have been freeze dried.

Only in recent years has freeze-drying of foods been seriously studied in a quantitative way to relate the physical and chemical

of the process on physical properties of the product and parameters of the system in which the process is conducted (Sandell, et al., 1967; Dyer and Sunderland, 1962). Such analyses invariably show

CHAPTER I

INTRODUCTION

Atmospheric freeze-drying is the process of sublimation in the presence of a cold, desiccated gas at atmospheric or near atmospheric pressure. It differs from the more familiar process, normally called freeze-drying, in which the system pressure is usually maintained below the triple point of water, approximately 4.58 mm Hg absolute. Vacuum freeze-drying of food products has been the subject of an intensive research and development effort especially since 1945 (Burke and Decareau, 1964). The highlights of this development will be briefly mentioned as a means of putting atmospheric freeze-drying in perspective.

Freeze-dehydration is preferred from a product quality standpoint over other dehydration methods for many biological products because sublimation of water vapor from the cell and intercellular spaces at low temperatures causes a minimum of irreversible biochemical changes. Many products can be rehydrated easily and rapidly to the original state with little or no functional modification. Vacuum freeze-drying has been expanded from a laboratory technique to include many commercial pharmaceuticals. However, only relatively high unit cost food items such as military rations and coffee have been freeze dried on a commercial scale.

Only in recent years has freeze-drying of solid foods been studied in a quantitative way to relate the rate-limiting factors

of the process to physical properties of the product and parameters of the system in which the process is conducted (Sandall, et al., 1967; Dyer and Sunderland, 1968). Such analyses invariably show the conventional freeze-drying process to be heat transfer limited due to two factors. First, heat must be transferred largely by radiation from some heat source through a near vacuum to the product surface without excessively heating that surface. Second, heat must be transferred through a porous, semi-dry zone of the product to the ice-vapor interface where sublimation is taking place. Effective conductivity of the porous zone at low system pressures is on the order of good insulation materials, approximately $.00004 \text{ cal/sec-cm}^{\circ}\text{C}$ (Harper, 1962). To provide the heat of sublimation to the ice zone, dielectric heating using a microwave field has been suggested. This idea would appear to have merit in that the polar water molecule couples efficiently to the microwave field compared to the dry porous zone. Thus heat is generated in the desired part of the product, and as the product dries the amount of heat generated is reduced so the process is self-limiting. Extensive research on the use of dielectric heating in freeze-drying indicates that, if a sufficiently strong microwave field is used to increase the drying rate significantly, ionization of inert gases present in the chamber takes place causing burning and rapid chemical decomposition of the porous product (Meryman, 1964; Burke and Decareau, 1964).

From time to time during the development of vacuum freeze-drying various investigators have noted the possibility of atmospheric freeze-drying (Meryman, 1959; Duncoyer and Larousse, 1961;

Woodward 1961; Lewin and Mateles, 1962). Few investigators have carried out tests designed to study the process (work which has been done will be reviewed in the next chapter). Most researchers have noted that mass transfer at atmospheric pressure is by molecular diffusion and that the rate is inversely proportional to total or system pressure (Harper and Tappel, 1957). It has generally been assumed this fact would make atmospheric freeze-drying rates too slow to be economically feasible.

While it is true the potential mass transfer rate of atmospheric drying is lower than vacuum freeze-drying, other factors should be considered when evaluating the overall usefulness of the process. First, vacuum freeze-drying does not utilize the available potential for mass transfer due to the process being heat transfer controlled. Several factors favor heat transfer in atmospheric freeze-drying over vacuum freeze-drying. At atmospheric pressure, the effective heat transfer coefficient in the porous zone of the product is substantially increased over the same value at low pressures. In addition heat transfer external to the sample is primarily by convection from the gas rather than by radiation. Second, if necessary, full use can be made of microwave radiation for supplying sublimation energy since no ionization problem exists at atmospheric pressures for the field strength required. These factors can be combined to allow the atmospheric freeze-drying process to utilize the full potential for mass transfer by eliminating heat transfer restrictions.

Unit costs of atmospheric freeze-drying should be competitive with vacuum freeze-drying at slower drying rates due to lower

equipment costs realized by elimination of the vacuum system and the associated structural requirements. In addition, atmospheric freeze-drying might be easily designed into a continuous system, an advantage never realized in vacuum freeze-drying on a commercial basis.

It is proposed that these potential advantages warrant careful analysis of the heat and mass transfer mechanisms in atmospheric freeze-drying. Specifically it is proposed to:

(1) derive and solve numerically an adequate mathematical model of atmospheric freeze-drying.

(2) obtain sufficient experimental data to evaluate the parameters of the model using nonlinear estimation.

(3) use the complete model to study optimum operating conditions and maximum feasible rates which might be obtained from the process.

Knowledge of the internal heat and mass transfer coefficients of the product under study is basic to understanding the transport mechanisms and to predicting the rates of atmospheric freeze-drying. These transport coefficients, or constants within the mathematical expressions comprising the coefficients, are dependent on structure and composition of the product. A statistical technique called nonlinear estimation will be used to evaluate, or, more correctly, estimate, these physical parameters. Nonlinear estimation of parameters from mathematical models has only recently come into significant practical usage (Pfahl and Mitchell, 1969). The technique requires voluminous amounts of computation, which has only recently become possible by use of the digital computer. An accurate, solvable mathematical model is also a requirement for accurate parameter estimation. The proposed

mathematical model, which is derived, solved, and tested in subsequent chapters, will be shown to accurately predict the rate of atmospheric freeze-drying over the entire moisture content range. Numerical analysis was used to obtain a solution to the mathematical model.

Application of the model solution and the physical parameter estimates is made in studying the mechanism of mass transport in atmospheric freeze-drying, in evaluating the effective heat transfer coefficient in the presence of a counter flow of water vapor, and in determining the effect of all operating variables and sample size on the rate of drying.

Precooked beef, longissimus dorsi muscle, was chosen as the product in which to study the process. This choice was made on a basis of large potential usage in dehydrated form, extensive available information on structure and composition, possibility of cutting geometrically simple samples from the muscle, and ready availability.

Preliminary tests were also conducted with sections of raw apple. Excessive shrinkage due to large amounts of soluble solids in the product moisture was observed when atmospheric freeze-drying was conducted at temperatures above -10°C . These results confirmed previous findings as will be discussed in the following chapters. Since it was desirable to investigate atmospheric freeze-drying at higher temperatures further testing in apples was abandoned.

CHAPTER II

REVIEW OF LITERATURE

Far less research has been done on atmospheric freeze-drying than on vacuum freeze-drying. In the past quarter century a large number of technical articles and books have been written on various aspects of applying vacuum freeze-drying to foods. Many of these presentations have been product-oriented studies dealing with biochemical aspects of freeze-dried foods. However, some quantitative studies of the process itself have been conducted especially in attempting to accelerate the drying rate by increasing heat transfer to the ice portion of the product. Rarely has the drying rate been related to basic transport mechanisms and physical parameters of the product.

This review will not include discussion of product-oriented articles except as they specifically apply to atmospheric freeze-drying. A more complete review has been published by Burke and Deceareau (1964).

Atmospheric Freeze-Drying

A few published papers and reports have dealt specifically with atmospheric freeze-drying in a descriptive or exploratory way. Meryman (1959) demonstrated the possibility of atmospheric freeze-drying by constructing a small laboratory device which dried histological samples in a stream of cold, desiccated air. The samples

were reportedly of comparable quality to vacuum freeze-dried samples when evaluated microscopically as tissue plates.

Preliminary studies of atmospheric freeze-drying applied to foods have been conducted by Lewin and Maletes (1962) and Woodward (1961, 1963). These works covered a wide variety of products and are valuable in that they demonstrated the basic technical feasibility of the process in food dehydration. These reports agree that atmospheric drying rates are appreciably slower than conventional freeze-drying rates for comparable size samples. They also agree the drying rate is highly dependent on air temperature and nearly independent of air velocity above one-half to one meter/sec.

The large dependence of drying rate on air temperature cannot be entirely explained by variation of the vapor diffusion coefficient with temperature. The effective mass diffusivity for vapor phase diffusion increases with absolute temperature to the .75 power. Data for diced roast beef presented by Woodward (1961) indicate a much stronger dependence of the drying rate on temperature above -10°C . It appears possible that drying rates for air temperatures above approximately -4°C are accelerated by liquid phase transport of water to the product surface. Due to freezing point depression caused by solutes in the cell moisture, significant amounts of unfrozen water exist in beef at temperatures above -4°C (Hohner and Heldman, 1970). Drying times were reported by Woodward (1963) for air temperatures as high as 4.5°C . The wet-bulb temperature for fully dry air at atmospheric pressure and 4.5°C is approximately -3.3°C ; thus it seems possible some transport of liquid water occurred accounting partially for faster drying rates. Since

no product temperatures were reported this cannot be confirmed.

Woodward (1961) indicated shrinkage takes place in high sugar products unless they are dried with air temperatures considerably below the initial freezing point. This fact is further indication that liquid transport was taking place causing soluble components to be brought to the surface and allowing cell collapse resulting in shrinkage. Burke and Deceareau (1964), in discussing Woodward's work, pointed out atmospheric drying at partially frozen conditions may still be a valuable process for some products provided product quality is near that of vacuum freeze-dried products. Since both Lewin and Maletes (1962) and Woodward (1961) found atmospheric drying rates in diced foods to be independent of air velocity above .5 meter/sec, internal transport resistances are indicated as the rate-limiting parameters. For such a situation the drying rate per unit weight of product can be increased by reducing the particle size. This concept has been tested in recent research by Malecki et al. (1969) in which atmospheric fluidized-bed freeze-drying was attempted with spray-frozen droplets of egg albumin and apple juice. Investigations by Dunoyer and Larousse (1961) also led to the conclusion that the effective rates of sublimation obtained from small particles can be of the same order of magnitude as in vacuum freeze-drying. Economic analysis by Woodward (1961) indicated an energy cost per unit of water removed in atmospheric freeze-drying of diced foods approximately equal to that of vacuum freeze-drying of the same product.

Mechanisms and Parameters of Heat and Mass Transfer
in Freeze-Dried Foods

Accurate analysis of the mechanisms and rate of atmospheric or vacuum freeze-drying is dependent upon knowledge of the heat and mass transfer parameters of the semi-dry porous zone of the product. Considering first the heat transfer properties, the effective thermal conductivity and specific heat of the porous layer must be known.

Harper (1962) and Harper and El Sahrighi (1964) have reported effective thermal conductivity data for freeze-dried peach, pear, apple and beef over a range of total pressure from near zero to atmospheric. All products tested exhibited results typical of other porous media. A nearly constant value was found for pressures less than .1 mm Hg and another higher constant value for pressures greater than 400 mm Hg. At intermediate pressures a transition region exists where the effective thermal conductivity increased sharply with gas pressure. Harper and El Sahrighi (1964) explained these results by reference to kinetic gas theory. At low pressures the mean free path of the gas molecules is large compared to mean pore diameter of the media, and effective thermal conductivity is limited by conductivity of the solid. At higher pressures where the mean free path of the gas molecule is of the order of the mean pore diameter, both the gas and the solid contribute to the effective conductivity, and its value increases sharply to the higher limiting value. Harper (1962) found the effective thermal conductivity of freeze-dried beef to have a lower limiting value of .00009 cal/sec-cm-^oC and a higher limiting

value of .00015 cal/sec-cm^oC. Harper and El Sahrigi (1964) established that the mechanisms of thermal convection and radiation are insignificant in freeze-drying of foods. All conductivity data reported by Harper and El Sahrigi were obtained by steady-state methods.

Triebes and King (1966) also used steady-state methods to evaluate effective thermal conductivity in freeze-dried turkey meat. Their results are similar in form to those of Harper (1962). Triebes and King included tests with water vapor as the gas present in the turkey meat. The upper limiting value increased with increasing relative humidity of the gas. Sixty percent relative humidity caused approximately a 30 percent increase in effective conductivity at atmospheric pressure. Sufficient data are not available to determine to what extent the increase in conductivity was caused by moisture adsorbed on the porous solid. Sparse data plotted by Triebes and King (1966) indicated no change in thermal conductivity at low pressures. This may mean that little increase in effective thermal conductivity was due to adsorbed moisture. The same authors found no change in thermal conductivity due to temperature over the range -26^oC to 67^oC.

Saravacos and Pilsworth (1965) also reported higher effective thermal conductivity for freeze-dried food gels when equilibrated with water vapor at high relative humidity. They showed an increase of 2 to 12 percent in effective thermal conductivity over dry gas measurements for relative humidity of approximately 50 percent. The effective thermal conductivity value in the presence of a counter flow of water vapor has apparently never been investigated.

As sublimation occurs at the ice-vapor interface during freeze-drying, water vapor is transported outward through the semi-dry, porous region. The mechanisms of such fluid flow in porous media have been extensively investigated (Carman, 1956; Scheidegger, 1957). The controlling mechanism depends upon structure of the media, system pressure and type of gas or gases present.

Flow of a single gas through porous media is dependent upon the mechanisms of hydrodynamic flow and Knudsen or free molecular flow. The appropriate controlling equation is a modification of the D'Arcy equation.

$$\dot{m} = M_w \left[\frac{C_0 P}{\mu RT} + K_w \right] \frac{dP}{dx} \quad (2.1)$$

In vacuum freeze drying at pressures below the ice vapor pressure, little or no inert gas remains in the system, and equation (2.1) is applicable to the flux of pure water vapor. Gunn and King (1969) point out that a plot of specific flux rate versus pressure in most porous media gives a linear relationship as suggested by equation (2.1). Conversely, a similar plot for flow in long capillary tubes always shows a minimum. Harper (1962) presented permeability data for freeze-dried apple, peach, and beef as functions of pressure which confirm this linear relationship. The two material constants, C_0 and C_1 , can be evaluated for a particular product from the permeability data.

In atmospheric freeze-drying water vapor is transported in the presence of an inert gas. At atmospheric pressure the mean pore diameter of freeze-dried foods is generally large compared

to mean molecular free path of the gases present. Total pressure gradient is almost zero. As a result the controlling mechanism of vapor transport is mutual diffusion of water vapor through the inert gas (Harper and Tappel, 1957). For nonisobaric vapor transport at much lower pressures in the transition region where mean molecular path and pore diameter are of the same order of magnitude, all three mechanisms of mutual diffusion, Knudsen diffusion and hydrodynamic flow may be significant. The significance of each component as a function of pressure can be clearly seen from the general expression for binary flux in porous media presented by Gunn and King (1969). From previous derivations of isobaric transition region diffusion by Scott and Dullien (1962) and Evans et al. (1961), Gunn and King derived the following expression for mass flux of water vapor not restricted to isobaric flow.

$$\dot{m} = \frac{-C_w \bar{D}_w M_w}{(C_w \bar{D}_w + K_m P) RT} \frac{dP}{dx} - \left[\frac{K_w (C_w \bar{D}_w + K_a P)}{C_w \bar{D}_w + K_m P} + \frac{C_o P}{\mu} \right] \frac{P M_w}{PRT} \frac{dP}{dx} \quad (2.2)$$

Simplification of equation (2.2) for the situation of interest will be discussed in the next chapter.

Numerous other equations have been presented for nonisobaric vapor transport in porous media. Many of these were derived by initially assuming the porous medium to be equivalent to a group of modified capillaries (Wakao, et al., 1965; Dyer and Sunderland, 1966). As discussed by Gunn (1967) these expressions fail to predict well-established experimental results for flow in porous media. On the other hand, equation (2.2) reduces to correct expressions for limiting cases at pressures both above and below the transition

region. The assumption was made that it also predicts the correct flux in the transition region. Differences between the various derivations for flux of multicomponent gases in porous media are confined to the transition region between bulk and diffusion transport under nonisobaric conditions. For isobaric diffusion, as approximated in the case of atmospheric freeze-drying, it can be shown that the derivations by Wakao, et al. (1965) and Gunn and King (1969) both reduce to the same expression as obtained by Scott and Dullien (1962) and Evans, et al. (1961).

Freeze-Drying Rate

No comprehensive study of drying rate has previously been completed in atmospheric freeze-drying. Sandall, et al. (1967) reported what is probably the most complete analysis of heat and mass transfer in freeze-drying. They used experimental results obtained from controlled studies in precooked turkey breast muscle to test a mathematical model based on a uniformly retreating ice front. The model was pseudo steady-state in that time derivatives in the heat and mass transport equations were neglected. Sandall (1966) justified this approach by the low velocity of the ice front which caused the change in temperature or vapor pressure with time to be small with respect to change in position at any point in the porous zone. The thermal requirement for heating the water vapor as it flows to the surface and the effect of adsorbed water remaining in the porous zone were also neglected. The author claimed a maximum error of four percent was induced in the heat flux to the ice front due to neglecting the thermal requirement for heating the vapor flow. They also claimed, for turkey muscle, the mean

moisture content in the porous zone was only approximately three percent of the initial moisture content if the product was in equilibrium with water vapor passing through it. Therefore, the adsorbed moisture was neglected.

Results of the experimental studies agreed with the prediction of Sandall's model until 75 to 90 percent of the initial moisture was removed. At lower moisture levels the model predicted substantially shorter drying times than were obtained experimentally. Nevertheless, the simplicity of the model makes it quite attractive for predicting the drying rate up to the time all free moisture has been removed by sublimation.

Effective thermal conductivity was evaluated from the model and compared with directly measured results by Triebes and King (1966). Values obtained from the model were approximately eight percent higher than those directly measured by steady-state procedures. The authors felt this comparison afforded striking confirmation of the retreating ice front model.

Dyer and Sunderland (1968) investigated heat and mass transfer mechanisms in sublimation dehydration of beef muscle. The process of freeze-drying was analyzed, and optimum operating conditions were discussed, but no experimental data were presented. Significant differences exist between this and the analysis presented by Sandall, et al. (1967). Both groups neglected the time derivatives of the heat and mass transfer equations by assuming the movement of the interface was so slow that the time rate of change at any point in the porous region was negligible compared to the space rate of change. Dyer and Sunderland (1968) calculated

that this assumption induced an error of approximately two percent in the heat flux to the ice interface. However, they noted the error may be somewhat greater if microwave heating is used. Like the previous analysis Dyer and Sunderland (1968) did not consider adsorbed moisture in the porous zone, but unlike Sandall, et al. (1967) they did include the thermal effect of heating the water vapor as it flows to the product surface. The mathematical model to be presented in the next chapter and used in the current research is not limited by the assumptions discussed above.

An additional, more basic, difference between the analysis by Dyer and Sunderland (1968) and the one previously discussed is concerned with the mechanism of mass transfer. Dyer and Sunderland (1968) considered the porous zone to be equivalent to a group of capillaries which were modified to account for the tortuous path of gas through the pores. The expression used for mass transfer in the transition zone between bulk and diffusional transport was derived by Dyer and Sunderland (1966). As mentioned previously this derivation was critically reviewed in detail by Gunn (1967).

Several specific suggestions for optimization of sublimation dehydration were made by Dyer and Sunderland (1968). Their model indicated decreasing the water vapor concentration at the sample surface to zero did not appreciably increase the drying rate. This is true for vacuum freeze-drying since it is usually heat transfer limited anyway but would not be true for a mass transfer limited process. Second, the model indicated that decreasing the total pressure increased the drying rate. Since the model did not consider the effect of inert gases this result would be expected.

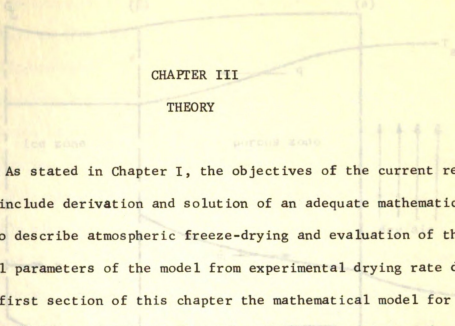
However, work by Kan and de Winter (1966) indicated increased drying rates in shrimp and diced peaches up to seven millimeter Hg total pressure when helium was used as the inert gas. Sandall, et al. (1967) showed the optimum drying rate for freeze-drying turkey breast meat in helium with parallel grain orientation of the meat was at about 14 mm Hg total pressure. The optimum pressure for nitrogen under the same conditions was about eight mm Hg.

A third suggestion was to heat the sample from the ice side to increase the drying rate in situations where the process is heat transfer limited. This valid suggestion is limited by the practical problem of holding a vapor tight seal against the ice which is being heated. The seal must prevent sublimation and subsequent formation of a porous zone which defeats the purpose of increasing heat transfer.

The preceding discussion of optimization of processes by use of mathematical models points out that often not all possible constraints on the system are included explicitly in the model. When this is true the model solution must be viewed critically.

Additional earlier works on use of mathematical models of the freeze-drying process have been published. Most of the models are over simplified, and little of this information is applicable to atmospheric freeze-drying and will not be reviewed. These works include Mink and Sachsel (1961), and Lambert and Marshall (1961).

dimensional rectangular coordinates. The sample vapor atmosphere freeze-drying can be represented schematically as shown in figure 2.1. An ice-vapor interface (I) recedes toward the centerline as sublimation progresses, and the necessary heat of sublimation is



CHAPTER III

THEORY

As stated in Chapter I, the objectives of the current research include derivation and solution of an adequate mathematical model to describe atmospheric freeze-drying and evaluation of the physical parameters of the model from experimental drying rate data. In the first section of this chapter the mathematical model for atmospheric freeze-drying is derived, and the assumptions and simplifications implied by the derivation are discussed. In the following section the expression for the mass transfer coefficient is obtained by simplification of a previously discussed derivation. The complete mathematical model is then transformed to the finite-difference model, the method of numerical solution is presented, and certain considerations of accuracy and stability in the numerical solution are discussed. The mathematical basis of sensitivity analysis and parameter estimation appears in the closing section of this chapter.

The Mathematical Model

The geometry used throughout the work reported was one-dimensional rectangular coordinates. The sample under atmospheric freeze-drying can be represented schematically as shown in Figure 3.1. An ice-vapor interface (f) recedes toward the centerline as sublimation progresses, and the necessary heat of sublimation is

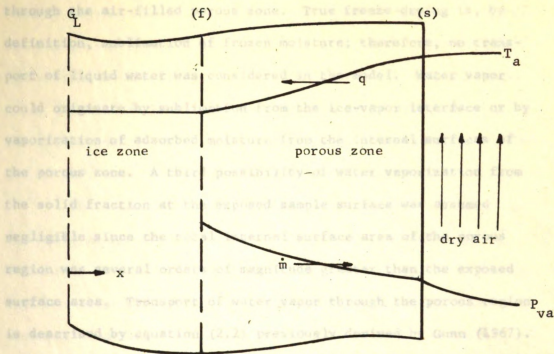


Figure 3.1. Schematic diagram of Atmospheric Freeze-Drying

transported from the surface (s) to the interface in response to a temperature gradient. Simultaneously water vapor is transported through the porous zone to the surface in response to a chemical potential gradient. Chemical potential of water vapor is represented in Figure 3.1 and throughout the current work as water vapor pressure. Derivation of the mathematical model for atmospheric freeze-drying required explicit statement of the mechanisms involved in the process. Since a priori proof cannot be provided to support the accuracy of these mechanisms, they are stated as hypotheses supported by previous work in vacuum freeze-drying and later will be tested with experimental data. As indicated in Figure 3.1, the mechanism of mass transfer was assumed to be water vapor diffusion

through the air-filled porous zone. True freeze-drying is, by definition, sublimation of frozen moisture; therefore, no transport of liquid water was considered in the model. Water vapor could originate by sublimation from the ice-vapor interface or by vaporization of adsorbed moisture from the internal surfaces of the porous zone. A third possibility of water vaporization from the solid fraction at the exposed sample surface was assumed negligible since the total internal surface area of the porous region was several orders of magnitude greater than the exposed surface area. Transport of water vapor through the porous region is described by equation (2.2) previously derived by Gunn (1967). Simplification of this equation to yield the appropriate effective vapor diffusivity for atmospheric freeze-drying will be the subject of the next section of the chapter.

Transfer of heat through the porous region to the ice-vapor interface was assumed to be by thermal conduction. As discussed in Chapter II, Harper and El Sharigi (1964) have shown the heat transfer mechanisms of convection and radiation are negligible in freeze-drying of foodstuffs. In any case, values for thermal conductivity of freeze-dried beef reported by the above authors are effective values; thus, they include all mechanisms of heat transfer. These experimentally determined values of thermal conductivity were used in the current research. The effective thermal conductivity was assumed to be a function of system pressure only.

All free, unbound, product moisture was assumed to be removed by sublimation at the ice-vapor interface. The remaining product moisture was assumed to be adsorbed in the porous zone and

removed to the external air stream through vaporization. Throughout the porous region the product matrix and associated adsorbed water were assumed to be in local equilibrium with the air-water vapor mixture in the pores. Thus the amount of adsorbed moisture was a function of the temperature and water vapor pressure of the gas in the immediate vicinity of the point in question.

The assumption of gas-solid equilibrium was justified on the basis of the slow movement of the ice front resulting in a small time rate of change of conditions at any point in the porous region. In processes where the rate of drying is very rapid this assumption may be of questionable validity. If it is violated the model will tend to predict a more rapid drying rate than would be observed experimentally. In freeze-drying this assumption is relevant only to the adsorbed moisture which is the minor component of the total moisture present. In addition, all sublimation dehydration processes are quite slow, therefore, the assumption was accepted as valid for atmospheric freeze-drying.

The energy and mass transfer equations for the porous zone were derived from the appropriate conservation principle applied to a differential volume of the porous zone, dV . Considering first the energy equation,

$$\left[\begin{array}{l} \text{rate of change} \\ \text{of internal} \\ \text{energy in } dV \end{array} \right] = \left[\begin{array}{l} \text{rate heat is} \\ \text{conducted into} \\ dV \end{array} \right] - \left[\begin{array}{l} \text{rate heat is} \\ \text{conducted out} \\ \text{of } dV \end{array} \right] + \left[\begin{array}{l} \text{rate of energy} \\ \text{input due to} \\ \text{vapor flow} \end{array} \right] \\ - \left[\begin{array}{l} \text{rate of energy} \\ \text{loss due to} \\ \text{vapor flow} \end{array} \right] + \left[\begin{array}{l} \text{heat of vaporization liberated} \\ \text{due to rate of change of adsorbed} \\ \text{moisture in } dV \end{array} \right]$$

which was written,

$$\rho (C_{pd} + M C_{pw}) \frac{\partial T}{\partial \theta} = \frac{\partial}{\partial \phi} \left(\frac{k}{D} \frac{\partial T}{\partial \phi} \right) + \frac{D_e}{D} C_{pw} \frac{\partial P_v}{\partial \phi} \frac{\partial T}{\partial \phi} + \rho \Delta H_v \frac{\partial M}{\partial \theta}, \quad (3.1)$$

where: θ and ϕ are dimensionless independent variables of time and space, respectively. Details of the derivation of equation (3.1) are given in Appendix I.

Likewise the water vapor transport equation was derived from a mass balance on the same differential volume element,

$$\left[\begin{array}{l} \text{rate of change} \\ \text{of water vapor} \\ \text{in volume } dV \end{array} \right] = \left[\begin{array}{l} \text{mass rate of} \\ \text{water vapor} \\ \text{flow into } dV \end{array} \right] - \left[\begin{array}{l} \text{mass rate of} \\ \text{water vapor} \\ \text{flow from } dV \end{array} \right] - \left[\begin{array}{l} \text{rate of change of} \\ \text{adsorbed moisture} \\ \text{in } dV \end{array} \right],$$

which was expressed

$$\frac{eM_w}{RT} \frac{\partial P_v}{\partial \theta} = \frac{\partial}{\partial \phi} \left(\frac{D_e}{D} \frac{\partial P_v}{\partial \phi} \right) - \rho \frac{\partial M}{\partial \theta}. \quad (3.2)$$

Details of the derivation are given in Appendix II.

In general, the amount of water adsorbed on a hygroscopic surface is a function of both temperature and vapor pressure of the surrounding gas. However, in the temperature range where atmospheric freeze-drying can be conducted, experimental data for freeze-dried beef indicated dependence of the amount of adsorbed moisture on temperature was negligible compared to dependence on relative humidity of the surrounding gas. These data are presented and discussed in a later chapter. Because of the relative independence of adsorbed moisture and temperature the time rate of change of adsorbed moisture in equation (3.2) was written

$$\frac{\partial M}{\partial \theta} = \left(\frac{\partial M}{\partial T} \right)_P \frac{\partial T}{\partial \theta} + \left(\frac{\partial M}{\partial P_v} \right)_T \frac{\partial P_v}{\partial \theta} \approx \left(\frac{dM}{dr} \right) \left(\frac{dr}{dP_v} \right) \frac{\partial P_v}{\partial \theta} = \frac{1}{P_{sat}} \left(\frac{dM}{dr} \right) \frac{\partial P_v}{\partial \theta}, \quad (3.3)$$

where use was made of the definition of relative humidity,

$r = P_v / P_{sat}$. Equation (3.2) was rewritten to give

$$\left[\frac{eM}{RT} + \frac{\rho}{P_{\text{sat}}} \left(\frac{dM}{dr} \right) \right] \frac{\partial P}{\partial \theta} = \frac{\partial}{\partial \phi} \left(\frac{D}{D} \frac{\partial P}{\partial \phi} \right) \quad (3.4)$$

Equations (3.1) and (3.4) represent the heat and mass transfer equations of the mathematical model and must be solved simultaneously to yield temperature and vapor pressure at all points as a function of dimensionless time. Appropriate boundary conditions must be specified to allow solution. At the product surface a finite porous zone was assumed to form instantaneously as heat and water vapor were exchanged with the air stream by convection. Convective conditions at the sample surface gave the following boundary conditions:

$$-\frac{k}{D} \left(\frac{\partial T}{\partial \phi} \right)_{\phi=1} = \frac{hs}{D} (T - T_a) \quad (3.5a)$$

and

$$-\frac{D_e}{D} \left(\frac{\partial P}{\partial \phi} \right)_{\phi=1} = \frac{h_v s}{D} (P_v - P_{va}) \quad (3.5b)$$

Boundary conditions at the ice-vapor interface were more complex. Vapor pressure at the interface was saturation vapor pressure of the ice surface at the interface temperature. The boundary condition for the energy equation was derived from an energy balance on the interface,

$$\Delta H_s \frac{df}{d\theta} \rho (M_o - M_f) = -\frac{ks}{D} \left(\frac{\partial T}{\partial \phi} \right)_{\phi=f} + \frac{k_s}{D} \left(\frac{\partial T}{\partial \phi} \right)_{\phi=f} \quad (3.6)$$

Equation (3.6) was simplified since the thermal conductivity of frozen beef at -6.7°C is approximately $.025 \text{ cal/sec-cm}^\circ\text{C}$ (Lentz, 1961), while the effective thermal conductivity of the porous zone is approximately $.00015 \text{ cal/sec-cm}^\circ\text{C}$ (Harper, 1962). Thus

the temperature gradient in the frozen core was small compared to the porous zone, and the ice core was considered by lumped-parameter analysis. Equation (3.6) then reduced to

$$\Delta H_s \frac{df}{d\theta} \rho (M_o - M_f) = - \frac{ks}{D} \left(\frac{\partial T}{\partial \phi} \right)_{\phi=f} + f \rho (1 + M_o) C_{pc} \frac{\partial T_c}{\partial \theta}. \quad (3.7)$$

The rate of vapor transfer away from the interface was written as

$$\frac{df}{d\theta} \rho (M_o - M_f) = \frac{D_e s}{D} \left(\frac{\partial P_v}{\partial \phi} \right)_{\phi=f}. \quad (3.8)$$

Finally, substitution of (3.8) into (3.7) led to the appropriate boundary condition for the energy equation at the ice-vapor interface. These constants are evaluated in

$$- \frac{ks}{D} \left(\frac{\partial T}{\partial \phi} \right)_{\phi=f} = \Delta H_s \frac{D_e s}{D} \left(\frac{\partial P_v}{\partial \phi} \right)_{\phi=f} - f \rho (1 + M_o) C_{pc} \frac{\partial T_c}{\partial \theta}. \quad (3.9a)$$

After the interface reached the centerline and free moisture was no longer present in the sample the boundary conditions at the centerline were

$$\left(\frac{\partial T}{\partial \phi} \right)_{\phi=0} = \left(\frac{\partial P_v}{\partial \phi} \right)_{\phi=0} = 0, \quad \text{at } \phi = 0. \quad (3.9b)$$

The amount of specific heat liberated due to change in ice core temperature with time had a negligible effect upon the velocity of the ice-vapor interface, but changes in ice core temperature had a significant effect upon the vapor pressure at the interface and thus upon the rate of mass transfer. Therefore, the remaining boundary condition for the mass transfer equation was written

$$P_v = F(T_c) = \text{saturation condition, } \phi = f. \quad (3.9c)$$

Various additional assumptions and simplifications not specifically mentioned during derivation of model were made.

These are listed as follows:

1. In a macroscopic sense the product was assumed to be of uniform and constant porosity; thus shrinkage was assumed to be zero.

2. All transport was assumed to be in one dimension.

3. Convective surface parameters were assumed to be constant, that is, independent of water vapor concentration at low concentrations involved at the sample surface.

4. Certain physical parameters including bulk density of the porous zone (ρ), specific heat of the porous zone (C_{pd}), specific heat of water (C_{pw}), heat of sublimation (ΔH_g), heat of vaporization (ΔH_v), and specific heat of the frozen core (C_{pc}) were assumed constant. These constants are evaluated in Chapter V.

5. The energy content of the vapor in the pores was neglected.

Complexity of the simultaneous solution of equations (3.1) and (3.4) precluded closed form integration. Instead the methods of numerical analysis were used, and the large amount of computation necessary was done on a digital computer (Control Data Corp. Model 3600). Before discussing the method of numerical solution the derivation of the effective mass transfer expression is presented.

The mass transfer coefficient

As previously reviewed in Chapter II, Gunn (1967) and Gunn and King (1969) have derived an expression for vapor-phase mass transport in porous media in the presence of gradients of total pressure and concentration. This expression was given as equation (2.2) and is repeated here for convenience,

$$\dot{m} = \frac{-C_2 \bar{D} K_w M_w}{(C_2 \bar{D} + K_m) RT} \frac{\partial P}{\partial x} - \left[\frac{K_w (C_2 \bar{D} + K_a P)}{C_2 \bar{D} + K_m} + \frac{C_0 P}{\mu} \right] \frac{P_w M_w}{PRT} \frac{dP}{dx}, \quad (3.10)$$

where: $K_w = C_1 / \sqrt{RT/M_w}$, $K_a = C_1 / \sqrt{RT/M_a}$ and $K_m = \frac{P}{P} K_a + \frac{P_a}{P} K_w$.

Three experimentally determined constants, C_0 , C_1 and C_2 which are functions of the porous structure are necessary to completely describe the flow of gases through a porous medium under all flow conditions. The above authors presented convincing experimental proof of the validity of the derivation and its superiority over similar expressions based on familiar capillary tube assumptions.

In atmospheric freeze-drying the transported gas is water vapor, and the stagnant gas is air, or some inert gas. The maximum possible total pressure differential across the porous zone is approximately 4.5 mm Hg compared to a total pressure of over 700 mm Hg. Thus, the second term of equation (3.10) was considered negligible. The remaining term was written

$$\dot{m} = \frac{-C_2 \bar{D} M_w}{\left(\frac{C_2 \bar{D}}{K_w} + \frac{K_m P}{K_w} \right) RT} \frac{dP_w}{dx}, \quad (3.11)$$

$$\text{but } \frac{K_m}{K_w} = \frac{P_a}{P} + \frac{P_w K_a}{P K_w} = 1 - \frac{P_w}{P} \left(1 - \frac{K_a}{K_w} \right) \quad \text{and} \quad \frac{K_a}{K_w} = \sqrt{\frac{M_w}{M_a}} \quad (3.12)$$

$$\text{so } \dot{m} = \frac{-C_2 \bar{D} M_w}{\left[\frac{C_2 \bar{D}}{K_w} + P - P_w \left(1 - \sqrt{\frac{M_w}{M_a}} \right) \right] RT} \frac{dP_w}{dx}. \quad (3.13)$$

For the gas mixture of air and water vapor (3.13) gave

$$\dot{m} = \frac{-C_2 \bar{D} M_w}{\left[\frac{C_2 \bar{D}}{K_w} + P - .209 P_w \right] RT} \frac{dP_w}{dx}. \quad (3.14)$$

Sandall, et al. (1967) evaluated K_w in the outer breast meat of turkey to be approximately $20 \text{ cm}^2/\text{sec}$ for transport parallel to the fibers and approximately $10 \text{ cm}^2/\text{sec}$ perpendicular to the fibers. These data were obtained with nitrogen as the inert gas. Assuming the same order of magnitude for K_w in beef with air as the inert gas, equation (3.14) was further simplified. By definition C_2 is less than one and \bar{D} is approximately $.2 \text{ cm}^2\text{-atm}/\text{sec}$ for air and water vapor at zero $^\circ\text{C}$. By order of magnitude analysis on the effective mass transfer coefficient, the following evaluation was obtained:

$$D_e = \frac{C_2 \bar{D} M_w}{\left[\frac{(.8)(.2)}{10} + 1 - \frac{(.209)(4.5)}{760} \right] RT} \quad (3.15)$$

Clearly, the first and last terms of the denominator are not only insignificant compared to P , but also of opposite sign. As a result, the effective mass transfer coefficient for atmospheric freeze-drying was written

$$D_e = \frac{C_2 \bar{D} M_w}{PRT} \quad (3.16)$$

It is unlikely significant thermal gradients exist in food products sized for practical application of atmospheric freeze-drying; if they do equation (3.16) can be modified to account for thermal gradients by the familiar $7/4$ power rule (Eckert and Drake, 1959).

$$D_e = \frac{C_2 D^1 \left(\frac{T}{T^1}\right)^{7/4}}{PRT} = \frac{C_2 D^1 T^{3/4}}{PRT^{7/4}} \quad (3.17)$$

The Finite-Difference Model

With larger, faster and more flexible digital computers which have been developed in recent years have come more sophisticated and reliable numerical methods. The present level of computer capability and numerical solution technique has elevated applied numerical solutions from crude approximations to an accurate and preferred method of solving real-world problems. Numerical solution of partial differential equations was discussed in an excellent manner by Smith (1965).

Two general approaches exist for transforming a complex physical situation and its associated mathematical model (partial differential equations in this case) into algebraic, finite-difference equations which constitute the numerical model. The first approach can be described as merely writing finite-difference equations to correctly approximate the partial differential equations without regard for the physical problem. The other approach is to derive the numerical model directly from the physical process by application of conservation laws to a differential volume increment. The current situation is an excellent example of the usefulness of the latter approach.

The domain of the equations which were to be solved to describe the process of atmospheric freeze-drying was the porous zone of the sample. At time equal to zero the domain was also zero. Furthermore, the domain continuously increased until the ice front reached the centerline. Finite-difference approximations of the partial differential equations were written at (m) -space

grid points or nodes across the domain of the partial differential equations. Obviously, since the domain increased, either the nodes had to shift position or additional nodes had to be added to the domain as time progressed. The later case was chosen. Geometrically the numerical solution was represented as shown in Figure 3.2.

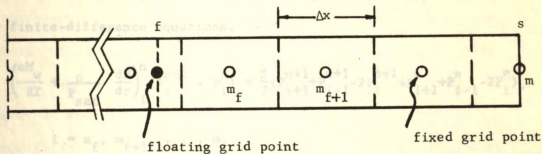


Figure 3.2. Geometric Basis for the Numerical Solution

Fixed position grid points were equally spaced from center-line to surface of the sample. An additional floating grid point remained on the ice-vapor interface (f). As the interface passed a fixed grid point that node was included into the numerical solution. No volume of the porous zone was associated with the floating grid point; it represented conditions of the ice core. The point nearest the interface represented a variable volume which increased as the interface receded. When the interface passed a new grid point the variable volume of the previous nearest grid point was truncated to normal size, and the dependent variables at the new grid point assumed a linearly interpolated value between the value of the floating grid point and node in the newly truncated grid volume. Computation continued until the floating grid point reached the

centerline at which time all grid points represented a constant volume.

Turning attention to numerical approximation of the partial differential equations, the domains of the independent variables, dimensionless time and distance, were divided into small increments $\Delta\theta$ and $\Delta\phi$ respectively. Using the procedure presented by Crank and Nicolson (1947), the mass transfer equation was approximated by finite-difference equations.

$$\left(\frac{eM_w}{RT} + \frac{\rho}{P_{sat}} \frac{dM}{dr} \right)_i^n (P_i^{n+1} - P_i^n) = \frac{Z}{2} (P_{i+1}^{n+1} + P_{i-1}^{n+1} - 2P_i^{n+1} + P_{i+1}^n + P_{i-1}^n - 2P_i^n), \quad (3.18)$$

$$i = m_f, m_f+1, \dots, m,$$

$$n = 1, 2, 3, \dots$$

Equations (3.18) were written from a conservation of mass in the differential volume element, $Ad\phi$, rather than being written directly from equation (3.4).

Ideally the energy equation should also be approximated by the Crank-Nicolson method since this method has the smallest truncation error of commonly used finite difference approximations (Smith, 1965). However, in spite of the fact that the Von Neumann stability analysis (Smith, 1965) predicted the Crank-Nicolson approximation of equation (3.1) to be stable, trial solutions demonstrated the numerical solution to be unstable. The apparent inconsistency is probably explained by the nonconstant coefficients and expanding domain of the model which were not considered in the Von Neumann analysis. For these reasons the energy equation was transformed to finite-difference equations using the backwards-difference technique (Smith, 1965).

$$\begin{aligned}
 (C_{pd} + M_i C_{pw}) (T_i^{n+1} - T_i^n) = & ZZ (T_{i+1}^{n+1} + T_{i-1}^{n+1} - 2T_i^{n+1}) \\
 + \frac{C_{pw} Z}{4} (P_{i+1}^{n+1} - P_{i-1}^{n+1}) (T_{i+1}^{n+1} - T_{i-1}^{n+1}) & + \Delta H_{v,p} (M_i^{n+1} - M_i^n), \quad (3.19)
 \end{aligned}$$

$$i = m_f, m_{f+1}, \dots, m,$$

$$n = 1, 2, 3, \dots$$

Boundary conditions at the surface and the ice interface were transformed to finite-difference equations in a similar manner. Details of the numerical derivations are shown in Appendix III.

Equations (3.18) and (3.19) each represented $(m - m_f + 1)$ algebraic equations which were solved simultaneously for the temperature and vapor pressure at each node point in the porous zone during time frame $\Delta\theta$. In each time step a solution was obtained for equations (3.18) first. Rearranging (3.18) the following equations were obtained:

$$\begin{aligned}
 -Z P_{i-1}^{n+1} + 2 \left(\frac{eM_w}{RT} + \frac{\rho}{P_{sat}} \frac{dM}{dr} + Z \right)_i P_i^{n+1} - Z P_{i+1}^{n+1} = \\
 Z P_{i-1}^n + 2 \left(\frac{eM_w}{RT} + \frac{\rho}{P_{sat}} \frac{dM}{dr} - Z \right)_i P_i^n + Z P_{i+1}^n, \quad (3.20)
 \end{aligned}$$

$$i = m_f, m_{f+1}, \dots, m.$$

Equations (3.20) were represented in matrix notation as

$$\underline{A} \cdot \underline{P}_v^{n+1} = \underline{B} \cdot \underline{P}_v^n = \underline{C}, \quad (3.21)$$

where \underline{A} and \underline{B} are both tridiagonal matrices. All quantities on the right-hand side of equation (3.21) were known allowing them to be evaluated to yield a known column matrix, \underline{C} . Row operations were performed on tridiagonal matrix \underline{A} to eliminate the lower

diagonal which in turn allowed direct evaluation of the vapor pressure matrix, \underline{P}_v^{n+1} , by back substitution. The appropriate matrix row and back substitution operations are summarized in an algorithm presented by Smith (1965).

The moisture content at each space node in the (n+1)th time frame was immediately computed from the equilibrium moisture relationship as soon as the vapor pressure was known. The temperature column matrix in the (n+1)th time frame was computed in the same manner as outlined above for vapor pressure. Vapor pressure and adsorbed moisture content at each space node for the (n)th and (n+1)th time frames were substituted into equations (3.19). The equations were rearranged into tridiagonal matrix form and solved for the temperature column matrix by use of the above mentioned algorithm.

Use of finite-difference equations for solution of partial differential equations raises questions of accuracy and stability. Stability implies convergence of the numerical solution to the actual solution. Absence of stability usually results in increasing oscillation of the numerical solution about the true solution. As previously mentioned not all methods of finite-difference approximation are equally stable or accurate. The Crank-Nicolson approximation used for the mass transfer equation has the smallest truncation error of any commonly used numerical approximation. This error is $O(\Delta\phi)^2 + O(\Delta\theta)^2$ for approximation of second order, diffusion-type, partial differential equations in one dimension. As previously mentioned this approximation is stable for all values of $\Delta\phi$ and $\Delta\theta$ with constant coefficients and a constant domain;

however, accuracy decreases with increasing increment size. The backward difference approximation provided a stable representation of the energy equation; however, it has no minimum truncation error (Smith, 1965). From these facts it is obvious improved accuracy can be obtained from the numerical solution, within the limit of computer round-off error, by reducing the increment sizes. The cost of improved accuracy is computation time. In the final analysis no presently available analytical stability investigation is highly definitive in complex models such as the one under consideration. The investigator is left with the practical method of trial solution of the model while varying increment size until an acceptable compromise between solution time and accuracy is obtained. Selection of appropriate increment sizes is discussed in Chapter V.

Numerical approximation of convective boundary conditions such as equations (3.5) are not stable for all values of $\Delta\theta$, the time increment. Also, the truncation error of the finite-difference equation for the convective boundary condition is of the order of $\Delta\phi$ which is, of course, larger than $O(\Delta\phi)^2$. Stability of the entire numerical solution depended upon stable numerical approximation of the convective boundary condition. This approximation is derived below and the maximum allowable dimensionless time step, $\Delta\theta$, was computed for a given dimensionless space increment. Considering the numerical approximation of the mass transfer surface boundary conditions:

$$\frac{\Delta\phi}{2} \left(\frac{eM_w}{RT} + \frac{\rho}{P_{sat}} \frac{dM}{dr} \right)_m^n \left(\frac{.75 P_m^{n+1} + .25 P_{m-1}^{n+1} - .75 P_m^n - .25 P_{m-1}^n}{\Delta\phi} \right) = \quad (3.22)$$

$$\frac{D_e}{2D} \left(\frac{P_{m-1}^{n+1} - P_m^{n+1}}{\Delta\phi} + \frac{P_{m-1}^n - P_m^n}{\Delta\phi} \right) - \frac{h_D s}{2D} \left(P_m^{n+1} + P_m^n - 2P_{va} \right)$$

Rearranging (3.22) into tridiagonal matrix form gave

$$\begin{aligned} P_{m-1}^{n+1} \left[.25 \left(\frac{eM_w}{RT} + \frac{\rho}{P_{sat}} \frac{dM}{dr} \right)_m^n - Z \right] + P_m^{n+1} \left[.75 \left(\frac{eM_w}{RT} + \frac{\rho}{P_{sat}} \frac{dM}{dr} \right)_m^n + Z + H \right] = \\ P_m^n \left[.25 \left(\frac{eM_w}{RT} + \frac{\rho}{P_{sat}} \frac{dM}{dr} \right)_m^n + Z \right] + P_m^n \left[.75 \left(\frac{eM_w}{RT} + \frac{\rho}{P_{sat}} \frac{dM}{dr} \right)_m^n - Z - H \right] \\ + 2P_a H, \end{aligned} \quad (3.23)$$

$$\text{where: } Z = \frac{D_e \Delta\theta}{D(\Delta\phi)^2} \quad \text{and} \quad H = \frac{h_D s \Delta\theta}{D \Delta\phi}.$$

Smith (1965) has shown equation (3.23) is stable provided the coefficient of $P_{v_m}^n$ is always positive. Then,

$$\Delta\theta \leq \frac{.75 \left(\frac{e M_w}{RT} + \frac{\rho}{P_{sat}} \frac{dM}{dr} \right)_m^n}{\frac{D_e^n}{D(\Delta\phi)^2} + \frac{h_D s}{D \Delta\phi}} \quad (3.24)$$

gives the relationship between $\Delta\phi$ and $\Delta\theta$ which satisfies stability requirements.

Sensitivity Analysis and Estimation of Model Parameters

A primary objective of this research was to use experimental atmospheric freeze-drying data and the mathematical model to obtain estimates of transport parameters for atmospheric freeze-drying in beef. The discussion of this section will be limited to the

mathematical basis of parameter estimation in nonlinear models and the associated subject of sensitivity analysis. The goal of sensitivity analysis is to predict what values of the independent variables correspond to conditions where the model is most sensitive to changes in the value of the parameters and, therefore, at what point the most useful data can be taken to evaluate a particular parameter.

The subject of parameter estimation in nonlinear models is relatively new. Few references are dated prior to 1960. Draper and Smith (1966) gave a one-chapter introductory coverage of the subject and provided a sizeable list of references. They pointed out three general methods are used for obtaining parameter estimates from nonlinear models. First, the method of linearization, which is presented later in this section, has been used by Beck (1966) and by Pfahl and Mitchell (1969) in parameter estimation from numerical solutions of models of partial differential equations in the field of heat transfer. Second is the method of steepest descent, which may have some advantages over the linearization (Gauss-Newton) method when the initial parameter estimates are considerably different from the final optimum estimates. The third (Marquardt's compromise) combines desirable features of both previous methods by using the method of steepest descent during early cycles of parameter improvement and gradually switching to the method of linearization. Marquardt's compromise has been written into a general computer routine, called GAUSHAUS, for parameter estimation in nonlinear models (Meeter, 1964). Use of this program is discussed in Chapter VI.

For the situation under consideration experimental data corresponding to the model solution were dimensionless mean moisture content as a function of dimensionless time. Solution to the model can be written in terms of the same variables,

$$\bar{M}(\theta, \underline{\beta}) = f + \int_f^1 \frac{M(\theta, \underline{\beta})}{M_o} d\phi, \quad (3.25)$$

where $\underline{\beta}$ is the parameter column matrix.

The observed data were represented as

$$Y_j = \bar{M}_j(\underline{\beta}) + \epsilon_j, \quad j = 1, 2, 3, \dots, L, \quad (3.26)$$

where ϵ_j was the random error of measurement associated with the (j)th experimental reading. The optimum values of the parameter matrix were determined by minimization of the deviation between the experimental data and the model according to some pre-selected criterion. For the proposed model the selected criterion was to minimize the sum of squared deviations. Based on this selection a risk function was defined as,

$$R(\underline{\beta}) = (\underline{Y} - \underline{\bar{M}}(\underline{\beta}))' \Psi^{-1} (\underline{Y} - \underline{\bar{M}}(\underline{\beta})), \quad (3.27)$$

where Ψ was the covariance matrix of the observations. It can be demonstrated that weighting the quadratic risk function with the inverse of the covariance matrix produces a minimum variance estimate of the parameter matrix (Deutsch, 1965). From a practical point of view it is probably impossible to know the value of all elements of the covariance matrix. If they were known it would be a large computational task to obtain the inverse since the matrix has L^2 elements; where L is the number of experimental

measurements. This difficulty is commonly circumvented by assuming the experimental data are independent observations. The assumption of independence implies zero covariance between two separate observations and reduces the covariance matrix to diagonal form. The matrix can then be easily inverted. The assumption of independence between any two experimental readings was made in the analysis presented herein.

Following previous derivations (Draper and Smith, 1966; Beck, 1969A), the minimum variance parameter vector was derived. The optimum value of the parameter vector exists when the gradient of the risk function is zero, that is, at the minimum of the risk function.

$$\nabla_{\beta} R(\beta) = 2(\nabla_{\beta} \bar{M}'(\beta)) \Psi^{-1} (\underline{Y} - \bar{M}(\beta)) = 0 \quad (3.28)$$

By expanding the expression for the model in Taylor series and retaining only the first two terms, the model was written as

$$\bar{M}(\beta) = \bar{M}(\beta_0) + \underline{S}(\beta_0)(\beta - \beta_0) \quad (3.29)$$

where: $\underline{S}(\beta_0) = \nabla_{\beta} \bar{M}(\beta) |_{\beta_0}$.

The expressions represented by $\underline{S}(\beta_0)$ are called sensitivity coefficients. Their magnitude indicated how sensitive the model was with respect to a given parameter at a particular value of the independent variable, dimensionless time. Substitution of equation (3.29) into (3.28) and rearranging gave

$$\underline{S}'(\beta_0) \Psi^{-1} \underline{Y} - \underline{S}'(\beta_0) \Psi^{-1} \left[\bar{M}(\beta_0) + \underline{S}(\beta_0)(\beta - \beta_0) \right] = 0. \quad (3.30)$$

Solving for β , the improved estimate of the parameter matrix, gave

$$\underline{\beta} - \underline{\beta}_0 = \left[\underline{S}'(\underline{\beta}_0) \underline{\Psi}^{-1} \underline{S}(\underline{\beta}_0) \right]^{-1} \underline{S}'(\underline{\beta}_0) \underline{\Psi}^{-1} (\underline{Y} - \underline{M}(\underline{\beta}_0)). \quad (3.31)$$

Repeated calculation by reinserting $\underline{\beta}$ into (3.31) as $\underline{\beta}_0$ led to a further refined parameter matrix. This procedure was repeated until some minimum change in any element of the parameter matrix was not exceeded. Alternately, computation could have been terminated if some preselected change in the total sum of squared deviations between the data and the model was not exceeded.

Whether or not the calculations suggested by equation (3.31) yield accurate estimates of all elements of the parameter matrix simultaneously, or whether the equation even exists depends upon the sensitivity coefficients. Inspection of equation (3.31) shows the answer to both questions is found by analysis of the matrix

$$\underline{N} = \underline{S}'(\underline{\beta}_0) \underline{\Psi}^{-1} \underline{S}(\underline{\beta}_0). \quad (3.32)$$

If the determinant of \underline{N} is zero the matrix is singular and the right side of equation (3.31) does not exist. The magnitude of the determinant of \underline{N} is dependent upon the values of the sensitivity coefficients. If any combination of the sensitivity coefficients of the parameters are linearly dependent two or more columns of \underline{N} are identical and \underline{N} is singular. Further discussion of this point is presented in the next chapter.

Values of the sensitivity coefficients as functions of the independent variable, dimensionless time, were computed from the numerical solution of the mathematical model.

$$S_{ij} = \frac{\partial \bar{M}(\theta_j, \underline{\beta})}{\partial \beta_i} = \frac{\bar{M}(\theta_j, \beta_i(1+\delta), \beta_{\neq i}) - \bar{M}(\theta_j, \underline{\beta})}{\delta \beta_i} \quad (3.33)$$

where: δ was a small number such as .01,

$i = 1, 2,$ or 3 ; the number of parameters in the model and

$\theta = j\Delta\theta$.

Use of the sensitivity equations as computed by equation (3.33)

in design of experiments is discussed in the next chapter.

CHAPTER IV
EXPERIMENTAL DESIGN AND PROCEDURES

Experimental design may be considered as two subjects when applied to problems of estimating physical parameters in mathematical models of biological processes. One type of experimental design makes use of the sensitivity coefficients derived in the previous chapter. The sensitivity coefficients can be used to define an optimum experiment for producing data to estimate the model parameters. An experiment can be optimum in the sense that data obtained from it will yield least variable estimates of the model parameters, provided the mathematical model is correct. The sensitivity coefficients may also be used to determine if all of the parameters can be simultaneously estimated, if nonuniform weighting of the data is desirable or necessary, and how accurately the parameters can be estimated.

Experimental design also refers to the concept of random selection and assignment of experimental units to the various test conditions. Random selection of test samples is especially important in studies such as the current research. Almost invariably the complexity of biological systems exceeds the ability of the investigator to explain all of the possible variables in mathematical terms. Therefore, relatively minor variables are omitted from the model or are assumed to be constant. Random selection of samples from a relatively large population of similar samples allows

statistical analysis of the results to minimize the effects of external and uncontrolled variables.

Experimental Design: Sensitivity Analysis

The mathematical model presented in Chapter III contains two internal transport parameters to be estimated from experimental data which are functions of the structure and composition of the product. These parameters are effective thermal conductivity of the porous zone, k , and the structural constant, C_2 , in the effective mass transfer coefficient.

The most accurate data for estimating a particular parameter are obtained under experimental conditions which maximize the sensitivity of the dependent variable to the parameter of interest. In freeze-drying heat and water vapor must be transferred through both internal and external transfer resistances. Since internal transport parameters were of primary interest, the optimum experiment was one which caused the dependent variable, dimensionless mean moisture content, to be dependent on internal transport resistances. This was accomplished by minimizing external resistances to heat and water vapor transfer. Therefore, the optimum atmospheric freeze-drying experiment for estimating internal transfer parameters was conducted with maximum possible air flow over the sample surface. The upper limit on air flow rate in the current research was dictated by experimental equipment limitations.

If sufficient air velocity over the sample could have been used to assure the surface transfer coefficients to be effectively infinite relative to the internal transfer coefficients, the external parameters could have been neglected, and, in turn, the surface

boundary conditions for the mathematical model would have been simplified. Calculations based on the Reynold's analogy for a flat plate indicated a dimensionless ratio of external to internal mass transfer coefficients of approximately ten for the air velocity used. This value was not sufficiently large to warrant neglecting the surface mass transfer parameter, h_D ; thus, it was included with the internal parameters to be evaluated from the data. The surface heat transfer coefficient, h , was not required since surface temperature was monitored experimentally and used in the numerical solution as a boundary condition.

By assuming the proposed mathematical model accurately simulated the process in question, the numerical solution of the model was used to compute sensitivity coefficients as a function of elapsed time for each of the three unknown parameters. Figure 4.1A shows the absolute value of dimensionless sensitivity coefficients for each parameter for typical test conditions at .97 atmosphere total pressure (the approximate atmospheric pressure at East Lansing, Michigan). Similiar results for a total pressure of .58 atmosphere are shown in Figure 4.1B. Sensitivity coefficients in Figures 4.1A and 4.1B were computed for a sample half-thickness of .45 cm and air temperature of -2.8°C . Values of the unknown parameters were estimated at $.012 \text{ gm/cm}^2\text{-sec-atm}$ for h_D , .8 for C_2 and $.00015 \text{ cal/sec-cm-}^{\circ}\text{C}$ for k .

The magnitude of the dimensionless sensitivity coefficient for C_2 , $S_{C_2}^*$, increased monotonically with elapsed time until the ice-vapor interface reached the centerline. At this time free ice no longer existed in the sample, and the boundary condition at the

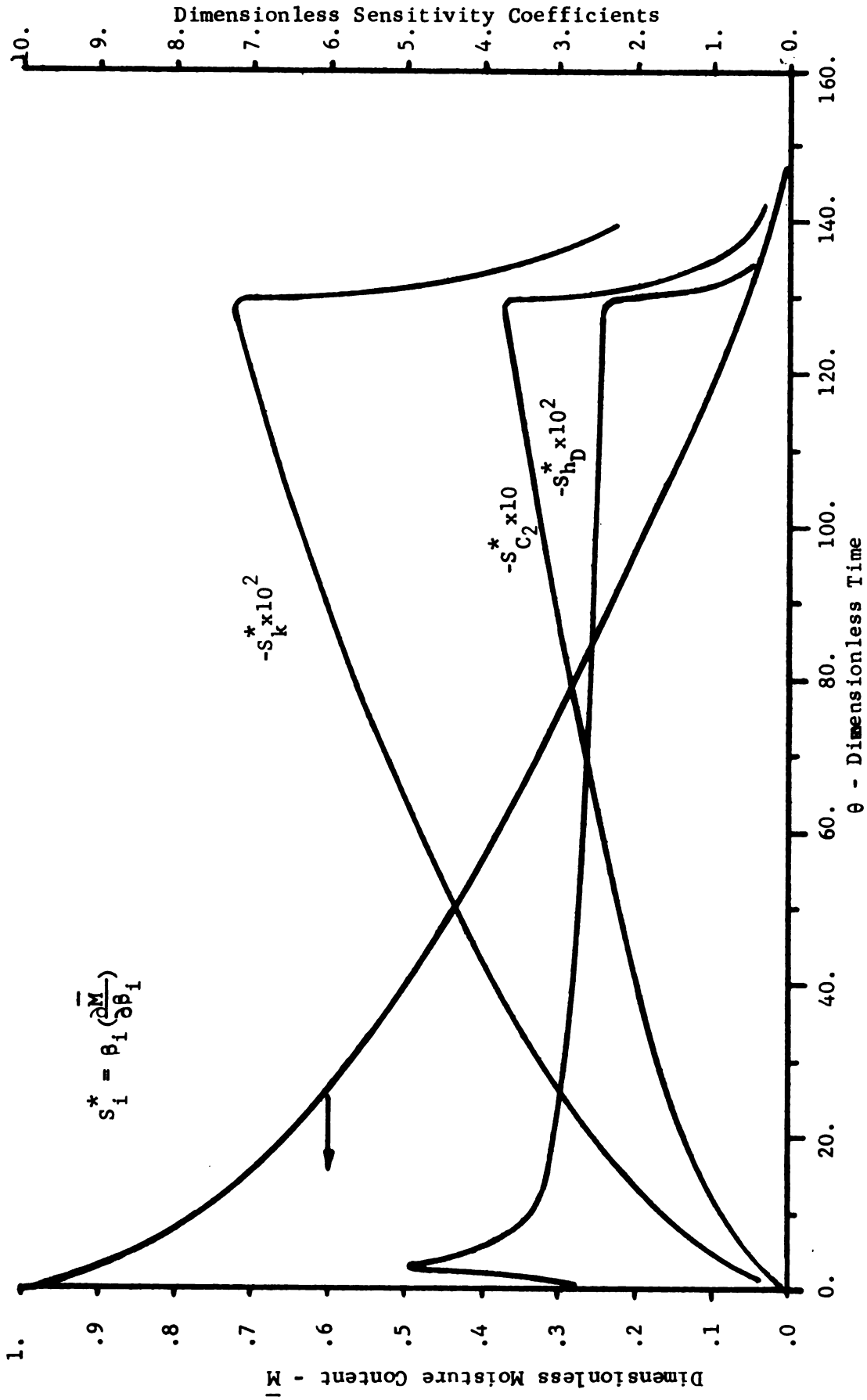


Figure 4.1A. Dimensionless Sensitivity Coefficients of Unknown Parameters for Freeze-Drying at .97 Atmosphere Pressure.

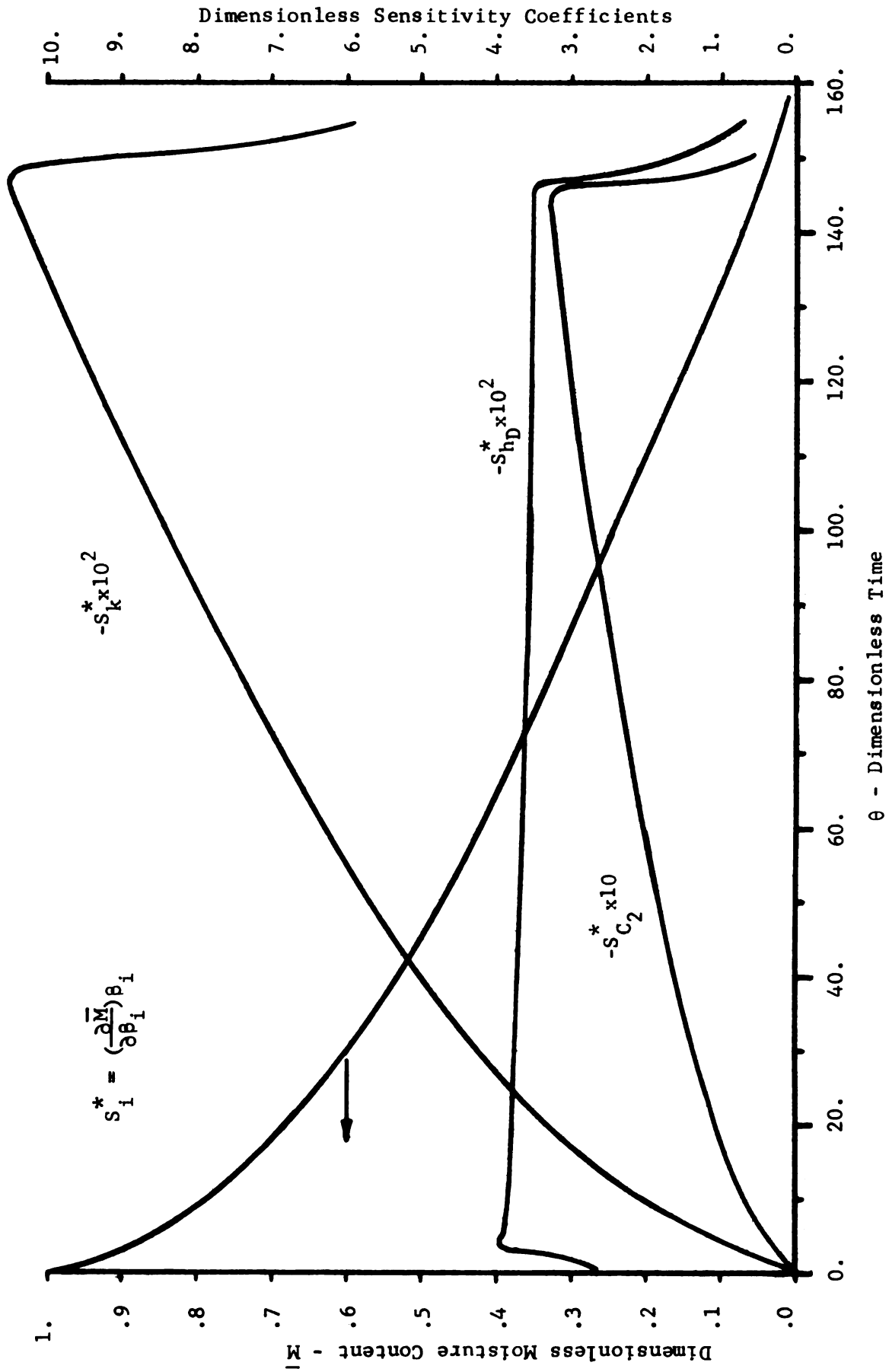


Figure 4.1B. Dimensionless Sensitivity Coefficients of Unknown Parameters for Freeze-Drying at .58 Atmosphere Pressure.

centerline abruptly changed from a saturated temperature and vapor pressure condition to an adiabatic condition. Change in the boundary condition caused an immediate drop in the magnitude of all sensitivity coefficients. They all decreased to zero as the sample reached equilibrium.

The magnitude of $S_{h_D}^*$ increased rapidly to a peak early in the drying process at both pressure levels. It then declined slowly to a nearly constant value while most of the free ice was removed from the sample. Absolute value of $S_{h_D}^*$ was approximately one order of magnitude less than $S_{C_2}^*$ over most of the drying time.

The sensitivity coefficient for effective thermal conductivity, S_k^* , also increased until all free moisture had been removed; however, the magnitude of S_k^* was approximately one-fifth that of $S_{C_2}^*$ throughout most of the process. This difference in magnitude indicated freeze-drying is mass transfer controlled at both pressure levels considered. Decreasing the system pressure increased the effective mass diffusivity while the effective thermal conductivity remained relatively constant. This caused the process to shift in the direction of heat transfer control with a corresponding increase in S_k^* and a decrease in $S_{C_2}^*$. These results can be noted in Figures 4.1A and 4.1B by comparing the coefficient magnitudes between the two figures at the same dimensionless time. Further reduction in system pressure to the range of conventional vacuum freeze-drying would have caused the process to be almost totally heat transfer controlled. The process would then have been relatively more sensitive to the heat transfer parameter, k , and less sensitive to C_2 . The magnitude

of S_k^* would then have been greater than $S_{C_2}^*$. This discussion illustrates that no single experiment can be designed to simultaneously maximize the sensitivity coefficients of both heat and mass transfer parameters. Thus an experiment cannot be the optimum experiment for estimating both heat and mass transfer parameters at the same time.

Another potential difficulty in simultaneously obtaining accurate estimates of k and C_2 is the proportional relationship that seems to exist between S_k^* and $S_{C_2}^*$ in both Figure 4.1A and 4.1B. Perfect linear dependence between the two sensitivity coefficients would cause \underline{N} to be singular and prevent simultaneous estimation of any combination of parameters which included both k and C_2 . To further assess the seriousness of the near linear dependence of S_k^* and $S_{C_2}^*$ the risk function of the experimental data obtained in test number 4 (See Appendix V) was plotted over the domain of k and C_2 in the vicinity of the minimum computed by the nonlinear estimation procedure. The surface mass transfer coefficient was held constant at the estimated value, $.0116 \text{ gm/cm}^2\text{-sec-atm}$. Contour lines of the risk function surface in the vicinity of the computed minimum are shown in Figure 4.2. These results indicated a single minimum does exist and confirmed that S_k^* and $S_{C_2}^*$ are not perfectly linearly dependent. Nonlinear estimation of all three parameters was possible but the distended nature of the contours of the risk function surface indicated limited accuracy in the computed estimates of k .

Magnitude of the sensitivity coefficients indicated how accurately the corresponding parameter could be estimated for a

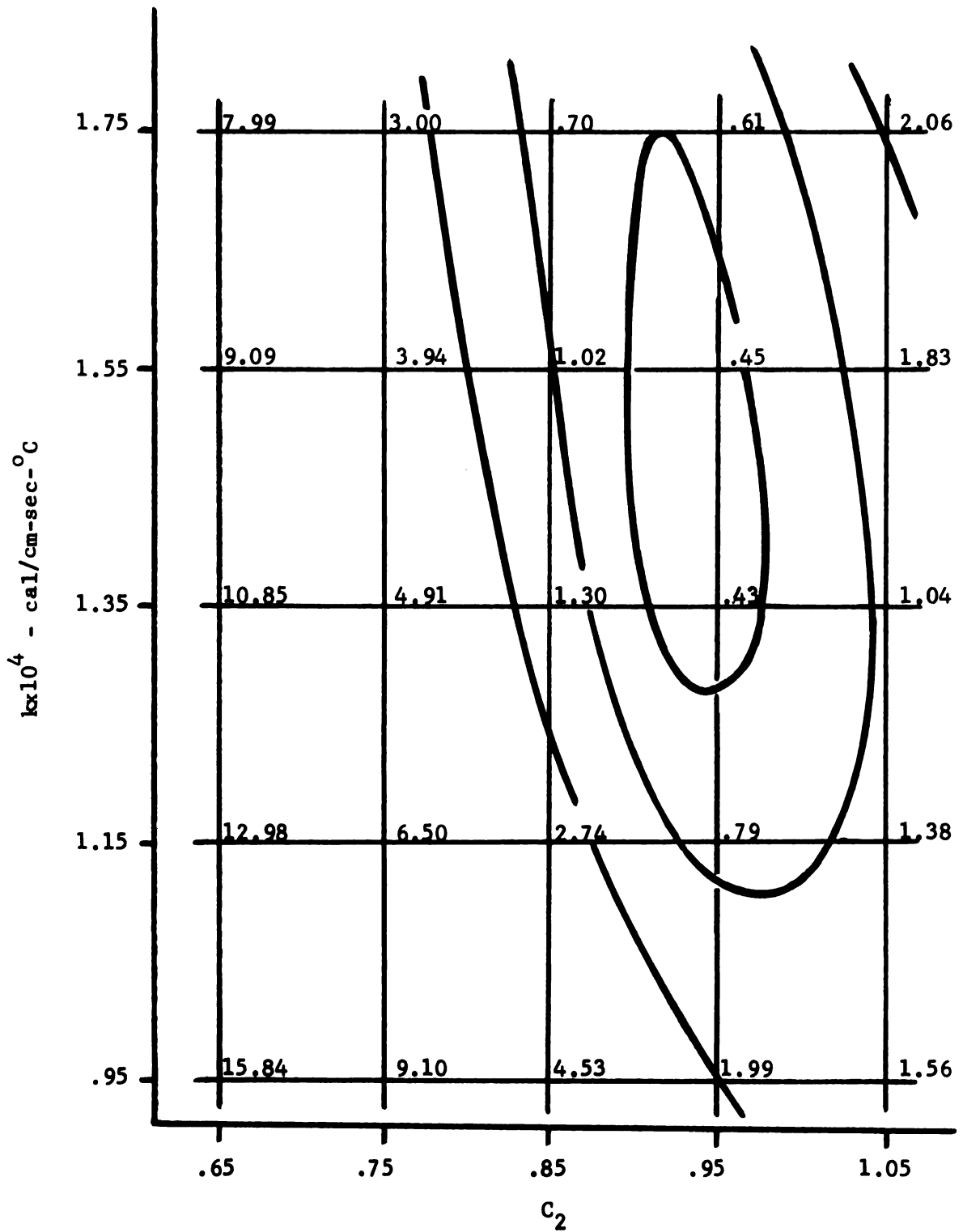


Figure 4.2. Contours of the Risk-Function Surface in the Vicinity of the Computed Minimum.

given level of accuracy in determining the dependent variable. The dependent variable, dimensionless mean moisture content, was determined from sample weight which was read from a scale with minimum divisions of .05 mm. Associated with this reading was a spring constant of .0243 gm/mm. Therefore, sample weight was determined to approximately .001 gm. Initial sample weight was approximately one gram. Accuracy of the parameter estimates was approximated from the average magnitude of the respective sensitivity coefficients shown in Figure 4.1A. Rearrangement of the dimensionless sensitivity coefficients gave the minimum detectable error in the parameter for a given average magnitude of the sensitivity coefficient.

$$c_2 \left(\frac{\Delta \bar{M}}{\Delta C_2} \right) = .2, \text{ then } \frac{\Delta C_2}{C_2} = \frac{.001}{.2} = .005$$

$$k \left(\frac{\Delta \bar{M}}{\Delta k} \right) = .05, \text{ then } \frac{\Delta k}{k} = \frac{.001}{.05} = .02$$

$$h_D \left(\frac{\Delta \bar{M}}{\Delta h_D} \right) = .03, \text{ then } \frac{\Delta h_D}{h_D} = \frac{.001}{.03} = .03$$

These results indicated all parameters could be estimated to within a maximum of three percent of their true value.

Finally, the sensitivity coefficients of Figures 4.1A and 4.1B could be used to weight the experimental data so that data taken when a particular sensitivity coefficient was maximum were given more weight in determining the parameter values than data taken when the sensitivity coefficient was smaller. Due to the relatively uniform values of the coefficients for the parameters of the proposed model it was decided that nonuniform weighting of

the data was not necessary.

Preparation and Assignment of Samples

Experimental samples were prepared from the loin eye muscle of beef, longissimus dorsi. A section of the muscle, grade U.S.D.A. Choice, was obtained from MSU Food Stores and roasted at 163°C until the temperature at the center of mass reached 74°C . Average composition of 10 samples of the cooked beef was 9.8% fat (ether extract) with a moisture content of 150% d.b. The cooked meat was then frozen at -29°C and later cut into approximately one-centimeter cubes with an electric band saw. Special effort was made when cutting the cubes to align the natural fibers of the meat with the planes of the cube. The cubes were wrapped in foil and stored at -29°C in a sealed container until needed for a test. Cubes in which the fibers of the meat projected at an oblique angle to the faces of the cube were discarded. From the remaining population cubes were assigned randomly to a particular set of test conditions.

Selection of Test Conditions

Conditions under which experimental data were to be obtained were selected to investigate the practical operating space of atmospheric freeze-drying in precooked beef and to adequately test the proposed mathematical model. As cited in Chapter II, previous investigators have found atmospheric freeze-drying rates are greatly accelerated by small increases in air temperature over the range from -20°C to zero $^{\circ}\text{C}$ (Woodward, 1961; Lewin and Maletes, 1962). Preliminary tests conducted in the current research indicated significant product shrinkage in beef dried with air temperatures

above zero °C. Calculation of the amount of unfrozen water in beef from apparent specific heat data indicated a large change of unfrozen water per unit change in product temperature in the range from -10°C to zero °C (Hohner and Heldman, 1970). Presumably the mechanism of moisture transfer during dehydration and qualitative factors in the dehydrated product may be significantly altered by the amount of unfrozen water present in the product during drying. These considerations and the fact that sublimation is exceedingly slow at temperatures below -10°C led to selection of two levels of air temperature, -2.8°C and -8.2°C.

Woodward (1961) has also shown that practical applications of atmospheric freeze-drying in foods are limited to small sample sizes. All drying results reported herein were obtained in samples approximately one-centimeter thick.

By definition, atmospheric freeze-drying is conducted at or near one atmosphere pressure. Nevertheless, for purposes of adequately testing the proposed mathematical model, data were obtained at two levels of total pressure, .97 atmosphere and .58 atmosphere. Data by Harper (1962) indicate the value of effective thermal conductivity in freeze-dried beef is the same for both of these pressure levels, approximately 1.5×10^{-4} cal/cm-sec-°C. From the discussion of Chapter III related to simplification of the effective mass transfer expression, it may be noted that the model predicts vapor diffusion is still the predominate mechanism of transport at .58 atmosphere; however, the effective mass transfer coefficient is inversely related to system pressure.

Estimation of C_2 from data obtained at both pressure levels represented a strenuous test of the validity of the model. The model assumed this parameter was a function of the structure of the product only and not of system pressure; therefore, C_2 should be estimated as the same value at both pressure levels. The same is true for thermal conductivity.

Finally, because of the prominent natural fiber structure of beef it was assumed that heat and mass transfer rates might be different for transport perpendicular to, as opposed to parallel to, the fiber structure. Therefore, both orientations were investigated. Three repetitions of each of six combinations of the above variables were conducted.

Experimental Apparatus and Procedures: Equilibrium Studies

As discussed previously in Chapters II and III, some fraction of the total moisture in beef is adsorbed on the non-aqueous fraction of the product by various types of bonding and is not removed by sublimation (Ngoddy, 1969). The specific amount of adsorbed moisture in equilibrium with various temperature and relative humidity conditions was required for accurate computer simulation of atmospheric freeze-drying. The experimental apparatus described in the following paragraphs was assembled to obtain the necessary equilibrium moisture isotherm data.

The experimental device, shown schematically in Figure 4.3, was capable of subjecting a sample of freeze-dried beef to an atmosphere of pure water vapor over ice at controlled temperatures. The device consisted of a modified mass sorption spring balance (Worden Quartz Products, Inc., Model 4401) connected through a

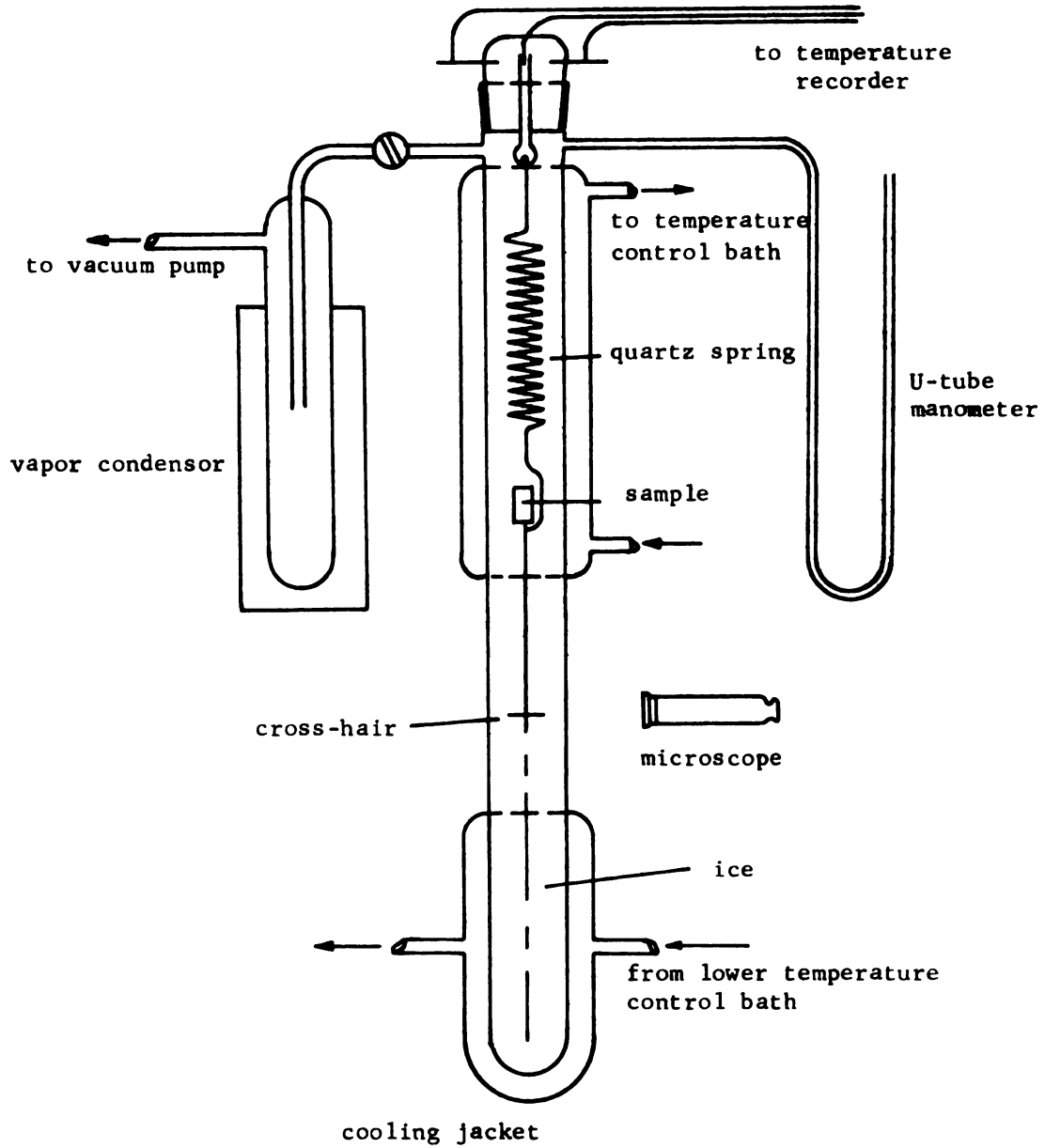


Figure 4.3. Schematic Drawing of Experimental Apparatus for Equilibrium Moisture Content Studies.

vapor condensor to a vacuum pump (Welch, Model 1400). The vapor condensor was cooled with a mixture of solid carbon dioxide and acetone to prevent water vapor from entering the vacuum pump. The freeze-dried beef sample was mounted on a nichrome wire hook suspended on a quartz spring inside the upper jacketed part of the vertical glass test cylinder.

The upper jacket was connected by Tygon tubing to a heat exchanger located in a constant temperature chamber. The coolant, fifty percent ethylene glycol-water solution, was pumped through the jacket and heat exchanger by a 1/15-horsepower centrifugal pump. The lower jacket, surrounding the ice, was controlled separately by a constant temperature bath (American Instrument Co., Model 4-8600) containing a built-in 1/30-horsepower pump. The upper end of the vertical cylinder was connected to a mercury manometer.

The top of the mass sorption balance was sealed with a glass cap through which four tungsten probes had been placed to facilitate reading thermocouples inside the cylinder. Copper-constantan thermocouples were located near the sample in the area surrounded by the upper temperature control jacket and on the ice surface near the bottom of the cylinder. Thermocouples were read alternately on 30-second intervals by a recording potentiometer (Brown Division, Honeywell Inc., Model 153X65P12-X-2F). Temperature range of the recorder was -40°C to 60°C with a minimum readable division of approximately $.2^{\circ}\text{C}$. The temperature control equipment could control both jacketed areas to approximately $\pm .3^{\circ}\text{C}$ of the respective settings.

The amount of moisture adsorbed or desorbed by the sample was determined from the position of a cross-hair on a quartz fiber which was suspended below the sample so the cross-hair was visible between the two temperature control jackets. Position of the cross-hair was determined by sighting through the glass cylinder wall with a 10X ocular microscope (Nikken, No. 39837) with a readability of .01 mm. The quartz spring had an extension constant of .0243 gms/mm with a maximum load of five grams.

Approximately .2 gm samples of freeze-dried beef were mounted on the nichrome hook. The stopcock and upper cap were lightly coated with Apezion vacuum seal grease and turned into place. The cylinder was evacuated with the vacuum pump until the manometer recorded only the vapor pressure of ice at the prevailing temperature. The stopcock was then turned isolating the cylinder. Final adjustments were made on the two temperature control units to reach the desired condition, and the system was allowed to equilibrate.

For a given isotherm the upper jacket temperature (which controlled the sample temperature) was left unchanged at the isotherm temperature. The lower jacket was set at a temperature corresponding to the desired vapor pressure, the sample was allowed to equilibrate, and a reading of spring deflection was recorded. The lower jacket temperature setting was then changed to correspond to a new vapor pressure, and the process was repeated.

Only desorption equilibrium moisture data were required, so that sample was first equilibrated to saturated vapor pressure conditions. The relative humidity of the water vapor surrounding

the sample was then lowered stepwise to give approximately seven data points over the entire relative humidity range. The lowest ice temperature which could be attained was -26°C . This temperature established the corresponding lower limit to the water vapor pressure which could be reached.

Experimental Apparatus and Procedures: Rate Studies

Atmospheric freeze-drying rate studies were conducted in a modification of the apparatus described in the previous section. A schematic drawing on the modified apparatus is shown in Figure 4.4. The lower end of the vertical cylinder was extended approximately 60 cm to assist in obtaining laminar flow of air over the sample. Also, the lower cooling jacket was removed, and a cartesian manostat (Manostat Corp., Model 7A) was installed between the vapor condensor and the vacuum pump. The manostat controlled the total pressure in the cylinder to approximately plus or minus one millimeter Hg of the desired value when operating at pressures below one atmosphere.

Air was circulated upward through the test chamber, then through a 6-cm by 25-cm cylinder of silica gel to remove water vapor from the air. From the desiccator air was pumped through a heat exchanger submerged in the Amico constant temperature bath and back to the lower end of the vertical cylinder. The heat exchanger consisted of fifty feet of 3/8-inch I.D. copper tubing. Connections between the various components were made with 3/8-inch thick-walled Tygon tubing clamped at each end. The entire air circuit excluding the heat exchanger was insulated with 3/8-inch thick refrigeration insulation (Armstrong, Armaflex).

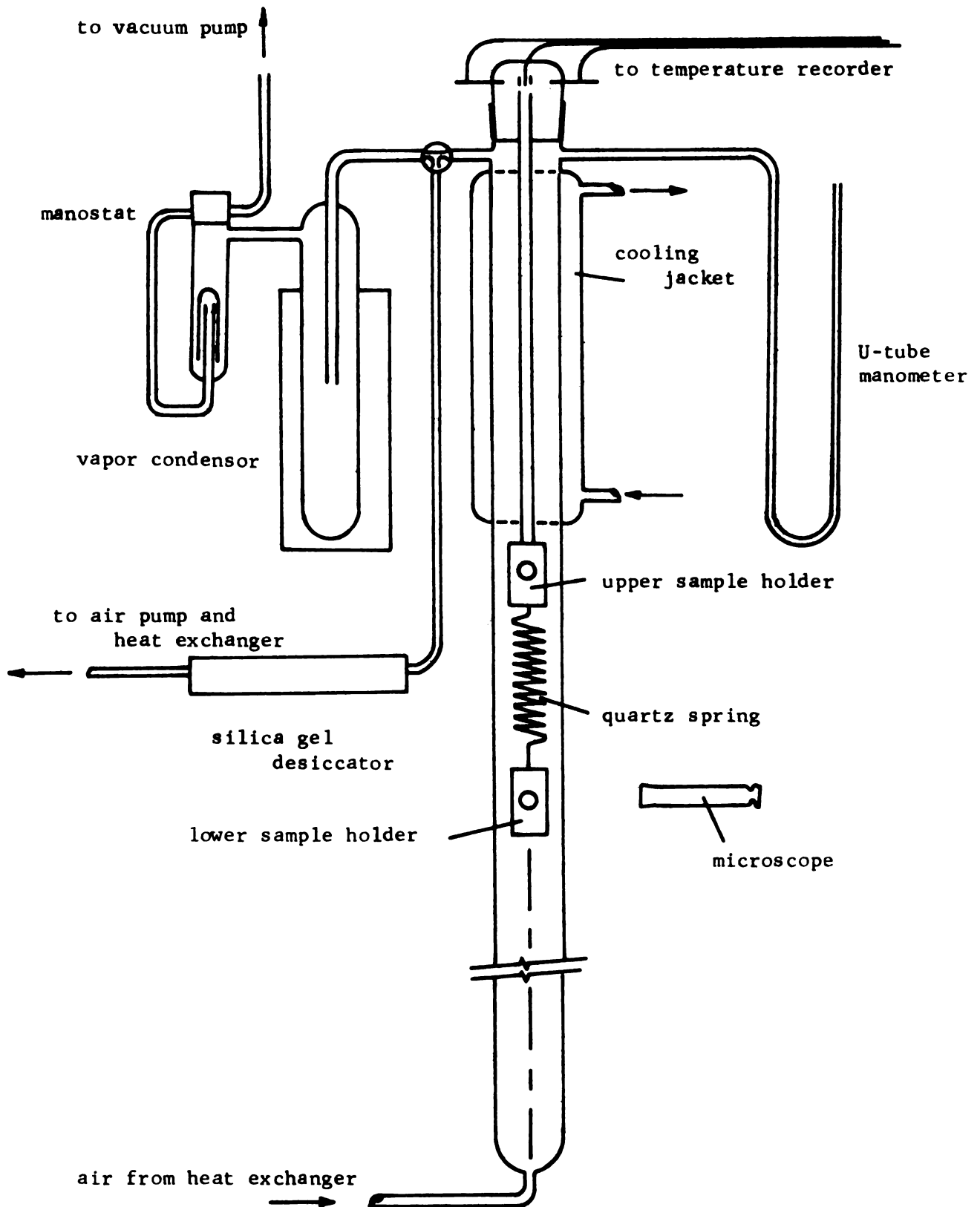


Figure 4.4. Schematic Drawing of Experimental Apparatus for Atmospheric Freeze-Drying Rate Studies

The sample holder used in the rate studies is shown schematically in Figure 4.5. Due to sensitivity of the spring it was impossible to attach thermocouples to the sample being weighed. For this reason two sample holders, oriented one above the other, were used. The lower sample holder was suspended from the upper holder by the quartz spring. Surface temperature and temperature of the frozen core were monitored by fine wire copper-constantan thermocouples in the upper sample. The upper sample holder was attached rigidly to a glass rod connected to the cap which sealed the upper end of the test chamber. Air temperature was measured just below the upper sample holder. Surface temperature, ice-core temperature, and air temperature were recorded in order on 30-second intervals using the same recording potentiometer described in the previous section.

Atmospheric freeze-drying tests were conducted in samples of the shape of a finite cylinder cut from frozen beef cubes described in an earlier section of this chapter. An eight-millimeter diameter sharpened cork cutter was used to cut finite cylinders from the precut cubes. The radial surface of the cylindrical sample was sealed with saran film glued to the sample with Duco cement. The cylindrical sample was then mounted in a styrafoam sample holder as shown in Figure 4.5 such that the radial surface was thermally insulated. Thickness of the sample was trimmed to match the holder thickness (approximately one cm). Heat and mass transport were effectively one dimensional through the ends of the sample cylinder. Natural grain of the meat was oriented either parallel to or perpendicular to the ends of the cylinder at the time of sample

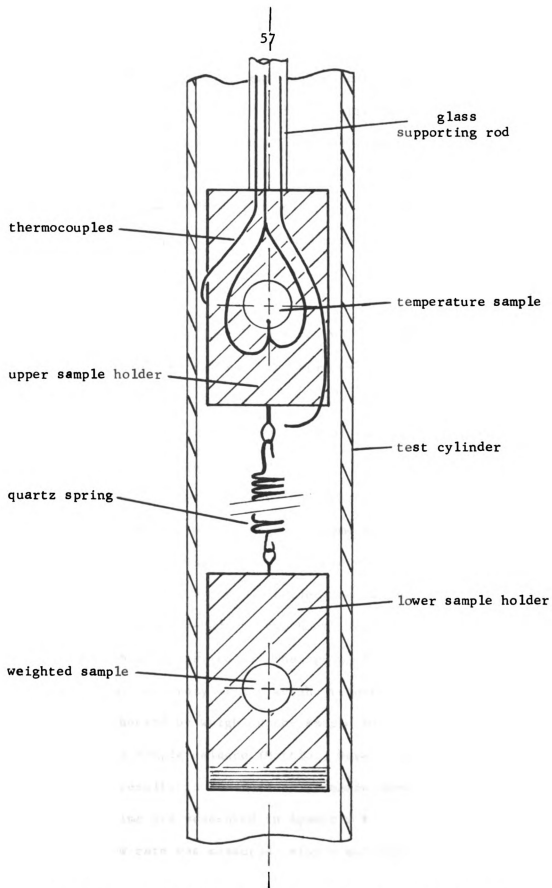


Figure 4.5. Sample Holders, Spring and Thermocouple Assembly for Drying Rate Studies.

preparation as required by the particular test conditions.

Effectiveness of the vapor seal in preventing radial mass transfer was tested by atmospherically freeze-drying several samples approximately one-half way through the complete process. The samples were removed from the holder and the vapor seal was removed. The ice-vapor interface was distinctly visible on the radial surface indicating little or no sublimation had taken place from this surface.

Prior to placing the samples in the test chamber the system was equilibrated to the desired test temperature. At the start of each test the silica gel in the desiccation cylinder was replaced. Used silica gel was regenerated by being placed in a drying oven at 100°C for not less than three days.

Sample weight was monitored throughout a test by measuring extension of the quartz spring with the same microscope as previously described. Spring deflections were measured to the nearest .05 mm during drying rate tests. Deflection readings were taken on intervals of from one-half to two hours such that 15 to 50 readings were obtained per test. The spring extension constant was .0243 gm/mm. Accuracy of the weight recorded from spring deflections was checked by weighing the sample before and after each drying test on a sample balance (Mettler, Serial no. 222912). Test conditions and results in the form of dimensionless weight versus dimensionless time are presented in Appendix V.

Air flow rate was measured using a vertical tube flowmeter inserted in the air circuit between the pump and the heat exchanger. Mean air velocity over the sample was computed to be

approximately .45 meter/sec. Because of excessive air pressure drop across the flow meter the meter was removed from the air circuit during a test. Therefore, air flow during a test was somewhat greater than .45 meter/sec.

Zero moisture content in any biological product is difficult to define and much harder to measure. This difficulty is caused by various types of bonding between the moisture and other components of the product. Throughout the current research this problem was circumvented by defining the dry, moisture-free, state to be that level of moisture content reached by freeze-dried beef in equilibrium with silica gel at -17.8°C . All test samples were equilibrated to this moisture content after atmospheric freeze-drying. The defined zero moisture content corresponds approximately to the same level reached by drying oven determinations, but does not damage the sample by subjecting it to high temperatures for extended periods of time.

CHAPTER V

THE NUMERICAL SOLUTION

The nature of numerical solutions of complex mathematical models is such that the investigator faces numerous decisions on points of competition between completeness, accuracy, stability, and computation time of the model. The various compromises and decisions made with regard to the proposed model are discussed in this chapter. The numerical representation of the mathematical model derived in Chapter III was solved with computer subroutine MODEL listed in Appendix IV. The computer program required explicit evaluation of several functional relationships and physical constants which appear in the model. These evaluations are discussed in this chapter. Last, qualitative results are presented to support the hypothesis that the proposed model is an adequate representation of atmospheric freeze-drying.

The most important functional relationship required for the numerical solution was the equilibrium moisture content of freeze-dried beef. The mathematical model, as derived in Chapter III, assumed adsorbed moisture in the porous zone was in equilibrium with the air-water vapor mixture in the pores. Equilibrium adsorbed moisture in freeze-dried beef was determined using the apparatus and procedures described in Chapter IV. Results of these tests are presented in Figure 5.1 as a function of the relative humidity of

the water vapor. Other investigators (Saravacos and Stinchfield, 1965) have obtained adsorption isotherms in freeze-dried beef for temperatures below zero °C. Adsorption data by these investigators are presented in Figure 5.1 as a dashed line.

It is of particular interest to note that equilibrium moisture contents obtained in separate investigations are in excellent agreement at the saturation condition. Adsorption and desorption data are not expected to agree over all of the relative humidity range due to sorption hysteresis commonly found in biological products. As demonstrated by results presented in Figure 5.1, variations in equilibrium moisture content with temperature below zero °C. are small. Advantage was taken of this fact in derivation of the model. The variation in equilibrium moisture content with respect to temperature was considered negligible when compared to variation with respect to relative humidity of the water vapor.

The derivative of equilibrium moisture content with respect to relative humidity was required in the mathematical model. Inspection of Figure 5.1 shows the average value of the derivative for the desorption isotherm to be approximately .2. That is, $\Delta M/\Delta r \approx .2$. Deviation from this average value is significant above a relative humidity of .5; however, attempts to fit the desorption isotherm or its derivative with various expressions failed to produce sufficiently accurate results to allow a stable numerical solution of the model. Therefore, the derivative of equilibrium moisture content with respect to relative humidity was approximated as the mean value of the derivative, namely, .2.

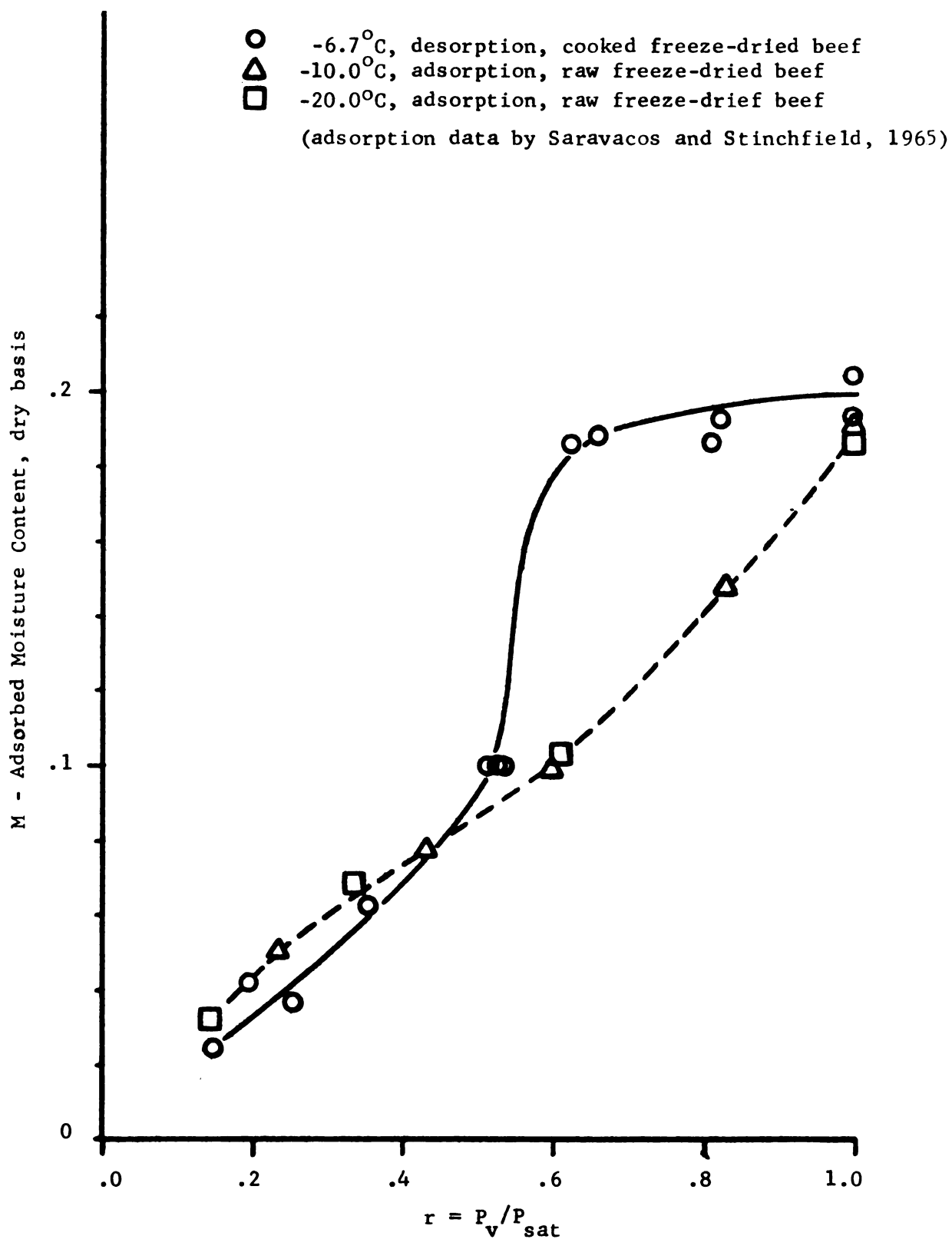


Figure 5.1. Equilibrium Moisture Isotherms of Freeze-Dried Beef Below Zero °C.

The total amount of adsorbed moisture present in the porous layer was important to accurate analysis of the freeze-drying process. Previous mathematical models of freeze-drying have neglected adsorbed moisture altogether (Sandall, et al., 1967; Dyer and Sunderland, 1968). Figure 5.1 shows that approximately $.2 \text{ gm-H}_2\text{O/gm-solid}$ exists in the porous zone in equilibrium with the ice interface. This is approximately 10-15 percent of the initial moisture content. In addition, the amount of heat required for desorption of this moisture increases as the moisture content decreases. Ngoddy (1969) has evaluated the heat of sorption for freeze-dried beef as a function of adsorbed moisture content. Above an adsorbed moisture content of approximately $.2 \text{ gm-H}_2\text{O/gm-solid}$ the heat of sorption is nearly constant at the value for free water vaporization. Below that moisture level the required heat of vaporization increases rapidly due to increasingly stronger bonding of the remaining water to nonaqueous components of the product. Since a gradient of adsorbed moisture remained in the porous zone when sublimation of free moisture was complete, neglecting the adsorbed moisture could be expected to have significant effect on the total drying time predicted by the model.

The saturated pressure of water vapor as a function of temperature was also required in the numerical solution. This expression was obtained by fitting a third degree polynomial to saturated vapor pressure data over the temperature range from -30°C to zero $^\circ\text{C}$. Values of the vapor pressure over ice were obtained from Threlkeld (1962). Coefficients of the polynomial were evaluated by minimizing the sum of squared deviations from

the data. Maximum absolute deviation of the polynomial was within three percent of the data over the temperature range of interest.

Various physical parameters which were assumed constant in the model also required evaluation. The constant numerical values used in the solution and the source of information are listed in Table 5.1.

The computer solution required the sample surface temperature as a known input. This temperature as well as the ice core temperature and air temperature were monitored during tests performed to collect parameter estimation data. For atmospheric freeze-drying it was found that the surface temperature remained nearly constant within one-half °C of the air temperature. Therefore, surface temperature was entered in the computer program as a constant value.

TABLE 5.1. Numerical Values of Physical Constants Used in the Mathematical Model

Constant	Value	Source
Bulk density of dry product, ρ	.46 gm/cm ³	Mean value of experimental measurements
Specific heat of dry product, C_{pd}	.38 cal/gm-°C	Computed from specific heat of frozen beef at -40°C (Short and Staph, 1951)
Specific heat of ice core, C_{pc}	1.15 cal/gm-°C	Riedel (1957)
Porosity of dry product, e	.76	Harper (1962)
Mutual diffusivity, air and water vapor, 1 atm, zero °C, D	.22 cm ² /sec	Perry (1963)
Heat of sublimation, ΔH_s	676 cal/gm	Threlkeld (1962)
Initial moisture content, M_o	approx, 1.5 d.b.	Measured for each test
Half-thickness of sample, s	approx. .45 cm	Measured for each test

If the computer subroutine, MODEL, were used to analyze data obtained in vacuum freeze-drying it would be expected that the surface temperature would vary with time. In this case values of surface temperature experimentally measured on some time increment could be stored in common storage by program MAIN much the same as experimental values of dimensionless mean moisture content and time were stored (See Appendix IV for listing of program MAIN). The surface temperatures could be used in subroutine MODEL as a boundary condition on the energy equation.

Solution of finite-difference equations to accurately approximate the partial differential equations from which they were written required careful selection of the incremental step size in the independent variables. There are two independent variables in the proposed model: dimensionless time and dimensionless distance. Size of the increment in dimensionless distance, $\Delta\phi$, was selected by repeatedly solving the model while varying the size of the increment. An increment of .1 gave three significant figures in the dependent variable (dimensionless mean moisture content) when compared to the solution obtained with an increment of .05. This level of accuracy was equal to the accuracy of experimentally determined dependent variables, so a distance increment of .1 was selected.

The maximum time step, $\Delta\theta$, compatible with stability of the convective mass transfer boundary condition was computed internally in computer subroutine MODEL using the inequality of equation (3.23). The computed time increment was approximately 40 seconds, real time. Computation time for one step in real time on the CDC-3600 computer

varied depending on the number of nodes in the numerical solution at any given time. Average simulation speed for solving the entire model was approximately 60 hours per minute of computer time.

Difficulty was encountered in finding a stable numerical representation of the energy equation, equation (3.1). As mentioned previously, application of the analytic stability analysis developed by Von Neumann (See Smith, 1965) to the energy equation indicated either the Crank-Nicolson or backward-difference approximation method should have been stable. This method of stability analysis is based on expressing an error from the correct solution in terms of a Fourier series. If the series converges the numerical approximation is stable. In application of the method the coefficients and domain of the equation in question are considered to be constant. In spite of the successful stability analysis of equation (3.1) trial solution of the proposed model revealed the energy equation was unstable. Use of the backward-difference method provided a stable solution longer than the Crank-Nicolson approximation; however, both methods eventually became unstable. The inconsistency between the stability analysis and actual solution was apparently explained by nonconstant coefficients and the expanding domain of the model.

Further trial solutions served to confirm that no feasible combination of space and time increments could maintain stability in the energy equation indefinitely. It was also established that instability in the energy equation was directly associated with the term accounting for the heat of vaporization of moisture being desorbed in the porous zone. This so-called sink term was time

dependent since the rate of moisture desorption at any point in the porous zone was a function of time. A stable representation of the energy equation was finally obtained by neglecting the energy requirement associated with the desorption of moisture in the porous zone. The amount of adsorbed moisture present was still accounted for in the mass transfer equation. The final energy and mass equations of the mathematical model which were solved simultaneously for the numerical solution are given in equations (5.1) and (5.2) respectively.

$$\rho(C_{pd} + MC_{pw})\frac{\partial T}{\partial \theta} = \frac{\partial}{\partial \phi} \left(\frac{k}{D} \frac{\partial T}{\partial \phi} \right) + \frac{D_e}{D} C_{pw} \frac{\partial P_v}{\partial \phi} \frac{\partial T}{\partial \phi} \quad (5.1)$$

$$\left[\frac{\epsilon M_w}{RT} + \frac{\rho}{P_{sat}} \left(\frac{dM}{dr} \right) \right] \frac{\partial P_v}{\partial \theta} = \frac{\partial}{\partial \phi} \left(\frac{D_e}{D} \frac{\partial P_v}{\partial \phi} \right) \quad (5.2)$$

Qualitatively the effect of disregarding the heat of vaporization for adsorbed moisture can be viewed as removing one of the requirements for the heat being transferred from the surface to the ice-vapor interface. The net result was that the model slightly overestimated the heat flux to the interface. Overestimating the heat flux to the interface caused the core temperature to be overestimated and a correspondingly higher vapor pressure at the interface to be computed. The higher vapor pressure in turn caused the sublimation rate to be slightly overestimated. Quantitatively, the error caused by neglecting the heat sink term in the energy equation was small. The total heat required to sublimate the free moisture from a unit weight of frozen beef was approximately ten times the heat required to vaporize adsorbed moisture.

Finally, some finite initial domain was required in order to write the finite-difference equations for heat and mass transfer in the porous zone. An initial domain was generated by assuming heat and water vapor were exchanged between the air stream and an exposed ice surface while the core temperature dropped from the initial temperature to the wet-bulb temperature of the air stream. This time was observed to be approximately five minutes in most tests. The initial domain was approximately two percent of the sample half-thickness. Initially the numerical solution contained only two nodes: one on the surface and the floating node on the ice-vapor interface (See Figure 3.1). As the ice-vapor interface receded more nodes entered the solution.

Trial solutions of the numerical model gave indication that the model was at least qualitatively correct. Figure 5.2 shows typical vapor pressure and temperature profiles computed from the proposed model for one-dimensional atmospheric freeze-drying of beef. For the elapsed time shown in Figure 5.2 three-fourths of the free moisture had been removed. The position of the ice-vapor interface is indicated by a dashed line. The most outstanding characteristic of the computed profiles is their almost perfect linearity. These computed results strongly supported the pseudo steady-state assumption used by previous investigators (Sandall, et al., 1967; Dyer and Sunderland, 1968). Clearly, movement of the ice front was so slow that the time derivatives of dependent variables in the porous zone were insignificant compared to the space derivatives.

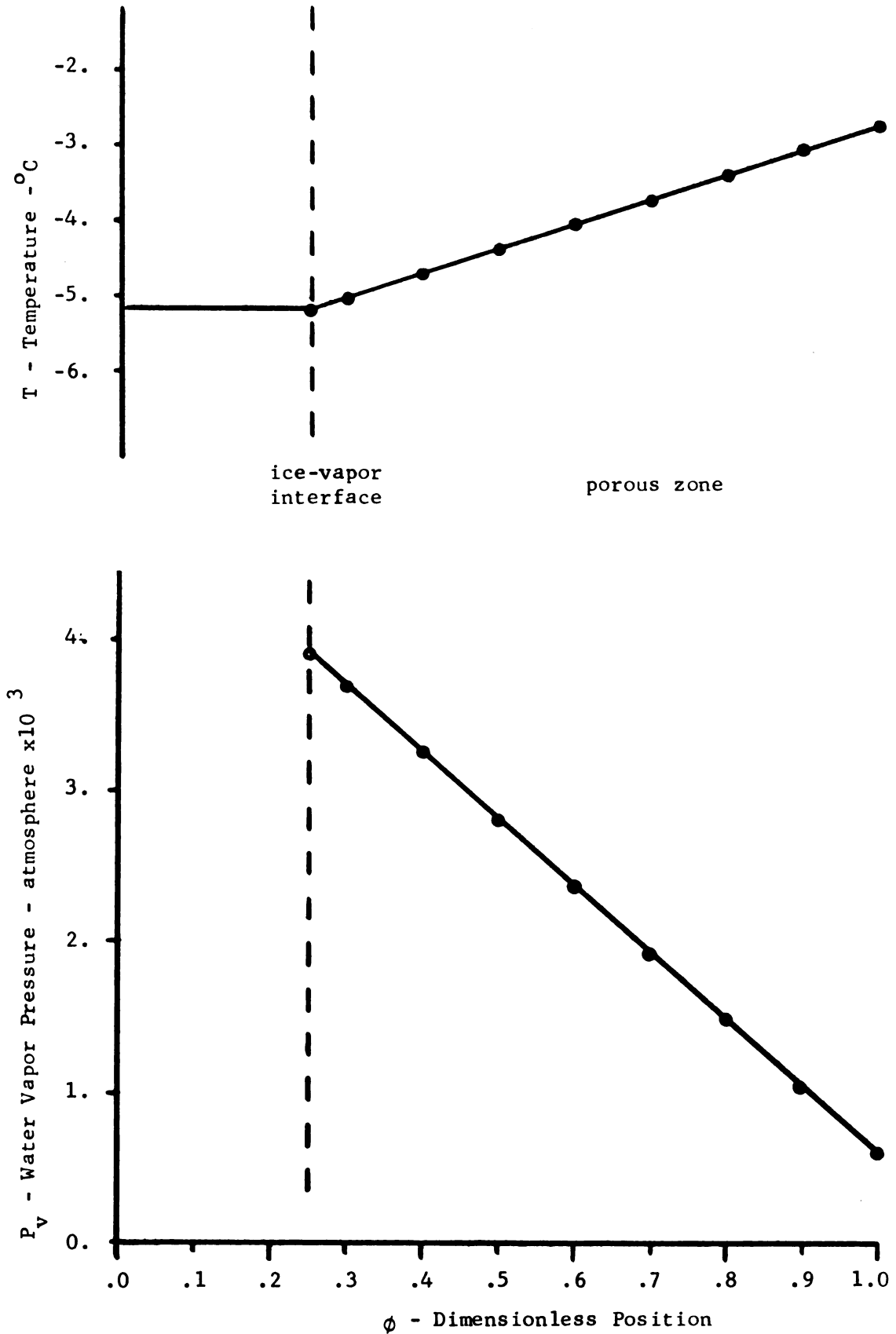


Figure 5.2. Computed Profiles of Vapor Pressure and Temperature for Typical Conditions of Atmospheric Freeze-Drying.

Linearity of the computed dependent variable profiles shown in Figure 5.2 provided increased confidence in the accuracy of the computer solution early in the process when only a few nodes were in the solution. If the profiles of the dependent variables were highly nonlinear, accuracy of the solution would have been restricted during the early portion of the process when the number of active nodes was small.

Linearity of the profiles also increased the accuracy with which the derivatives of vapor pressure and temperature were computed at the interface. The velocity of the interface and the rate of drying were dependent on calculation of these derivatives.

Figure 5.3 shows a solution of the proposed model in terms of dimensionless mean moisture content versus dimensionless time. The model solution has been converged to a typical set of atmospheric freeze-drying data obtained from a one-dimensional sample. Also shown in Figure 5.3 is a solution which neglected the same components of the heat and mass transfer equations as did the pseudo steady-state model. The most important component neglected was the adsorbed moisture. Both solutions included the same values for all constants and transport parameters of the model. The proposed model, at least qualitatively, predicted the extended time required to remove the adsorbed moisture after the ice front reached the centerline. Previous investigators (Sandall, *et al.*, 1967) have noted that models which neglected the adsorbed moisture were significantly in error after 75 to 90 percent of the original moisture had been removed. This observation was supported by results of the proposed model.

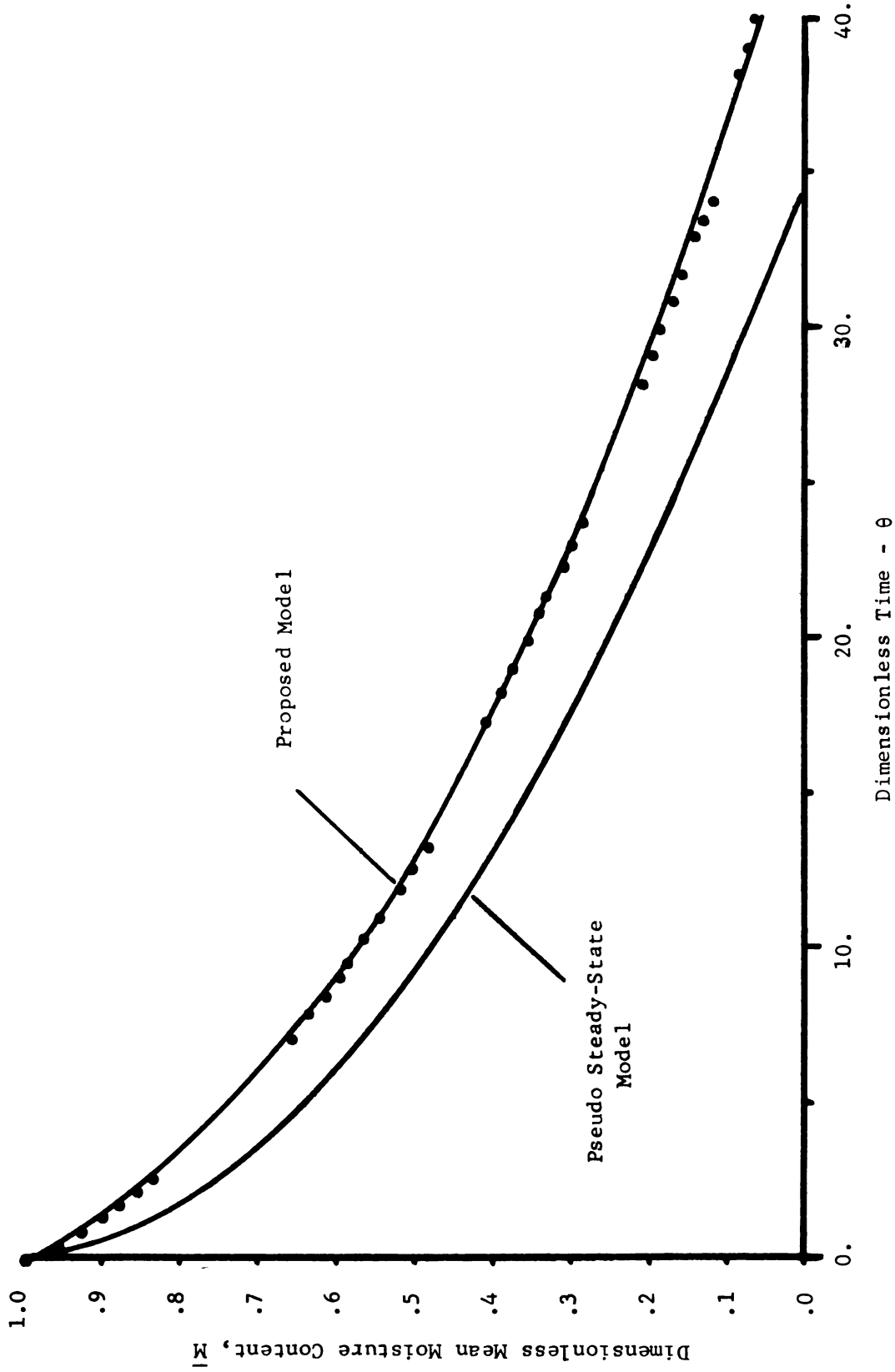


Figure 5.3. Comparison of Predicted Drying Curves of the Proposed Model and Pseudo Steady-State Model in One-Dimensional Samples.

Combined results shown in Figures 5.2 and 5.3 indicated the pseudo steady-state model was in error chiefly due to neglecting the adsorbed moisture in the porous zone. Clearly the assumption of linear dependent variable profiles was acceptable. However, for purposes of parameter estimation, the more complete description of atmospheric freeze-drying as included in the proposed model was preferred.

Qualitative results and discussion presented in the preceding paragraphs indicate the proposed model is probably an adequate representation of atmospheric freeze-drying. More quantitative and strenuous tests of the model will be discussed in the next chapter under the headings of parameter estimation and analysis of residuals.

CHAPTER VI
RESULTS AND DISCUSSION

Three transport parameters of the mathematical model were evaluated from data generated in atmospheric freeze-drying tests described in Chapter IV. Estimates of these physical parameters are presented and discussed in the first section of this chapter. The following section includes analysis of the residuals and further discussion of the validity of the one-dimensional mathematical model. In subsequent sections of the chapter the proven model is transformed into an approximate, three-dimensional model and used for practical analysis of the effect of all operating variables on the rate of atmospheric freeze-drying.

The parameter estimates

Three transport parameters were evaluated in each of 18 tests conducted at six different experimental conditions. At .97 atm total pressure, tests were conducted at all four possible combinations of air temperature (-2.8°C and -8.2°C) with fiber orientation (parallel and perpendicular to the direction of transport). In order to adequately test the accuracy of the mathematical model, data were also taken at a system pressure of .58 atm and -2.8°C air temperature for both parallel and perpendicular fiber orientation.

Before presenting the parameter estimation results a brief diversion is in order to explain the statistical information obtained with the parameter estimates when the GAUSHAUS program (Meeter, 1964) was used for nonlinear estimation. As mentioned previously, GAUSHAUS is a library program which utilizes a combination of methods to perform estimation of parameters in mathematical models which are nonlinear with respect to their parameters. This program was used chiefly because of the supplementary information which was obtained with the parameter estimates at little or no extra effort. This supplementary statistical information helped to evaluate the accuracy of the model and the parameter estimates; it included:

1. final functional or predicted values of the model using the optimum parameter estimates.
2. approximate 95 percent confidence limits on the predicted functional values and on the parameter estimates. The confidence limits were computed from a linear approximation of the model in the vicinity of the optimum parameter matrix, $\hat{\beta}$, and, therefore, were not exact.
3. residual values, that is, $(Y_i - \bar{M}_i)$ for $i = 1, 2, \dots, L$. These values are analyzed in the next section of this chapter to assess the accuracy of the model.
4. variance of the residuals which, in the case of a linear model, is an independent and unbiased estimate of σ^2 , the variance of the individual observations. In the nonlinear model the estimate is biased but can be used as a relative measure of the variance of observations between tests.
5. the correlation matrix, which revealed how the various parameters were correlated with each other.

This supplementary information is mentioned in the following discussion of the model and the parameter estimates.

Eighteen estimates each of three parameters are presented in Table 6.1. Initial observation indicated substantial variability in

all of the parameters. This was probably to be expected in a biological product where composition can vary from sample to sample. A more encouraging observation was that the internal transport parameters, k and C_2 , were estimated near the values expected. Harper (1962) reported the value of k in freeze-dried beef for pressures above approximately .5 atm in the absence of a counter-flow of water vapor to be approximately 1.5×10^{-4} cal/cm-sec- $^{\circ}$ C. The estimates of k shown in Table 6.1 are near this value. Sandall, et al. (1967) evaluated C_2 , the structural constant in the effective mass transfer coefficient, in the breast meat of turkey. They found C_2 to be between .44 and .66 for transport parallel to the fibers and approximately .27 for transport perpendicular to the fiber orientation. Similiar to slightly higher values are presented in Table 6.1 for precooked beef.

A summary of the analysis of variance of all three parameters is presented in Table 6.2. The variance of the experimental results was analyzed for significance due to air temperature, system pressure and orientation of the fibers. Interactions between these factors were assumed negligible. Testing for significant differences was done by use of the F-test at the 90% level of significance (Peng, 1967).

TABLE 6.1. Summary of Parameter Estimates and Variance of the Residuals

Test no.	h_D	C_2	k	σ^2
Air Temperature -8.2°C Pressure = .97 atm Orientation = parallel				
1	.0084	.56	$.46 \times 10^{-4}$	1.97×10^{-5}
17	.0091	.75	.44	9.78
2	.0079	.86	.47	5.72
Air Temperature -8.2°C Pressure = .97 atm Orientation = perpendicular				
7	.0087	.64	2.77×10^{-4}	1.05×10^{-5}
8	.0117	.80	.95	29.90
18	.0086	.51	1.59	13.80
Air Temperature -2.8°C Pressure = .97 atm Orientation = parallel				
3	.0126	.89	$.53 \times 10^{-4}$	21.82×10^{-5}
4	.0116	.95	1.35	1.97
15	.0056	.99	.51	16.44
16	.0092	.61	.31	5.36
Air Temperature -2.8°C Pressure = .97 atm Orientation = perpendicular				
5	.0072	.62	$.96 \times 10^{-4}$	9.24×10^{-5}
6	.0111	.64	.99	17.26
Air Temperature -2.8°C Pressure = .58 atm Orientation = parallel				
9	.0087	.74	1.21×10^{-4}	8.52×10^{-5}
10	.0087	.99	1.00	12.36
12	.0095	.74	1.02	7.54
Air Temperature -2.8°C Pressure = .58 atm Orientation = perpendicular				
11	.0133	.42	1.03×10^{-4}	14.12×10^{-5}
13	.0091	.72	1.75	8.76
14	.0107	.62	1.09	11.40

TABLE 6.2. Summary of Analysis of Variance in the Parameter Estimates

Analysis of Variance in Estimates of h_D

<u>Source of Variance</u>	<u>d.f.</u>	<u>Mean Square</u>	<u>F-ratio vs F(.90,14,1)</u>	
Air Temperature	1	2.007	.425	3.10
System Pressure	1	1.910	.405	3.10
Orientation of Fibers	1	3.759	.897	3.10
Experimental Error	14	4.717		

Analysis of Variance in Estimates of C_2

<u>Source of Variance</u>	<u>d.f.</u>	<u>Mean Square</u>	<u>F-ratio vs F(.90,14,1)</u>	
Air Temperature	1	1.395	.681	3.10
System Pressure	1	.319	.156	3.10
Orientation of Fibers	1	15.855	7.755	3.10
Experimental Error	14	2.045		

Analysis of Variance in Estimates of k

<u>Source of Variance</u>	<u>d.f.</u>	<u>Mean Square</u>	<u>F-ratio vs F(.90,14,1)</u>	
Air Temperature	1	.651	.231	3.10
System Pressure	1	6.264	2.224	3.10
Orientation of Fibers	1	7.978	2.76	3.10
Experimental Error	14	2.822		

Turning attention now to analysis of each parameter estimate, the surface mass transfer coefficient, h_D , is considered first. The value of this parameter was not expected to vary with temperature or pressure over the small range of these variables that was considered. Since h_D is not a function of product properties it was not expected to be a function of orientation of the fibers. Statistical analysis of the dependence of h_D on temperature, pressure and orientation as summarized in Table 6.2 confirmed that no significant difference exist for any of these factors at the 90 percent confidence level. The mean value of all estimates of h_D was approximately $.0095 \text{ gm/sec-cm}^2\text{-atm}$.

The internal heat and mass transfer parameters, being functions of the product under consideration, were of greater interest. The structural constant in the effective mass transfer coefficient, C_2 , can be viewed as an attenuation constant which accounted for the amount the free-gas value of the mutual diffusivity of air and water vapor was reduced due to constrictions of the porous media. Krischer (1959) has related this constant to the porosity of the porous zone by a factor to account for the tortuosity of the path of the water vapor molecule through the dried portion of the product.

$$C_2 = \frac{e}{\tau^2} \quad (6.1)$$

The porosity of freeze-dried beef has been reported by Harper (1962) to be approximately .76. Since it was expected that the tortuosity factor, τ , was greater for transport perpendicular to the fiber orientation of the meat than parallel to the fibers, C_2 was expected

to be less in those tests conducted with water vapor transport perpendicular to the fibers of the meat. The structural constant was not expected to be a function of any operating variable.

The estimates of C_2 shown in Table 6.1 were tested for significant differences due to temperature, pressure level and orientation of the fibers. Results of this analysis of variance are presented in Table 6.2. Only differences in C_2 due to orientation of the fibers were significant when tested at the 90 percent confidence level. Differences due to fiber orientation were also significant at the 95 percent confidence level. The mean for estimates of C_2 for vapor diffusion parallel to the fibers was .81 and .62 for diffusion perpendicular to the fibers.

Estimates of the effective thermal conductivity, k , presented an interesting comparison to results obtained by Harper (1962). Using steady-state methods on freeze-dried beef with no water vapor flux, Harper found the mean value of k to be 1.5×10^{-4} cal/cm-sec- $^{\circ}$ C. An overall mean value of 1.0×10^{-4} cal/cm-sec- $^{\circ}$ C was found in the current research. These estimates were made in the presence of a counterflow of water vapor and by parameter estimation from transient experiments. The estimated effective thermal conductivity was especially sensitive to variations in structure and composition of the meat sample as is evident from the results of Table 6.1. In addition, an unknown portion of the total variation in the estimated values of k can be attributed to the elongated contours of the risk-function surface in the k direction (See Figure 4.2). Ninety-five percent confidence limits were computed for the estimated value of k . Using the t-test

(Snedecor, 1956) these limits were found to be $.7 \times 10^{-4}$ to 1.3×10^{-4} cal/cm-sec- $^{\circ}$ C. Variations in k due to system pressure, air temperature and orientation were all insignificant at the 90% confidence level.

It may be argued that more powerful techniques are available for obtaining the single best estimate of the parameter matrix than by finding the arithmetic mean of each parameter individually. If the nonlinear model were represented with a linear approximation in the vicinity of the optimum parameter matrix of all the tests, the risk function would be an (n) -dimensional parabaloid over the domain of the parameter matrix, where (n) is the number of parameters estimated. The single best estimate of $\underline{\beta}$ could then be found by finding the minimum of the parabaloid. However, linearization of the nonlinear model can only be accomplished over incremental variations in the estimated parameters. It was concluded that the variation shown in the parameter estimates of Table 6.1 could hardly be construed to be incremental in magnitude. Therefore, the arithmetic mean value was computed to be the single best estimate of each parameter.

Evaluation of k and C_2 allowed certain observations to be made concerning details of the mechanisms of atmospheric freeze-drying. Heat transfer through the porous zone of the product has been assumed to be by conduction through the solid matrix and by some combination of conduction and convection through the gas-filled pores. The mean of the current estimates of k was approximately two-thirds of the magnitude which Harper (1962) found. While variability of the estimates of k was large it is noteworthy

that the 95 percent confidence limits on the mean of the current estimates did not include the mean value Harper obtained. Furthermore, the mean estimated value of k was between the values Harper found for atmospheric pressure and vacuum conditions (See Chapter II). These points tend to support the above concept of the mechanism of heat transfer with some additional insight. Apparently, the counter-flux of water vapor throughout the drying process substantially reduced the contribution to the pores to transfer of heat in the opposite direction. Thus the effective value of thermal conductivity measured under dynamic conditions at atmospheric pressure was found to be near the value obtained under static conditions in a vacuum.

Implication of the above results is that the effective transfer of heat through the porous zone during the drying process is substantially less than measured under steady-state conditions. Such findings are important to optimization of the freeze-drying process.

The rate of atmospheric freeze-drying has been observed to increase significantly with increasing air temperature in the range of -10°C to zero $^{\circ}\text{C}$. The question has been raised as to whether this phenomenon was partially caused by liquid transport of water which was unfrozen due to the presence of solutes. Tests were conducted in the current research in an attempt to answer this question.

The maximum temperature at which ice exists in frozen beef is approximately -1.75°C (Hohner and Heldman, 1970). Experimental atmospheric freeze-drying tests were conducted at air temperature

of -2.8°C and -8.2°C . If significant liquid transport had resulted in tests at the higher air temperature, the accelerated drying rate would have been reflected in an inflated estimate of the mass transfer parameter in these tests.

Statistical analysis of estimates of C_2 summarized in Table 6.2 indicates the mean value from tests at -2.8°C was slightly but not significantly larger than values from the lower temperature tests when tested at the 90 percent confidence level. Thus the concept of liquid transport was not supported by the results. The frozen core temperature was observed experimentally to remain three to five degrees C below the air temperature throughout most of the drying process. This observation was confirmed by the solution of the mathematical model. In summary, it appears unlikely that water was transferred in the liquid state when the air temperature remained below the initial freezing point. The fraction of product moisture in the form of ice increases rapidly with decreasing temperature in the range just below the initial freezing point; thus depression of the ice core temperature served to prevent liquid transport of water. In a later section of this chapter it is demonstrated that the proposed model does predict the observed increase in the drying rate with increasing air temperature.

Results of statistical analysis of the mass transfer parameter, C_2 , failed to reject the hypothesis that the mechanism of mass transfer was water vapor diffusion through stagnant air in the pores of the dried layer. Further insight into this process was gained from the magnitude of the estimated values of C_2 both parallel and perpendicular to the fiber orientation. The mean

value of C_2 parallel to the fibers was determined to be .81 compared to a value of one under free-gas conditions. In other words, the mean free path of the water vapor molecule led to contact with the porous solid only often enough to reduce the effective value of the free-gas mass diffusivity by 19 percent. Similarly transport perpendicular to the fibers was reduced by 38 percent. From the viewpoint of a water vapor molecule at freeze-drying temperatures, freeze-dried beef is a highly porous medium.

The fact that Sandall et al. (1967) estimated C_2 to be between .44 and .66 parallel to the fibers and .27 perpendicular to the fibers of turkey meat may have been because the structure of turkey meat is less porous than that of beef. However, these lower values for C_2 may also have been computed due to fitting the incomplete pseudo steady-state model to experimental freeze-drying data. From Figure 5.3 it can be observed that a lower mass transfer coefficient would have been required to cause the pseudo steady-state solution to fit the same data that the model used in this research fit with a higher value.

Accuracy of the Model

Qualitative results have been presented in Chapter V to support the accuracy of the numerical solution of the model and to compare it to previous models. Comparison of model solutions to experimental results and analysis of the residuals between the experimental data and the computed values are presented in this section to further confirm accuracy of the model.

Figure 6.1 compares the solution of the model to experimental results of one-dimensional transport tests at two different pressure levels. The computed solution represents the optimum fit of the model to each separate set of data. Ability of the model to fit results obtained at different levels of the operating variables is further demonstration of the accuracy of the numerical solution of the model. Results of Figure 6.1 indicate the model satisfactorily fits each set of experimental results.

The difference between the final functional value of the model and the experimental value at each recorded point is called the residual value. Draper and Smith (1966) discussed several methods of analyzing the size, randomness and various trends which the residual values may exhibit. If the mathematical model were a complete and accurate representation of the physical process under study and all experimental data were obtained with an unbiased procedure the residual values of any test would be a random variable with magnitude equal to the standard deviation of the experimental error. The objective of the methods of analysis presented by Draper and Smith (1966) was to answer the question whether the residual values have the characteristics of a random variable.

The residual values of all 18 one-dimensional atmospheric freeze-drying tests used to obtain parameter estimation data are shown in Appendix V. Variance of the residuals of all tests is shown in Table 6.1. In all cases the residuals were small, almost never greater than two percent of the initial functional value. In addition, the variance of the residuals was small and quite

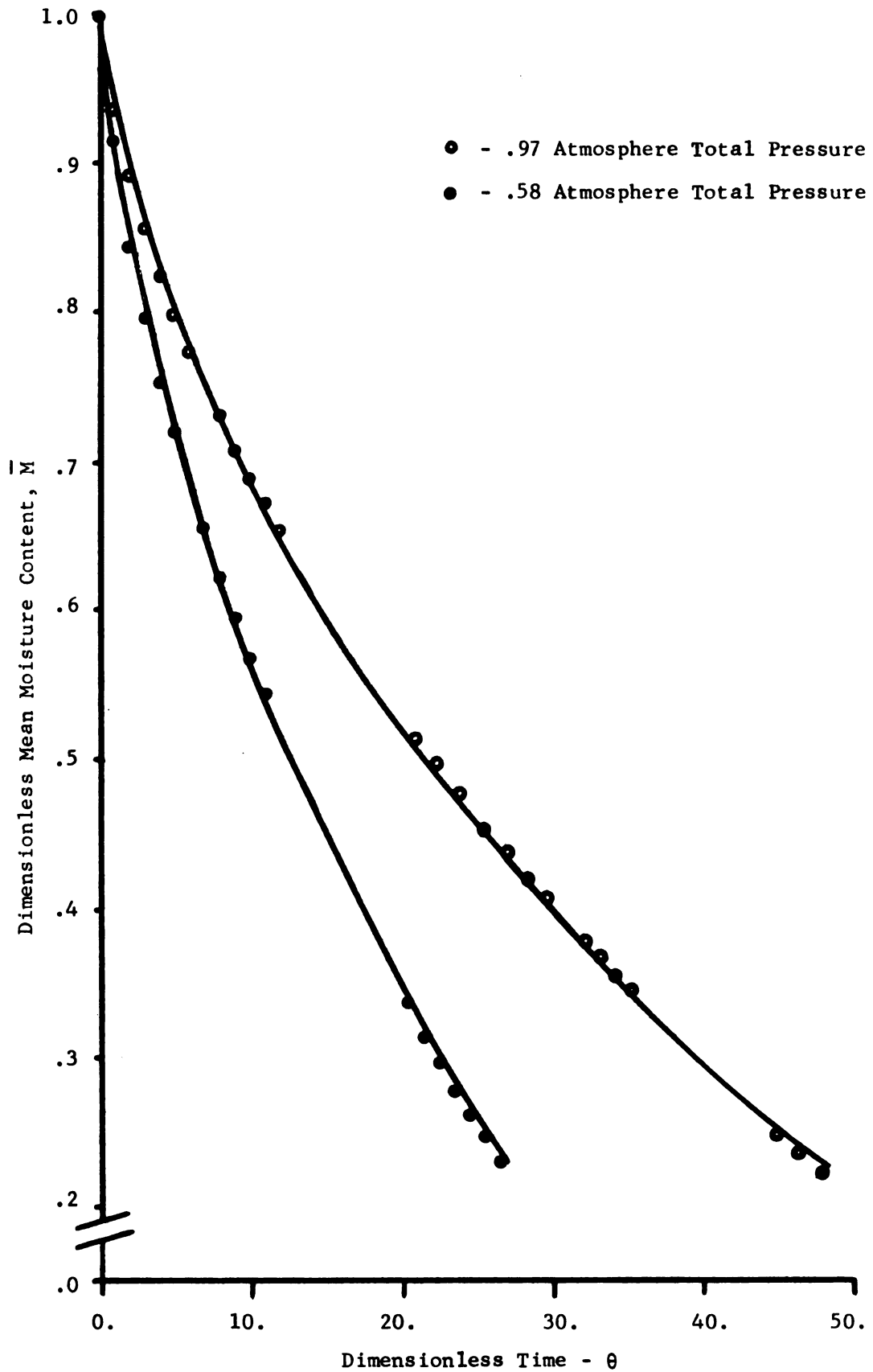


Figure 6.1. Comparison of the Proposed Model to Experimental Results at .97 and .58 Atmosphere Total Pressure.

uniform over the entire group of tests. Average variance of the residuals was approximately 1×10^{-4} .

Inspection of the time dependence of the residual values as they are listed in Appendix V revealed a cyclic nature in all tests. No formal testing was required to confirm that the residuals were not a random variable. Such nonrandom cyclic patterns of residuals with relatively small values have been encountered before when transport parameters have been estimated from numerical solutions of mathematical models (Beck, 1969B).

The small size of the residual values and the rather uniform variance of the residuals between tests tended to vindicate the experimental technique of inducing a biased error into the results. A more probable cause of the nonrandom residual values in all of the test results was the fact that several variables in the mathematical model were assumed constant. Assuming minor variables were constant tended to induce a small bias into the model. The parameter h_D can be taken as an example. The surface mass transfer coefficient was assumed constant; however, being a minor function of the water vapor concentration at the surface, this parameter may have declined in value as the vapor concentration declined. The effect of such a variation can be seen from Figure 6.1. The experimental results initially declined faster than the model. Later when the value of h_D had declined the experimental results fell more slowly than the solution of the model. Through the process of minimizing the squared deviations between the model solution and the data a mean value was found for parameters which actually were minor variables. The cyclic nature of the residuals

was caused by the model solution being based on the computer value of such parameters.

The small size of the residuals in all tests indicated the total error in the proposed model was small; however, there was no means of computing exactly how accurate the model was. Since any addition would only increase the complexity of the model and its solution without insuring an improvement in the accuracy as measured by analysis of the residuals, a cost-benefits decision remained with the investigator. Therefore, the model was described as adequate for parameter estimation and process analysis, but probably not a complete description of the physical process represented.

Simulation of Atmospheric Freeze-Drying in Three Dimensions

In all tests discussed previously in this thesis the transport of heat and water vapor in the sample has been limited to one dimension. Such tests were used for parameter estimation and analysis of the mechanisms of atmospheric freeze-drying. Obviously, practical application of the process occurs in samples where heat and water vapor are transported in three dimensions. Complexity of the mathematical model would defy even numerical solution if it were derived initially in three space coordinates. However, the one-dimensional model was transformed into a reasonably accurate approximation of atmospheric freeze-drying in cubical samples with transport of heat and water vapor from all six surfaces. Mean values of all parameters determined in the previous section were used, and the anisotropic effect induced by the fiber structure was disregarded.

Geometrically the three-dimensional model was visualized as a pyramid with height one-half the length of the base. The apex of the pyramid was located at the center of the cubical sample with the base of the pyramid on the sample surface. All transport of heat and water vapor was assumed to move perpendicular to the sample surface. Actually, of course, flow of heat and water vapor were not perpendicular to the surface of the cube except along a line from the center perpendicular to the surface. Nevertheless, considering the sample variability reflected in the parameter estimates of a previous section and the effect of this variability on the product-dependent constants of the model, the three-dimensional model was considered sufficiently accurate for process analysis work.

Results of the three-dimensional solution using the mean values of parameters are compared to experimental results of atmospheric freeze-drying of cubes of precooked beef in Figure 6.2. Both sets of experimental results shown in Figure 6.2 were obtained at -2.8°C air temperature and .97 atm total pressure. One sample had a half-thickness of .7 cm and the other .5 cm. These results confirm that the approximations included in the three-dimensional model were reasonably accurate until the dimensionless mean moisture content dropped below .1. At low moisture contents the three-dimensional model predicted excessively long drying times.

At low moisture content the ice core in the three-dimensional model was assumed to be reduced to a small cube in the center of the sample. Water vapor was assumed to flow outward only along a path with cross-sectional area equal to the area of

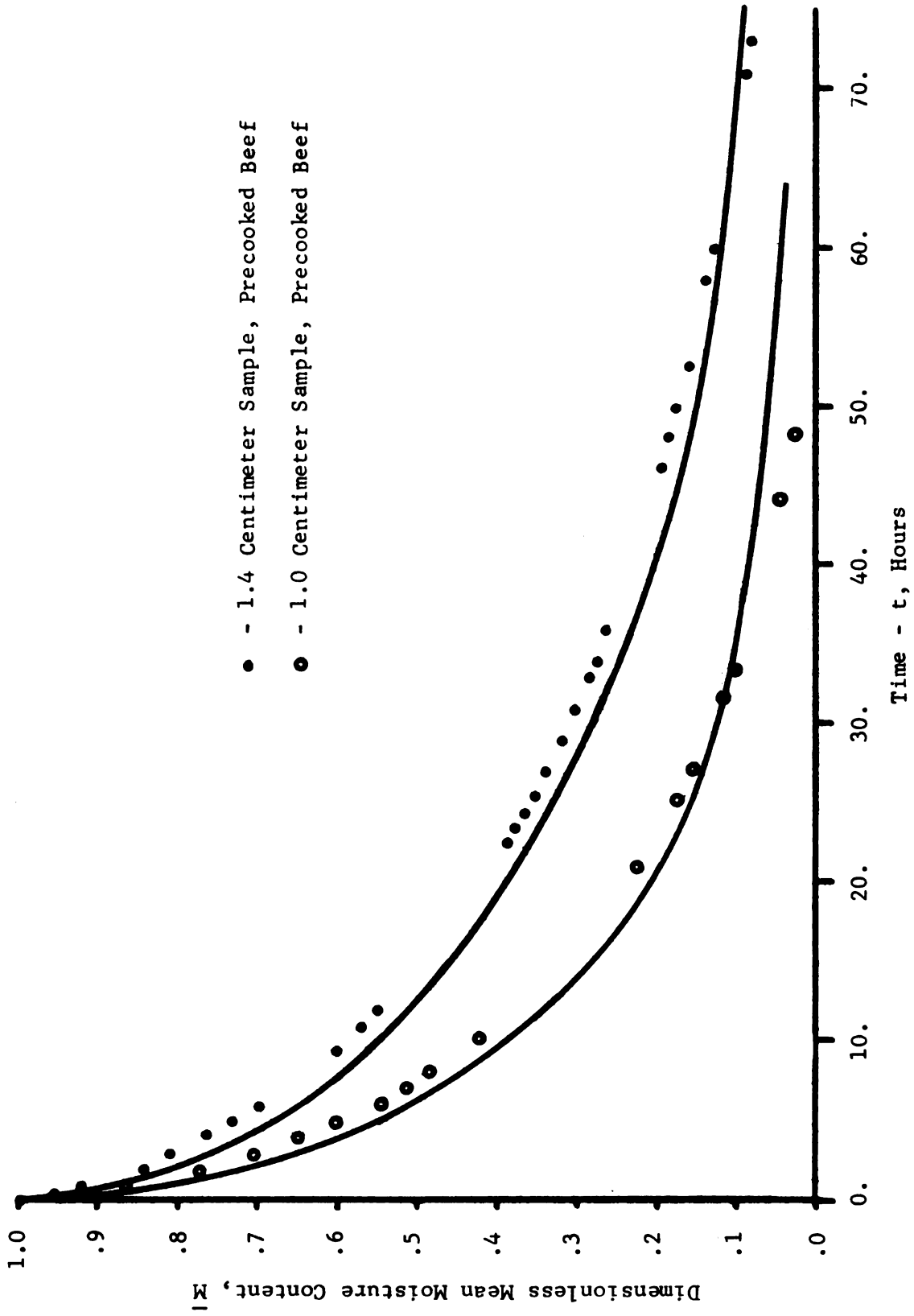


Figure 6.2. Comparison of Solutions of the Three-Dimensional Model to Experimental Results in Cubical Samples.

the ice core in the center of the sample. Clearly, near the end of the process, this assumption neglected a substantial amount of the effective transport area of the sample. In subsequent discussion, where the three-dimensional model will be used for analysis of the atmospheric freeze-drying process, prediction of the model will be disregarded below $\bar{M} = .1$.

Analysis of Atmospheric Freeze-Drying in Cubical Samples

The power and economy of a proven computer simulation for analysis of the effect of operating variables upon a physical process quickly becomes apparent when the speed and flexibility of the model solution are compared to acquiring the same information from experimental tests. The approximate three-dimensional model discussed above was used to investigate the effect of air temperature, system pressure, sample size, and magnitude of the surface mass transfer coefficient on the rate of atmospheric freeze-drying in cubical samples of cooked beef.

The practical operating range of all variables was investigated by changing the variables one at a time while holding all others at a standard condition. The standard condition was the following:

Air temperature, T_a	= -3.0°C
System pressure, P	= .97 atm
Sample half-thickness, s	= .5 cm
Surface mass transfer coef., h_D	= .0095 gm/cm ² -sec-atm
Structural constant, C_2	= .725
Thermal conductivity, k	= .0001 cal/cm-sec-°C
Initial Moisture content, M_0	= 1.5 gm-H ₂ O/gm-dry solid

Other product dependent constants were evaluated as shown in Table 5.1.

In Figure 6.3 the effect of air temperature on the rate of atmospheric freeze-drying of one centimeter cubes of cooked beef is shown. Air temperature was investigated at -3.0°C , -8.0°C , and -13.0°C . This modest range in air temperature caused a greater change in the predicted drying time than the changes investigated in any other variable. The predicted increase in drying rate with air temperature was approximately of the order witnessed by Woodward (1961) and Lewin and Maletes (1962). As has previously been noted the practical upper limit of air temperature is approximately -3.0°C due to depression of the freezing point caused by dissolved solutes. Results of Figure 6.3 demonstrate that any practical application of atmospheric freeze-drying must be carefully designed to operate as near the maximum allowable temperature as possible.

The large dependence of drying rate on air temperature was caused by two factors. First, higher air temperature resulted in a higher ice core temperature which in turn caused a higher saturated vapor pressure at the ice-vapor interface. The higher vapor pressure at the interface represented an increase in the mass transfer potential and caused more rapid vapor transport across the porous zone. The second and minor cause was an increase in the vapor diffusivity due to increase in temperature.

The effect of reducing system pressure on the rate of freeze-drying in one-centimeter cubes of precooked beef is shown in Figure 6.4. Little discussion is required concerning these results since it has been previously established that the maximum rate of freeze-drying occurs in the range of 8-25 mm Hg, far below atmospheric conditions. The justification of atmospheric freeze-drying centers

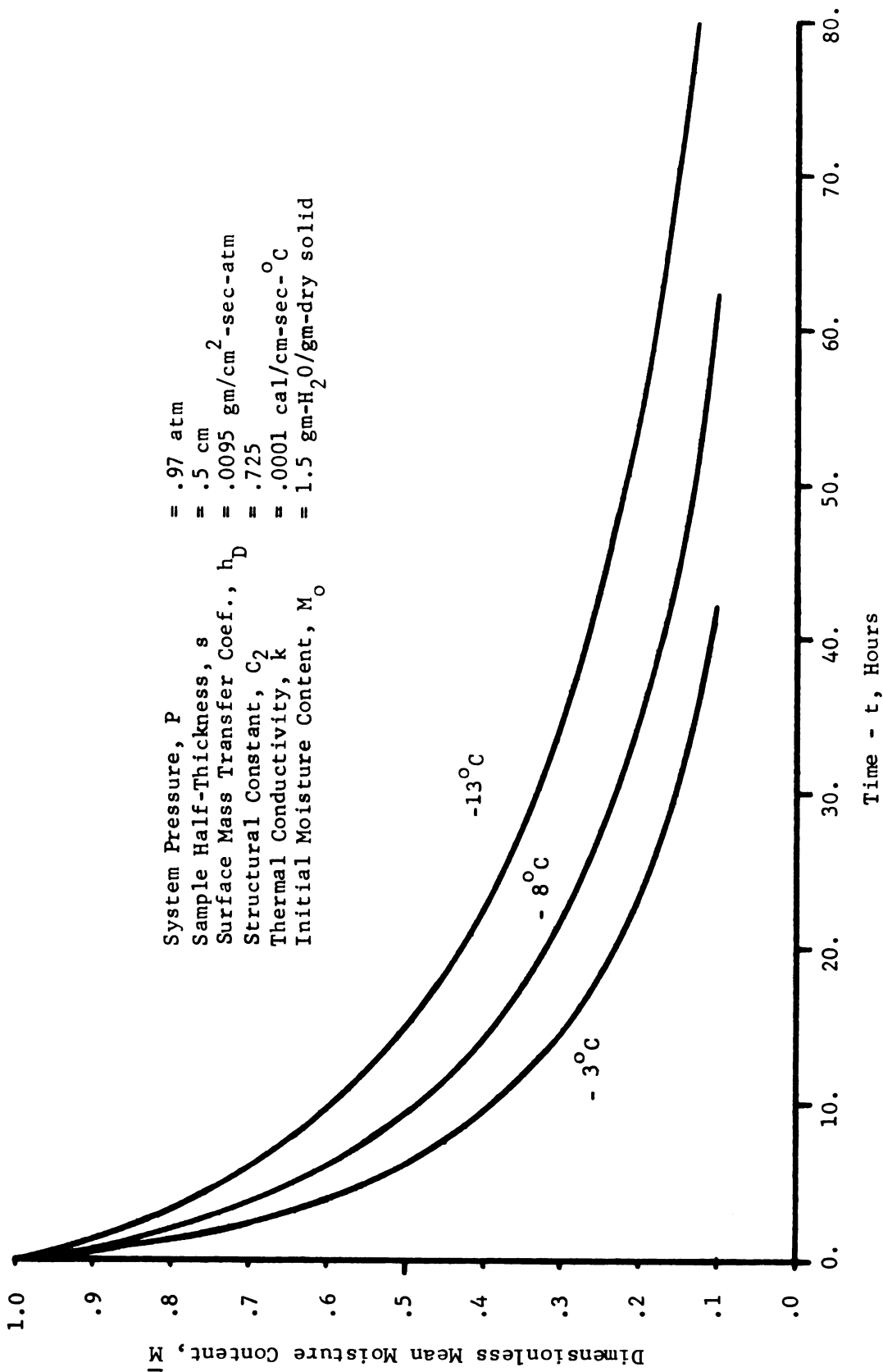


Figure 6.3. Predicted Effect of Air Temperature on Atmospheric Freeze-Drying Rates in One-Centimeter Cubes of Precooked Beef.

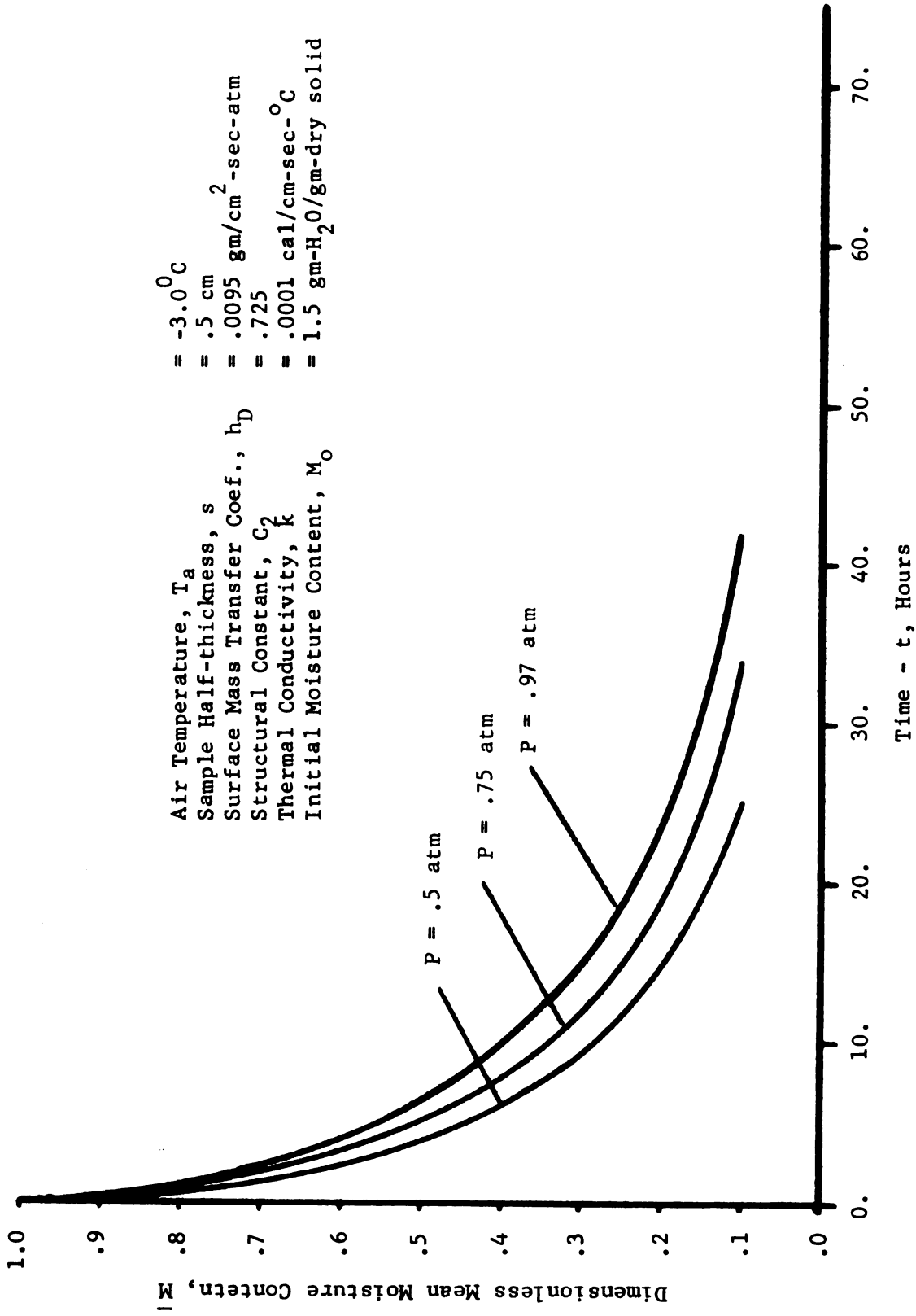


Figure 6.4. Predicted Effect of System Pressure on Atmospheric Freeze-Drying Rate in One-Centimeter Cubes of Precooked Beef.

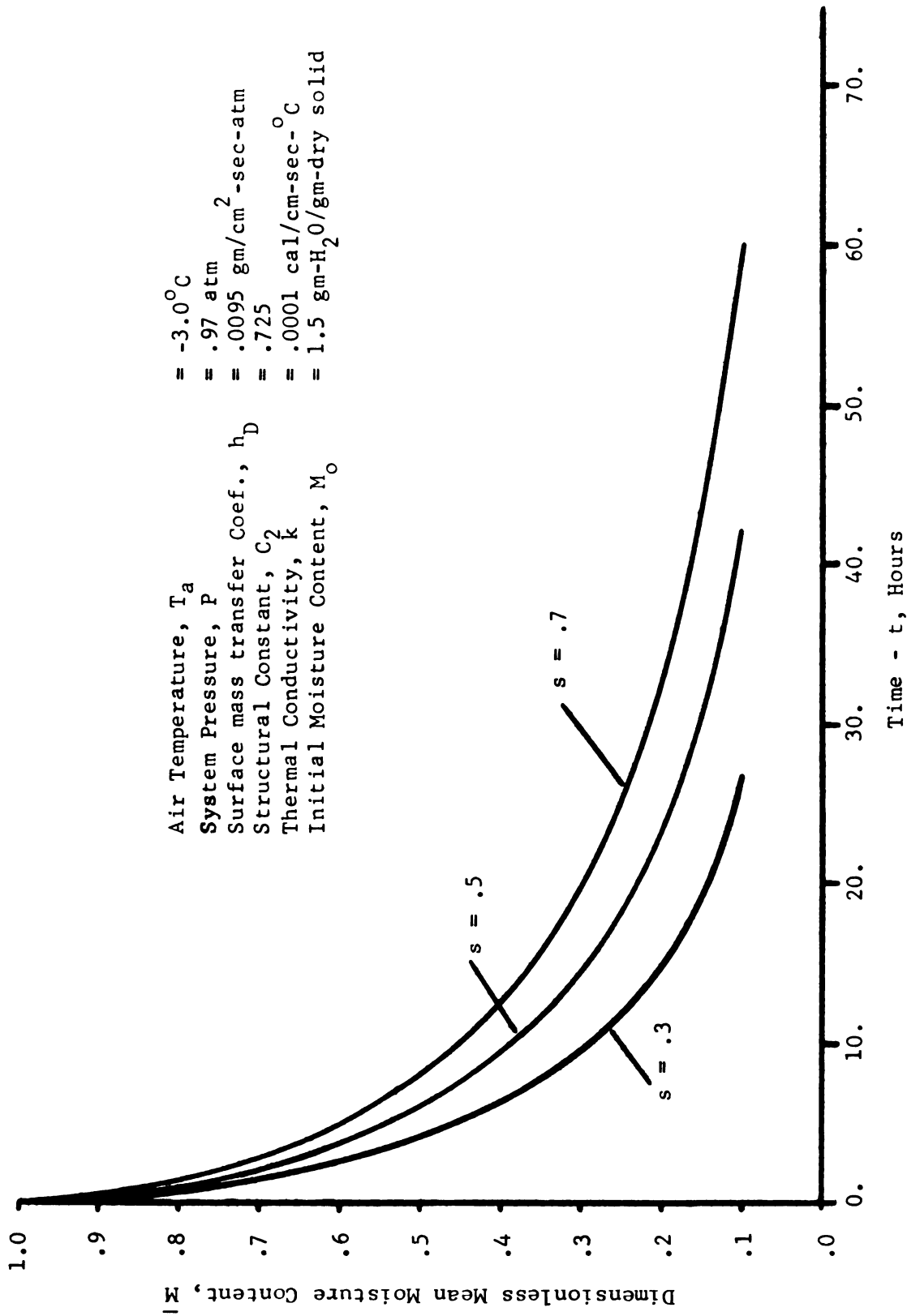
about elimination of equipment related to providing and maintaining a vacuum condition. However, process design for atmospheric freeze-drying should take full advantage of the increased drying rate due to reduced system pressure by arranging equipment to minimize the total pressure in the drying chamber.

The effect of sample size on the rate of atmospheric freeze-drying in beef cubes at the standard conditions listed above is shown in Figure 6.5. Time to dry to $\bar{M} = .1$ decreased rapidly with decrease in the dimension of the cubical samples. For freeze-drying with a very large surface mass transfer coefficient (so that the surface vapor concentration approximates the free-stream vapor concentration) the time to dry to any given dimensionless moisture content should vary with the ratio of the square of the sample size. Results shown in Figure 6.5 were computed with $h_D = .0095 \text{ gm/cm}^2\text{-sec-atm}$ which was not large enough to fulfill the above criterion. Nevertheless sample size was shown to greatly effect the drying rate.

Effect of the surface mass transfer coefficient on the rate of atmospheric freeze-drying is best illustrated by definition of a ratio of external to internal mass transfer coefficients analogous to the heat transfer Biot number.

$$\bar{H} = h_D s / D_e = h_D s RTP / C_2 \bar{D} M_w \quad (6.2)$$

Figure 6.6 illustrates the dimensionless time required to reduce \bar{M} to .1 in cubes of precooked beef as a function of \bar{H} . Clearly, the drying time and, therefore, the drying rate are independent of \bar{H} when it is greater than approximately 100. For values of \bar{H}



Air Temperature, T_a = -3.0°C
 System Pressure, P = $.97$ atm
 Surface mass transfer Coef., h_D = $.0095$ gm/cm²-sec-atm
 Structural Constant, C_2 = $.725$
 Thermal Conductivity, k = $.0001$ cal/cm-sec- $^{\circ}\text{C}$
 Initial Moisture Content, M_0 = 1.5 gm-H₂O/gm-dry solid

Figure 6.5. Predicted Effect of Sample Size on Atmospheric Freeze-Drying Rate in Cubes of Precooked Beef.

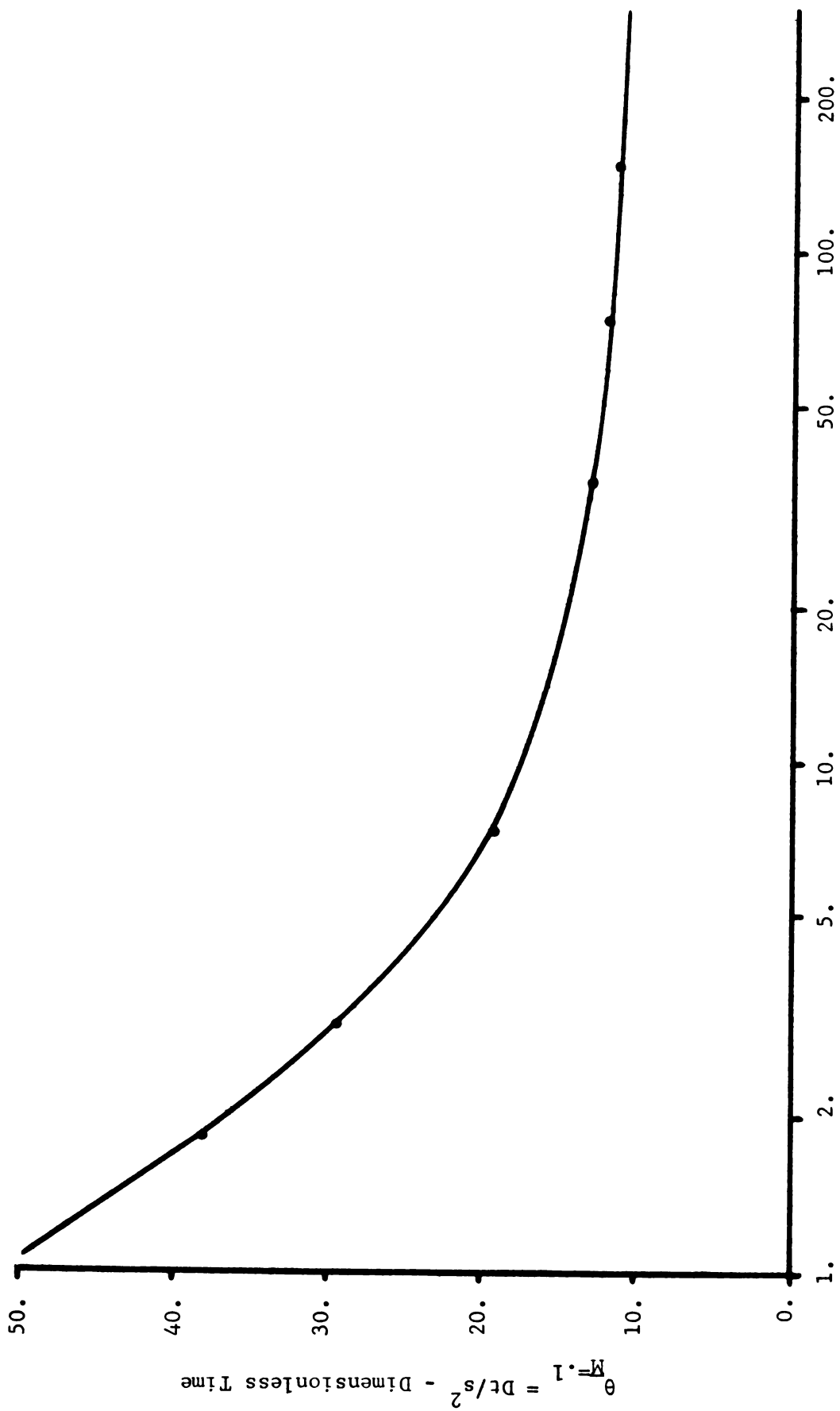


Figure 6.6. Dimensionless Time Elapsed to $\bar{M} = .1$ in Precooked Cubes of Beef as a Function of \bar{H} under Atmospheric Freeze-Drying.

greater than 100 the rate of mass transfer is effectively controlled by the internal mass transfer mechanism.

The maximum possible rate of atmospheric freeze-drying as predicted by the approximate three-dimensional model for one centimeter cubes of precooked beef is illustrated in Figure 6.7. A value of $h_D = .040 \text{ gm/cm}^2\text{-sec-atm}$ was used to compute the curve in Figure 6.7. This value of h_D corresponded to $\bar{H} = 148$. The curve illustrated in Figure 6.7 can be used to predict the maximum rate of atmospheric freeze-drying for cubes of precooked beef of any size. The ratio of drying times for two cubes of different size is proportional to the ratio of the sample size squared.

Economic analysis of the atmospheric freeze-drying process is beyond the scope of this research, however, some observations can be made from the results presented concerning its practical usefulness. Obviously the rate of atmospheric freeze-drying is slow even in relatively small samples. The most promising area of the operating variable space is where h_D is high and sample size is small. This vicinity was of interest to Malecki, et al. (1969) but other problems concerning fluidization of frozen particles in the fluidized bed hampered the investigation. Perhaps other configurations of equipment which could investigate this domain of the operating variable space would meet with more success.

Economic viability of the process must be based on low capital investment for equipment and a continuous process. In both of these areas great improvement is possible over conventional freeze-drying.

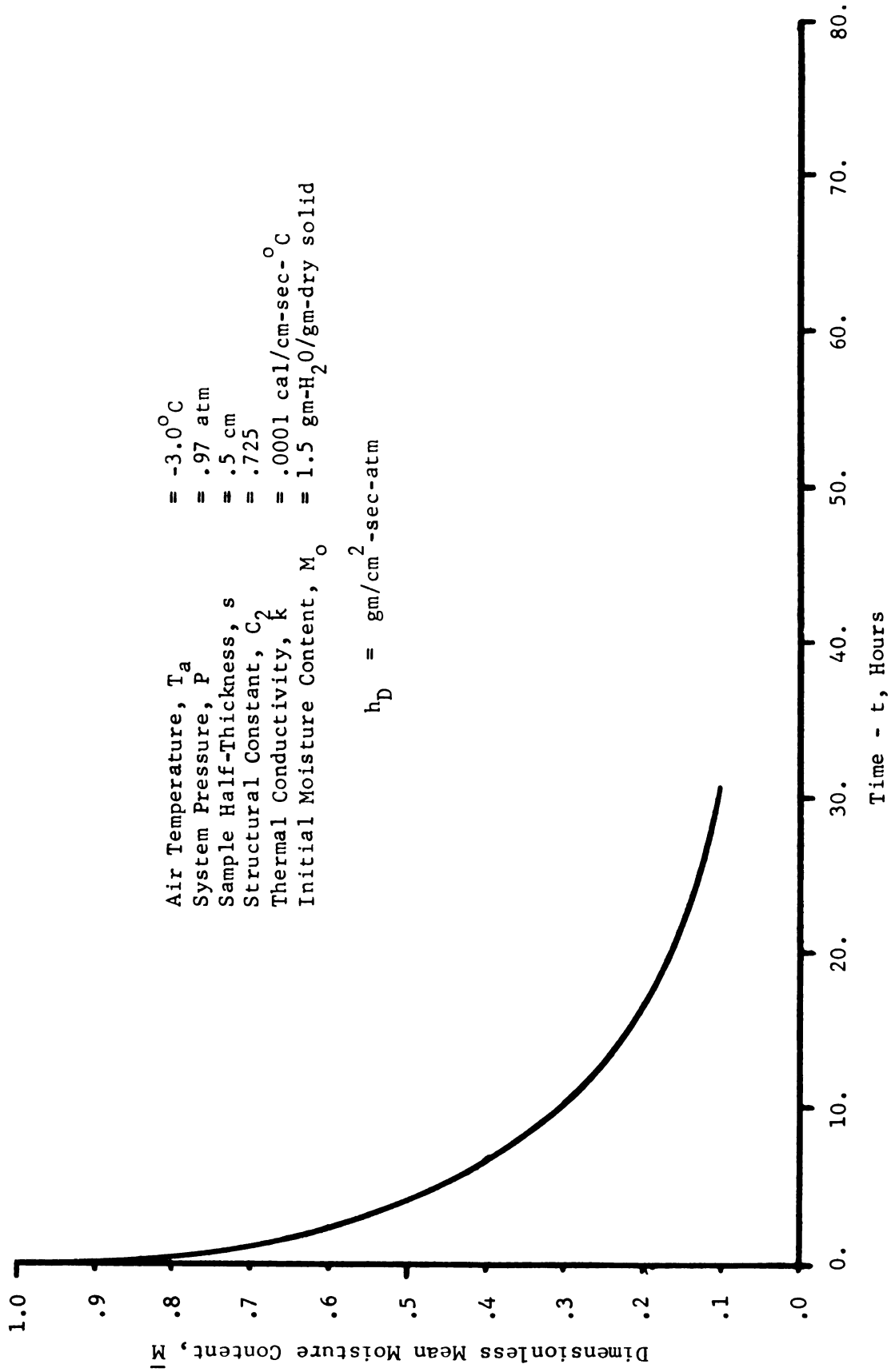


Figure 6.7. Predicted Maximum-Rate Drying Curve for Atmospheric Freeze-Drying of Cubical Samples of Precooked Beef.

CHAPTER VII

CONCLUSIONS

1. The rate of atmospheric freeze-drying in precooked beef was found to be adequately predicted by numerical solution of a mathematical model of simultaneous heat and mass transfer. The model assumed water vapor diffusion was the mechanism of mass transfer and thermal conduction was the heat transfer mechanism through the porous zone.

2. Nonlinear estimation of transport parameters in a mathematical model with an integrated dependent variable (mean moisture content) was successfully demonstrated.

3. The internal heat and mass transport parameters of atmospheric freeze-drying were evaluated by nonlinear estimation. The structural constant of the porous zone was evaluated at .81 for diffusion parallel to the fibers of the mean and .62 for diffusion perpendicular to the fibers. The mean value of the effective thermal conductivity was found to be .0001 cal/cm-sec-^oC.

4. The mechanism of thermal transport in the porous zone of a product under freeze-dehydration was shown to be largely limited to conduction through the solid fraction of the matrix. Counter-flow of water vapor substantially reduced the contribution by the porous fraction to the total heat transfer.

5. The process of atmospheric freeze-drying was analyzed in cubes of precooked beef by use of an approximate three-dimensional model. The operating variables of air temperature, system pressure, sample size and surface mass transfer coefficient were investigated. The rate of atmospheric freeze-drying was found to be strongly and directly related to air temperature. Sample size and the surface mass transfer coefficient were found to be the most promising variables to yield a practical process. Time to remove 90 percent of product moisture from one-centimeter cubes of cooked beef was approximately 30 hours for optimum conditions at atmospheric pressure. The drying time for other size cubes was proportional to the ratio of the sample size squared.

BIBLIOGRAPHY

BIBLIOGRAPHY

- Beck, J. V. 1966. Transient Determination of Thermal Properties. Nuclear Engineering and Design 3: 373-381.
- Beck, J. V. 1969A. Class Notes from M. E. 818, Estimation in Heat and Mass Transfer, Spring Term, 1969, Michigan State University, East Lansing.
- Beck, J. V. 1969B. Personal Communication.
- Burke, R. F. and R. V. Decareau. 1964. Recent Advances in Freeze-Drying of Food Products. Advances in Food Research 13: 1-89.
- Carmen, P. C. 1956. Flow of Gases Through Porous Media. Academic Press, New York.
- Crank, J. and P. Nicolson. 1947. A Practical Method for Numerical Evaluation of Solutions of Partial Differential Equations of the Heat Conduction Type. Proceedings of Cambridge Phil. Soc. 43 (17): 50-67.
- Deutsch, R. 1965. Estimation Theory. Prentice-Hall, Englewood Cliffs, N. J.
- Draper, N. R. and H. Smith. 1966. Applied Regression Analysis. John Wiley and Sons, Inc., New York.
- Dunoyer, J. M. and J. Larousse. 1961. Experiences Nouvelles sur la Lyophilisation. Trans. of Eighth Vacuum Symposium and Second International Congress 2: 1059-1063.
- Dyer, D. F. and J. E. Sunderland. 1966. Bulk and Diffusional Transport in the Region Between the Molecular and Viscous Conditions. International Journal of Heat and Mass Transfer 9: 519-526.
- Dyer, D. F. and J. E. Sunderland. 1968. Transfer Mechanisms in Sublimation Dehydration. Journal of Heat Transfer, ASME Trans. 90C: 379-384.
- Eckert, E. R. G. and R. M. Drake, Jr. 1959. Heat and Mass Transfer. McGraw-Hill Book Co., Inc., New York.

- Evans, R. B., G. M. Watson, and E. A. Mason. 1961. Gaseous Diffusion in Porous Media at Uniform Pressure. Journal of Chemical Physics 35: 2076-2083.
- Gunn, R. D. 1967. Mass Transport in Porous Media as Applied to Freeze-Drying. Ph.D. Dissertation, University of California, Berkeley.
- Gunn, R. D. and C. J. King. 1969. Mass Transport in Porous Materials Under Combined Gradients of Composition and Pressure. A.I.Ch.E. Journal 15(4): 507-514.
- Harper, J. C. and A. L. Tappel. 1957. Freeze-Drying of Food Products. Advances in Food Research 7: 172-235.
- Harper, J. C. 1962. Transport Properties of Gases in Porous Media at Reduced Pressures with Reference to Freeze-Drying. A.I.Ch.E. Journal 8(3): 298-302.
- Harper, J. C. and A. F. El Sahrighi. 1964. Thermal Conductivities of Gas-Filled Porous Solids. Industrial and Engineering Chemistry, Fundamentals 3(4): 318-324.
- Hohner, G. A. and D. R. Heldman. 1970. Computer Simulation of Freezing Rates in Foodstuffs. A paper to be presented before the Institute of Food Technology, San Francisco, Calif., May, 1970.
- Kan, B. and F. deWinter. 1966. The Acceleration of the Freeze-Drying Process Through Improved Heat Transfer. Paper presented at the 26th Annual Meeting of the Institute of Food Technology, Portland, Oregon, May, 1966.
- Krischer, O. 1959. Die Wissenschaftlichen Grundlagen der Trocknungstechnik. Springer, Berlin.
- Lambert, J. B. and W. R. Marshall, Jr. 1961. Heat and Mass Transfer in Freeze-Drying. In: Freeze-Drying of Foods., NAS-NRC publication, Frank R. Fisher, editor. 105-133.
- Lentz, C. P. 1961. Thermal Conductivity of Meats, Fats, Geletine Gels and Ice. Food Technology 15: 243-247.
- Lewin, L. M. and R. F. Mateles. 1962. Freeze-Drying Without Vacuum, a Preliminary Investigation. Food Technology 16(1): 94-97.
- Malecki, G. J., P. Shinde, A. I. Morgan, Jr., and D. F. Farkas. 1969. Atmospheric Fluidized-Bed Freeze-Drying of Apple Juice and Other Liquid Foods. Paper presented at the 29th Annual Meeting of the Institute of Food Technology, May, 1969, Chicago, Ill.

- Meeter, D. A. 1964. Program GAUSHAUS, Numerical Analysis Laboratory, University of Wisconsin, Madison.
- Meryman, H. T. 1959. Sublimation Freeze-Drying Without Vacuum. Science 130: 628.
- Meryman, H. T. 1964. Induction and Dielectric Heating for Freeze-Drying. In: Aspects Theoriques et Industriels de la Lyophilisation. 65-68.
- Mink, W. H. and G. F. Sachsel. 1961. Evaluation of Freeze-Drying Mechanisms Using Mathematical Models. In: Freeze-Drying of Foods, NAS-NRC publication, Frank R. Fisher, editor. 84-92.
- Ngoddy, P. O. 1969. A Generalized Theory of Sorption Phenomena in Biological Materials. Ph.D. Dissertation, Michigan State University, East Lansing.
- Peng, K. C. 1967. The Design and Analysis of Scientific Experiments. Addison-Wesley Co., Reading, Mass.
- Perry, J. H. 1950. Chemical Engineers' Handbook. McGraw-Hill Book Co., Inc., New York, 3rd Ed.
- Pfahl, R. C., Jr. and B. J. Mitchell. 1969. A General Method for Simultaneous Measurement of Thermal Properties. Preprint of a paper for presentation before the American Inst. of Aeronautics and Astronautics.
- Riedel, L. 1957. Kalorimetrische Untersuchungen über das Gefrieren von Fleisch. Kältetechnik 9(2): 38.
- Sandall, O. C. 1966. Interactions Between Heat and Mass Transfer in Freeze-Drying. Ph.D. Dissertation, University of California, Berkeley.
- Sandall, O. C., C. J. King and C. R. Wilke. 1967. The Relationship Between Transport Properties and Rates of Freeze-Drying of Poultry Meat. A.I.Ch.E. Journal 13(3): 428-438.
- Saravacos, G. D. and M. M. Pilsworth, Jr. 1965. Thermal Conductivity of Freeze-Dried Model Food Gels. Journal of Food Science 30: 773-776.
- Saravacos, G. D. and R. M. Stinchfield. 1965. Effect of Temperature and Pressure on the Sorption of Water Vapor by Freeze-Dried Food Materials. Journal of Food Science 30(5): 779-785.
- Scheidegger, A. E. 1957. The Physics of Flow Through Porous Media. MacMillian Co., New York.

- Scott, D. S. and F. A. L. Dullien. 1962. Diffusion of Ideal Gases in Capillaries and Porous Solids. A.I.Ch.E. Journal 8: 113-117.
- Short, B. E. and H. E. Staph. 1951. The Energy Content of Foods. Ice and Refrigeration 121(5): 23.
- Smith, G. D. 1965. Numerical Solution of Partial Differential Equations. Oxford University Press. New York and London.
- Snedecor, G. W. 1956. Statistical Methods. Iowa State University Press, Ames, Iowa.
- Threlkeld, J. L. 1962. Thermal Environmental Engineering. Prentice-Hall, Inc., Englewood Cliffs, N. J.
- Triebes, T. A. and C. J. King. 1966. Factors Influencing the Rate of Heat Conduction in Freeze-Drying. Ind. and Eng. Chem., Process Design and Development 5(4): 430-436.
- Wakao, N., S. Otani, and J. M. Smith. 1965. Significance of Pressure Gradients in Porous Materials: Part 1. Diffusion and Flow in Fine Capillaries, A.I.Ch.E. Journal 11: 435-439.
- Woodward, H. T. 1961. Study of Vapor Removal Systems in Dehydration of Food Products Having Piece or Block Conformation. Quartermaster Contract Report (DA 19-129-QM-1597).
- Woodward, H. T. 1963. Freeze-Drying Without Vacuum. Food Engineering 35(6): 96-98.

APPENDICES

APPENDIX I

DERIVATION OF THE ENERGY EQUATION, EQUATION (3.1)

From an energy balance at constant pressure on a differential volume of the porous zone, $dV = Adx$, the following equation for transport in the (x) direction is obtained:

$$dV\rho(C_{pd} + MC_{pw})\frac{\partial T}{\partial t} = A \left[\left(k\frac{\partial T}{\partial x} \right)_{x+dx} - \left(k\frac{\partial T}{\partial x} \right)_x + C_{pw}(\dot{m}T)_x - C_{pw}(\dot{m}T)_{x+dx} \right] + dV\rho\Delta H_v \left(\frac{\partial M}{\partial t} \right). \quad (A.1)$$

Variables at (x+dx) are expanded by Taylor Series in terms of the same variables at (x).

$$\left(k\frac{\partial T}{\partial x} \right)_{x+dx} = \left(k\frac{\partial T}{\partial x} \right)_x + dx \frac{\partial}{\partial x} \left(k\frac{\partial T}{\partial x} \right)_x + \dots \quad (A.2)$$

$$(\dot{m}T)_{x+dx} = (\dot{m}T)_x + dx \frac{\partial}{\partial x} (\dot{m}T)_x + \dots \quad (A.3)$$

Since the fraction of mass flux moving through dV was much greater than the change in mass flux rate in dV , (\dot{m}) was considered independent of (x). Also, the mass flux rate can be written in terms of vapor the pressure gradient,

$$\dot{m} = D_e \frac{\partial P_v}{\partial x}, \quad (A.4)$$

and then

$$(\dot{m}T)_{x+dx} = -D_e \frac{\partial P_v}{\partial x} \left[T_x + dx \left(\frac{\partial T}{\partial x} \right)_x \right]. \quad (A.5)$$

Substitution of equations (A.2) and (A.5) into (A.1) followed by appropriate simplification gives,

$$\rho (C_{pd} + MC_{pw}) \frac{\partial T}{\partial t} = \frac{\partial}{\partial x} \left(k \frac{\partial T}{\partial x} \right) + C_{pw} \frac{D}{e} \frac{\partial^2 v}{\partial x^2} \left(\frac{\partial T}{\partial x} \right) + \rho \Delta H_v \left(\frac{\partial M}{\partial t} \right), \quad (\text{A.6})$$

the heat transfer equation of the porous zone. It was desirable to express the equation in terms of the dimensionless variables: $\theta = Dt/s^2$ and $\phi = x/s$. Substitution of θ and ϕ into (A.6) gives the energy equation.

$$\rho (C_{pd} + MC_{pw}) \frac{\partial T}{\partial \theta} = \frac{\partial}{\partial \phi} \left(\frac{k}{D} \frac{\partial T}{\partial \phi} \right) + C_{pw} \frac{D}{e} \frac{\partial^2 v}{\partial \phi^2} \left(\frac{\partial T}{\partial \phi} \right) + \rho \Delta H_v \left(\frac{\partial M}{\partial \theta} \right) \quad (3.1)$$

APPENDIX II

DERIVATION OF THE MASS TRANSFER EQUATION, EQUATION (3.2)

The water vapor transport equation for atmospheric freeze drying is derived from a mass balance on a volume element of the porous zone of the sample. The volume element, $dV = Adx$, was assumed to have constant porosity, e . The one-dimensional transport of water was assumed to be solely by vapor diffusion. Water vapor was assumed to behave as an ideal gas so mass concentration can be expressed as $M_w P_v / RT$. Then,

$$dV \frac{eM_w}{RT} \frac{\partial P_v}{\partial t} = A \left[\left(-D_e \frac{\partial P_v}{\partial x} \right)_x - \left(-D_e \frac{\partial P_v}{\partial x} \right)_{x+dx} \right] - dV \rho \frac{\partial M}{\partial t} . \quad (A.7)$$

Expanding the vapor flux at $(x+dx)$ in terms of a Taylor Series gives

$$\left(-D_e \frac{\partial P_v}{\partial x} \right)_{x+dx} = \left(-D_e \frac{\partial P_v}{\partial x} \right)_x + dx \frac{\partial}{\partial x} \left(-D_e \frac{\partial P_v}{\partial x} \right) + \dots \quad (A.8)$$

Substitution of equation (A.8) into (A.7) and simplification gives the mass transfer equation.

$$\left(\frac{eM_w}{RT} \right) \frac{\partial P_v}{\partial t} = \frac{\partial}{\partial x} \left(D_e \frac{\partial P_v}{\partial x} \right) - \rho \frac{\partial M}{\partial t} \quad (A.9)$$

Equation (A.9) is expressed in terms of dimensionless independent variables, $\theta = Dt/s^2$ and $\phi = x/s$ to give equation (3.2)

$$\left(\frac{eM_w}{RT} \right) \frac{\partial P_v}{\partial \theta} = \frac{\partial}{\partial \phi} \left(\frac{D_e}{D} \frac{\partial P_v}{\partial \phi} \right) - \rho \frac{\partial M}{\partial \theta} . \quad (3.2)$$

APPENDIX III

DERIVATION OF FINITE DIFFERENCE APPROXIMATIONS OF THE HEAT AND MASS TRANSFER EQUATIONS, EQUATIONS (3.18) AND (3.19)

Finite difference approximations of the heat and mass transfer equation were required for the numerical solution. Considering the heat transfer equation first and using the backward-difference approximation (Smith, 1965), the change in internal energy in differential volume element $dV = Ad\phi$ during time step $\Delta\theta$ can be written

$$\begin{aligned} \Delta\phi\rho(C_{pd} + MC_{pw})_i^n \left(\frac{T_i^{n+1} - T_i^n}{\Delta\theta} \right) &= \frac{k}{D} \left[\frac{T_{i+1}^{n+1} - T_i^{n+1}}{\Delta\phi} - \frac{T_i^{n+1} - T_{i-1}^{n+1}}{\Delta\phi} \right] \\ &+ C_{pw} \frac{D}{e} \left(\frac{P_{i+1}^{n+1} - P_{i-1}^{n+1}}{2\Delta\phi} \right) \left(\frac{T_{i+1}^{n+1} - T_{i-1}^{n+1}}{2} \right) + \Delta\phi\rho\Delta H_v \left(\frac{M_i^{n+1} - M_i^n}{\Delta\theta} \right). \end{aligned} \quad (A.10)$$

Equation (A.10) is rearranged to yield equation (3.19),

$$\begin{aligned} \rho(C_{pd} + MC_{pw})_i^n (T_i^{n+1} - T_i^n) &= ZZ(T_{i+1}^{n+1} + T_{i-1}^{n+1} - 2T_i^{n+1}) \\ &+ \frac{C_{pw}Z}{4}(P_{i+1}^{n+1} - P_{i-1}^{n+1})(T_{i+1}^{n+1} - T_{i-1}^{n+1}) + \rho\Delta H_v(M_i^{n+1} - M_i^n). \end{aligned} \quad (3.19)$$

The mass transfer equation in finite difference form is derived from a mass balance on the void space of a differential volume element, $e dV = eAd\phi$, during time step $\Delta\theta$. The Crank-Nicolson approximation (Smith, 1965) is used and all coefficients are evaluated in the (n)th time frame.

$$\Delta\phi \left(\frac{eM_w}{RT} + \frac{\rho}{P_{\text{sat}}} \frac{dM}{dr} \right)_i^n \left(\frac{P_i^{n+1} - P_i^n}{\Delta\theta} \right) = \frac{D}{2D} \left[\frac{P_{i-1}^{n+1} - P_i^{n+1}}{\Delta\phi} + \frac{P_{i-1}^n - P_i^n}{\Delta\phi} - \frac{P_i^{n+1} - P_{i+1}^{n+1}}{\Delta\phi} - \frac{P_i^n - P_{i+1}^n}{\Delta\phi} \right]. \quad (\text{A.11})$$

Equation (A.11) is rearranged to yield equation (3.18),

$$\left(\frac{eM_w}{RT} + \frac{\rho}{P_{\text{sat}}} \frac{dM}{dr} \right)_i^n (P_i^{n+1} - P_i^n) = \frac{Z}{2} \left[P_{i+1}^{n+1} + P_{i-1}^{n+1} - 2P_i^{n+1} + P_{i+1}^n + P_{i-1}^n - 2P_i^n \right]. \quad (3.18)$$

APPENDIX IV

COMPUTER PROGRAM MAIN AND SUBROUTINE MODEL

```
PROGRAM MAIN
DIMENSION W(100),TIM(100)
DIMENSION TH(3),SIGNS(3),DIFF(3)
COMMON TS,TIM,DAW,MI,S,TWR,PS
EXTERNAL MODEL
NP =3
D01?J=1.1
READ(60,7) NOR,NTFST
7 FORMAT(2I5)
DO 10 I=1,NOR
10 READ(60,9) W(I),TIM(I)
9 FORMAT(F8.1,F10.1)
READ(60,8) TS,DAW,MI,S,TWR,PS,TH(1),TH(2),TH(3)
8 FORMAT(9F8.0)
DO 11 I=1,NP
SIGNS(I)=1.
11 DIFF(I)=.01
EPS1=1.0E-3
EPS2=1.0E-2
CALL GAUSHAUS(NTFST,MODEL,NOR,W,NP,TH,DIFF,SIGNS,EPS1,
1EPS2,20,.01,10.)
12 CONTINUE
END
```

```

SUBROUTINE MODEL (NPROB,TH,WFT,NOR,NP)
DIMENSION TH(1),WFT(1),TIM(100)
DIMENSION T(31),P(31),M(31),A(30,31),AA(31),AS(31)
DIMENSION OLDM(31),PSAT(31),DMDP(31),PI(31),TI(31)
DIMENSION OLDP(31),T5(31)
COMMON TS,TIM,DAW,MI,S,TWB,PS
REAL M,MI,MF
C  CONSTANTS OF THE MODEL ARE LISTED BELOW
C  UNITS OF THE MODEL ARE GM SEC CM ATM CALORIE K
C
C      RS= BULK DENSITY OF DRY PRODUCT
C      CPW= SPECIFIC HEAT OF WATER
C      CPS = SPECIFIC HEAT OF DRY PRODUCT
C      E = POROSITY OF DRY PRODUCT
C      DAW = FREE GAS MUTUAL DIFFUSIVITY, AIR AND WATER VAPOR
C      PA = VAPOR PRESSURE OF AIR STREAM
C      DHV = HEAT OF VAPORIZATION
C      DHS = HEAT OF SUBLIMATION, ICE
C      MI= INITIAL MOISTURE CONTENT
C      S = HALF THICKNESS OF SAMPLE
C      NN= NUMBER OF SPACE NODES
C      TIMWB = TIME REQUIRED TO DROP CENTERLINE TEMP TO WET-
C              BULB TEMPERATURE OF AIR STREAM
C      TWB = WET-BULB TEMPERATURE OF AIR STREAM
C      MF = SATURATION EQUILIBRIUM MOISTURE CONTENT
C      PS = SATURATION VAPOR PRESSURE OF ICE AT TWB
C      FK = TH(3)
C      RS=.46
C      CPW=1.
C      CPS=.38
C      CPC= 1.15
C      E=.76
C      PA=0.0
C      DHV=850.
C      DHS= 676.
C      NN=11
C      TIMWB= 300.
C      MF=.2
C
C  MODEL ASSUMES SUBLIMATION IS FROM FREE ICE SURFACE WHILE
C  CENTERLINE DROPS FROM T-AIR TO T-WET BULB
C
C      ENN=NN
C      KK=2
C      WFT(1) =1.0
C      DF=TIMWB*TH(1)*(PS-PA)*S/(RS*(MI-MF)*DAW)
C      F=1.-DF
C      DR=1./(ENN-1.)
C      DT=20.*DR*DAW/(S*TH(1))
C      K=0
C      DO 10 I=1,NN
C      T(I)=TWB
C      P(I)=PS
10  M(I)=MI

```

```

TIME = TIME + DT
NN1 = NN - 1
NFHOLD = NN
DRHLD = DF
Z7 = TH(3) * DT / ((DR**2) * DAW)
H = DT * TH(1) * S / (DAW * DR)
TC = TWB
11 K = K + 1
TIME = TIME + DT
IF (F.LE.0.) F = 0.
IF (K.GT.1) NFHOLD = NF
NF = (1.-F) / DR
NF = NN - NF
IF (F.EQ.0.) NF = 2
IF (NFHOLD.LF.NF) GO TO 12
RATIO = ((ENF - 2.) * DR - F) / ((ENF - 1.) * DR - F)
T(NF) = T(NF2) + RATIO * (T(NF + 1) - T(NF2))
P(NF) = P(NF2) + RATIO * (P(NF + 1) - P(NF2))
M(NF) = M(NF2) + RATIO * (M(NF + 1) - M(NF2))
XX = TC - 243.15
P(NF - 1) = (.255886464376 + .044891607089 * XX - .00061794492312
1 * (XX**2) + .00012993021895 * (XX**3)) / 760.
M(NF - 1) = MF
T(NF - 1) = TC
12 IF (K.GT.1) DRHLD = DR2
NF2 = NF - 1
NF1 = NF + 1
ENF = NF
DR2 = 1.-F - (ENN - ENF) * DR
DR2BR = (DR2 + DRHLD) / 2.
IF (NFHOLD.GT.NF) DR2BR = DR2
DO 20 I = NF2, NN
OLDP(I) = P(I)
OLDM(I) = M(I)
XX = T(I) - 243.15
PSAT(I) = (.255886464376 + .044891607089 * XX - .00061794492312 *
1 * (XX**2) + .00012993021895 * (XX**3)) / 760.
DMDP(I) = .2 / PSAT(I)
20 P1(I) = .219 * F / T(I) + RS * DMDP(I)
IF (F.GT.0.) OLDP(NF2) = PSAT(NF2)
Z = DT * TH(2) * .438 / ((T(NF2) + T(NN)) * (DR**2))
IF (F.GT.0.) OLDM(NF2) = 1F
IF (1.-F - DR) 21, 21, 22
21 T(NN) = TS
T(NF2) = TC
P(NF2) = PSAT(NF2)
P1(NN) = 2. * P1(NN)
P2 = P1(NN) + Z * ((DR / DR2)**2) + S * TH(1) * DT / (DR2)
P(NN) = (P1(NN) * OLDP(NF) + 7 * ((DR / DR2)**2) * (P(NF2) + OLDP(NF2)
1 - OLDP(NF)) - TH(1) * DT * (OLDP(NF) - 2. * PA) / (DR2)) / P2
DP = (P(NF) - P(NF2)) / DR2
OLDDP = (OLDP(NF) - OLDP(NF2)) / (DRHLD)
F = F + .5 * S * Z * (DR**2) * (DP + OLDDP) / (RS * (M1 - MF))
TC = TC + (DHS * Z * .5 * (DP + OLDDP) + Z7 * (T(NF) - T(NF2)) / DR2) * (DR**2)

```

```

1 *S/(F*RS*(1.+MI)*CPC)
19 M(NF2)=MF
   M(NN)= .2*P(NN)/PSAT(MN)
   WT=F+.5*(1.-F)*(MF+M(NN))/MI
   GO TO 101
22 IF(F) 23,23,24
23 A(1,1)=P1(1)+ Z
   A(1,2)=- Z
   A(1,NN+1)=(P1(1)- Z)*P(1)+ Z*P(2)
   GO TO 25
24 IF(DR2-1.0F-5) 26,26,27
26 A(NF,NF-1)=0.0
   A(NF,NF)=1.0
   A(NF,NF+1)=0.0
   A(NF,NN+1)=OLDDP(NF)
   GO TO 28
27 A(NF,NF-1)=-Z*DR/DR2
   A(NF,NF+1)=-Z
   A(NF,NF)=2.*P1(NF)*( .5+DR2HR/DR)-A(NF,NF2)-A(NF,NF1)
   A(NF,NN+1)=P(NF)*(A(NF,NF)+A(NF,NF-1)+A(NF,NF+1))
1 -A(NF,NF-1)*(P(NF-1)-P(NF))+A(NF,NF+1)*(P(NF)-P(NF+1))
28 A(NF2,NF2)=1.0
   A(NF2,NF)=0.0
   A(NF2,NN+1)=PSAT(NF2)
   IF(NF.EQ.NN1) GO TO 31
25 II=NF
   IF(F.GT.0.) II=NF1
   DO 30 I=II,NN1
   A(I,I-1)=-Z
   A(I,I)=2.*(P1(I)+Z)
   A(I,I+1)=-Z
30 A(I,NN+1)= Z*P(I-1)+2.*(P1(I)-Z)*P(I)+Z*P(I+1)
31 A(NN,NN-1)= .25*P1(NN)-Z
   A(NN,NN)= .75*P1(NN)+Z+H
   A(NN,NN+1)=( .25*P1(NN)+Z)*P(NN-1)+( .75*P1(NN)-Z+H)
1 *P(NN)+2.*H*PA
   AS(NF2 )=A(NF-1,NN+1)
   AA(NF2 )=A(NF-1,NF-1)
   DO 35 I=NF,NN
   AA(I)=A(I,I)-A(I,I-1)*A(I-1,I)/AA(I-1)
35 AS(I)=A(I,NN+1)-A(I,I-1)*AS(I-1)/AA(I-1)
   P(NN)=AS(NN)/AA(NN)
   NNF=NN-NF2
   DO 40 I=1,NNF
   J=NN-I
40 P(J)=(AS(J)-A(J,J+1)*P(J+1))/AA(J)
   IF(F.GT.0.) P(NF2)=PSAT(NF2)
   DO 50 I=NF2,NN
50 M(I)= .2*P(I)/PSAT(I)
   IF(F.GT.0.) M(NF2)=MF
   OLDDP=DP
   IF(DR2-1.0F-3) 48,48,49
49 DP=(DR2+DR)*(P(NF)-P(NF2))/(DR*DR2)+DR2*(P(NF2)
1 -P(NF1))/(DR*(DR+DR2))

```

```

GO TO 47
48 DP=(P(NF1)-P(NF2))/(DR+DR2)
47 IF(((TS-T(NF2))/TS).GT. .001) GO TO 59
TC=TS
DO 58 I=NF2,NN
58 T(I)=TS
GO TO 91
59 DO 60 I=NF2,NN
T1(I)=RS*(CPS+M(I)*CPW)
60 T5(I)=RS*DHV*(M(I)-O1DM(I))
IF(F.GT. .001) GO TO 52
51 A(1,1)=T1(1)+ZZ-.25*Z*CPW*(P(1)-P(2)+OLDP(1)-OLDP(2))
A(1,2)= .25*Z*CPW*(P(1)-P(2)+OLDP(1)-OLDP(2)) -ZZ
A(1,NN+1)=T(1)*(T1(1)*2.-A(1,1))-T(2)*A(1,2)+15(1)
GO TO 53
52 IF(DR2 -1.0E-5) 54,54,55
54 A(NF2,NF2) =1.
A(NF2,NF)=0.0
A(NF2,NN+1)=TC
A(NF,NF2) =0.0
A(NF,NF) =1.0
A(NF,NF1) =0.0
A(NF,NN+1) =T(NF)
GO TO 53
55 A(NF2,NF2)=F*RS*CPC*(1.+MI)+ ZZ*S*(DR**2)/DR2
A(NF2,NF)=- S*Z*(DR**2)/DR2
A(NF2,NN+1)=T(NF2)*F*RS*(1.+MI)*CPC+ DHS*S*Z*(DR**2)*DP
56 T2= (.5+DR2RZ/DR)*T1(NF)
T3=ZZ
T4= ZZ*DR/DR2
T6=-.25*Z*CPW*(P(NF1)+P(NF)-2.*P(NF2))/(.5+DR2/DR)
A(NF,NF2)=-T4-2.*T6
A(NF,NF)=T2+T3+T4+T6
A(NF,NF+1)=-T3+T6
A(NF,NN+1)=T(NF)*T2
53 II=NF
IF(F.GT.0.) II=NF1
IF(II.GT.NN1) GO TO 71
DO 70 I=II,NN1
A(I,I-1)=-ZZ+.25*CPW**Z*(P(I+1)-P(I-1))
A(I,I)=T1(I)+ZZ*2.
A(I,I+1)=-A(I,I-1)-ZZ*2.
A(I,NN+1)=T1(I)*T(I)
IF(F.LE. 0.0) A(I,NN+1)=T1(I)*T(I)+15(I)
70 CONTINUE
71 A(NN,NN-1)=0.0
A(NN,NN)=1.
A(NN,NN+1)=TS
AS(NF2)=A(NF2,NN+1)
AA(NF2)=A(NF2,NF2)
DO 80 I=NF,NN
AA(I)=A(I,I)-A(I,I-1)*A(I-1,I)/AA(I-1)
80 AS(I)=A(I,NN+1)-A(I,I-1)*AS(I-1)/AA(I-1)
T(NN)=AS(NN)/AA(NN)

```

```

      DO 90 I=1,NNF
      J=NN-I
  90  T(J)=(AS(J)-A(J,J+1)*T(J+1))/AA(J)
  91  WT=F*MI+.5*DR*(M(NF)+M(NF))
      IF(F.EQ.0.0) WT=.5*DR*(M(1)+M(2))
      DO 100 I=NF,NN1
  100  WT=WT+.5*DR*(M(I)+M(I+1))
      WT=WT/MI
  101  IF(ABS(TIME-TIM(KK)).GT. .5*DT) GO TO 102
      WFT(KK)=WT
      WRITE(61,122) WFT(KK)
  122  FORMAT(* *,F6.4)
      KK=KK+1
  102  IF(F.EQ. 0.0 .OR. NF.EQ. NN) GO TO 103
      DFP=Z*(DR**2)*.5*(DP+OLDP)*S/(RS*(MI-MF))
      F=F+DFP
  103  IF(KK.GT.NOR) GO TO 104
      IF(M(1).GT. .02) GO TO 11
  106  DO 107 I=KK,NOR
  107  WFT(I) =0.0
  104  RETURN
      END

```

APPENDIX V

SUMMARY OF RESULTS FROM PARAMETER ESTIMATION TESTS

Test number: 1	Fiber orientation: parallel
Air Temperature: -8.2 ^o C	Sample Half-thickness: .477 cm
System Pressure: .97 atm	Initial Moisture Content: 1.477

<u>Dimensionless Time</u> <u>$\theta \times 10^{-4}$</u>	<u>Experimental Dimensionless</u> <u>Mean Moisture Content, \bar{M}</u>	<u>Computed</u> <u>Residual</u>
0.00	1.000	.000
.38	.959	.008
1.70	.876	.002
2.30	.847	.000
2.69	.833	.001
3.07	.815	-.003
6.62	.704	.008
7.29	.679	.002
8.05	.657	.000
8.92	.635	-.001
9.21	.628	-.001
9.79	.614	-.001
10.55	.600	.002
11.13	.585	.000
11.51	.576	-.001
11.90	.569	.000
15.54	.495	-.004
16.12	.485	-.003
16.88	.474	-.001
17.65	.465	.003
18.04	.456	.000
18.61	.442	-.004
19.00	.436	-.004
19.86	.416	-.010
20.43	.409	-.008
21.11	.402	-.005
25.71	.337	-.003
26.29	.330	-.002
26.86	.327	.003
27.63	.319	.005
28.40	.310	.006
30.70	.280	.006
36.36	.215	.009

Test number: 2	Fiber orientation: parallel
Air temperature: -8.2°C	Sample half-thickness: .420 cm
System pressure: .97 atm	Initial moisture content: 1.505

<u>Dimensionless Time</u> <u>$\theta \times 10^{-4}$</u>	<u>Experimental Dimensionless</u> <u>Mean Moisture Content, \bar{M}</u>	<u>Computed</u> <u>Residual</u>
.00	1.000	.000
.43	.955	.002
.87	.924	-.003
1.30	.899	-.003
1.74	.877	.002
2.17	.854	.001
2.61	.837	.004
7.06	.658	.001
7.82	.635	.002
8.48	.613	.000
9.13	.594	.000
9.56	.585	.003
10.36	.561	.000
11.08	.543	.000
11.95	.517	-.004
12.61	.500	-.005
13.26	.490	.000
17.39	.408	.005
18.26	.389	.003
19.13	.372	.002
20.00	.354	.000
20.86	.337	-.001
21.30	.330	.000
22.39	.309	-.002
23.04	.299	-.001
23.69	.285	-.004
28.26	.208	-.008
29.12	.191	-.012
30.00	.181	-.009
30.86	.167	-.010
31.73	.153	-.012
32.82	.139	-.010
33.47	.129	-.011
34.12	.118	-.013
38.25	.083	.007
39.12	.070	.011
39.99	.063	.025

Test number: 3	Fiber orientation: parallel
Air temperature: -2.8°C	Sample half-thickness: .405 cm
System pressure: .97 atm	Initial moisture content: 1.723

<u>Dimensionless Time</u> <u>$\theta \times 10^{-4}$</u>	<u>Experimental Dimensionless</u> <u>Mean Moisture Content, M</u>	<u>Computed</u> <u>Residual</u>
.00	1.000	.000
.48	.940	.015
1.09	.883	.010
1.58	.843	.002
2.06	.800	-.014
2.55	.760	-.027
2.91	.733	-.029
3.40	.700	-.032
7.64	.526	-.016
8.12	.513	-.012
8.61	.496	-.012
9.34	.472	-.012
10.06	.451	-.011
10.55	.436	-.011
11.16	.419	-.010
11.52	.409	-.009
13.10	.366	-.008
14.67	.319	-.015
19.52	.215	-.005
20.01	.205	-.006
20.49	.194	-.006
21.10	.184	-.003
21.83	.172	-.001
22.80	.159	.006
23.28	.152	.009

Test number: .4
 Air temperature: -2.8°C
 System pressure: .97 atm

Fiber orientation: perpendicular
 Sample half-thickness: .472 cm
 Initial moisture content: 2.01

<u>Dimensionless Time</u> $\times 10^{-4}$	<u>Experimental Dimensionless</u> <u>Mean Moisture Content, M</u>	<u>Computed</u> <u>Residual</u>
.00	1.000	.000
.43	.937	.003
.86	.893	-.002
1.29	.857	-.001
1.72	.825	-.004
2.15	.799	-.007
2.58	.773	-.004
3.43	.731	.003
3.86	.708	.002
4.29	.689	.004
4.72	.671	.006
5.15	.653	.006
9.01	.515	.006
9.66	.498	.009
10.30	.476	.005
10.95	.452	-.000
11.66	.439	.006
12.23	.420	.003
12.77	.407	.004
13.88	.378	.003
14.30	.368	.003
14.74	.355	.000
15.17	.345	.000
19.32	.248	-.005
19.96	.235	-.004
20.61	.222	-.004

Test number: 5	Fiber orientation: perpendicular
Air Temperature: -2.8 ^o C	Sample half-thickness: .460 cm
System pressure: .97 atm	Initial moisture content: 1.688

<u>Dimensionless Time</u> <u>$\theta \times 10^{-4}$</u>	<u>Experimental Dimensionless</u> <u>Mean Moisture Content, M</u>	<u>Computed</u> <u>Residual</u>
.00	1.000	.000
.38	.943	.001
.75	.911	.000
1.13	.881	.003
1.50	.854	.002
1.88	.830	.000
2.73	.782	-.004
3.29	.760	-.001
3.85	.734	-.005
7.57	.602	.002
8.06	.585	.001
8.64	.572	.007
9.21	.554	.006
9.78	.539	.007
10.34	.525	.010
10.81	.511	.009
11.84	.489	.014
12.22	.477	.012
12.60	.469	.014
16.54	.359	-.004
17.10	.346	-.005
17.67	.336	-.003
18.23	.311	-.005
19.36	.299	-.006
19.93	.288	-.006
20.87	.271	-.004
21.25	.265	-.005
21.53	.260	-.003
21.90	.254	-.002
25.47	.196	.004
26.04	.188	.006

Test number: 6	Fiber orientation: perpendicular
Air temperature: -2.8°C	Sample half-thickness: .405 cm
System pressure: .97 atm	Initial moisture content: 1.757

<u>Dimensionless Time</u> <u>$\times 10^{-4}$</u>	<u>Experimental Dimensionless</u> <u>Mean Moisture Content, \bar{M}</u>	<u>Computed</u> <u>Residual</u>
.00	1.000	.000
.48	.932	.001
1.13	.869	-.011
1.45	.846	-.013
1.94	.816	-.016
2.43	.790	-.023
3.15	.756	-.018
3.64	.734	-.016
4.17	.711	-.017
5.34	.669	-.013
5.82	.653	-.012
6.31	.634	-.015
6.79	.620	-.014
11.64	.490	-.012
12.37	.476	-.009
13.10	.459	-.010
13.82	.443	-.010
14.60	.424	-.012
15.28	.411	-.011
16.81	.380	-.012
17.46	.367	-.012
18.19	.353	-.013
23.52	.262	-.010
24.73	.245	-.008
25.46	.233	-.008
26.19	.222	-.008
26.92	.213	-.005
27.40	.206	-.005
34.00	.133	.016

Test number: 7	Fiber orientation: perpendicular
Air temperature: -8.2°C	Sample half-thickness: .477 cm
System pressure: .97 atm	Initial moisture content: 1.813

<u>Dimensionless Time</u> <u>$\times 10^{-4}$</u>	<u>Experimental Dimensionless</u> <u>Mean Moisture Content, M</u>	<u>Computed</u> <u>Residual</u>
.00	1.000	.000
.46	.956	.004
.92	.921	-.003
1.39	.898	.001
2.36	.844	-.001
2.82	.824	-.001
3.28	.805	-.002
3.74	.791	.002
8.36	.662	.006
9.05	.646	.006
9.79	.626	.003
10.16	.616	.001
10.86	.597	-.003
11.55	.582	-.004
12.01	.572	-.005
13.28	.549	-.004
13.97	.536	-.005
14.67	.522	-.006
18.94	.459	.001
19.55	.449	.001
20.33	.438	.001
21.02	.429	.003
21.71	.420	.004
22.17	.410	.000
22.87	.399	-.001
24.03	.382	-.002
24.71	.374	-.001
25.41	.363	-.002
29.80	.308	-.001
30.49	.300	-.001
31.18	.292	.000
31.87	.283	-.001
32.57	.276	.000
33.26	.269	.001
33.95	.262	.002
35.10	.251	.004
35.80	.242	.003
36.49	.236	.005
40.61	.182	-.005

Test number: 8	Fiber orientation: perpendicular
Air temperature: -8.2°C	Sample half-thickness: .472 cm
System pressure: .97 atm	Initial moisture content: 2.01

<u>Dimensionless Time</u> <u>$\theta \times 10^{-4}$</u>	<u>Experimental Dimensionless</u> <u>Mean Moisture Content, M</u>	<u>Computed</u> <u>Residual</u>
.00	1.000	.000
.36	.946	-.006
.90	.894	-.024
1.26	.872	-.023
1.80	.843	-.021
2.33	.816	-.023
2.69	.799	-.025
3.41	.772	-.025
3.95	.749	-.025
4.49	.732	-.022
8.26	.619	-.021
8.88	.606	-.020
9.34	.592	-.021
9.88	.581	-.019
10.41	.568	-.020
10.90	.556	-.021
12.43	.525	-.019
12.93	.515	-.019
13.47	.505	-.018
17.42	.438	-.012
18.38	.425	-.009
18.86	.417	-.009
19.40	.410	-.007
19.93	.401	-.008
20.48	.392	-.008
21.02	.388	-.003
25.33	.325	-.002
25.87	.321	.001
26.76	.307	.000
27.30	.301	.001
29.10	.278	.002
29.64	.273	.004

Test number: 9
Air temperature: -2.8°C
System pressure: .58 atm

Fiber orientation: parallel
Sample half-thickness: .385 cm
Initial moisture content: 1.488

<u>Dimensionless Time</u> <u>$\theta \times 10^{-4}$</u>	<u>Experimental Dimensionless</u> <u>Mean Moisture Content, \bar{M}</u>	<u>Computed</u> <u>Residual</u>
.00	1.000	.000
.45	.957	.013
.90	.924	.015
1.80	.863	.017
2.70	.809	-.008
3.59	.766	.004
4.49	.722	.006
5.39	.686	.010
6.29	.647	.007
8.54	.567	.005
9.44	.535	.002
10.33	.513	.007
11.23	.488	.008
19.77	.283	.004
20.67	.261	.000
21.57	.243	.001

Test number: 10	Fiber orientation: parallel
Air temperature: -2.8°C	Sample half-thickness: .394 cm
System pressure: .58 atm	Initial moisture content: 1.48

<u>Dimensionless Time</u> <u>$\theta \times 10^{-4}$</u>	<u>Experimental Dimensionless</u> <u>Mean Moisture Content, \bar{M}</u>	<u>Computed</u> <u>Residual</u>
.00	1.000	.000
.86	.914	.014
1.72	.849	.013
2.57	.795	-.021
4.81	.671	.003
5.58	.637	.008
6.43	.599	.011
7.29	.562	.010
8.15	.531	.015
15.87	.267	-.002
16.73	.243	-.002
17.59	.216	-.007
18.44	.192	-.009
19.30	.178	-.002
20.16	.161	-.002

Test number: 11	Fiber orientation: perpendicular
Air temperature: -2.8°C	Sample half-thickness: .450 cm
System pressure: .58 atm	Initial moisture content: 1.027

<u>Dimensionless Time</u> <u>$\theta \times 10^{-4}$</u>	<u>Experimental Dimensionless</u> <u>Mean Moisture Content, \bar{M}</u>	<u>Computed</u> <u>Residual</u>
.00	1.000	.000
.33	.922	-.003
.66	.901	.013
1.32	.845	.008
1.97	.797	.001
2.30	.780	.001
3.95	.698	-.005
4.60	.672	-.007
5.26	.642	-.014
5.92	.620	-.018
12.41	.439	.002
13.55	.417	-.001
14.14	.396	-.002
15.13	.370	-.007
16.12	.344	-.004
17.10	.318	-.008
18.09	.296	-.009
19.89	.258	-.010
20.88	.236	-.012
21.87	.219	-.010
27.96	.111	-.010
28.94	.096	-.009
29.92	.085	.008
30.92	.079	.028
31.24	.072	.027

Test number: 12	Fiber orientation: parallel
Air temperature: -2.8°C	Sample half-thickness: .402 cm
System pressure: .58 atm	Initial moisture content: 1.61

<u>Dimensionless Time</u> <u>$\times 10^{-4}$</u>	<u>Experimental Dimensionless</u> <u>Mean Moisture Content, \bar{M}</u>	<u>Computed</u> <u>Residual</u>
.00	1.000	.000
.41	.956	.013
.83	.951	.005
1.65	.845	-.009
2.48	.797	-.019
3.31	.753	-.017
4.13	.720	-.007
5.79	.655	.001
6.61	.624	.001
7.44	.596	.003
8.26	.568	.002
9.09	.544	.004
16.94	.339	.001
17.76	.314	-.006
18.60	.297	-.006
19.42	.279	-.006
20.25	.262	-.007
21.07	.249	-.003
21.90	.229	-.007

Test number: 13	Fiber orientation: parallel
Air temperature: -2.8°C	Sample half-thickness: .422 cm
System pressure: .58 atm	Initial moisture content: 1.57

<u>Dimensionless Time</u> <u>$\theta \times 10^{-4}$</u>	<u>Experimental Dimensionless</u> <u>Mean Moisture Content, \bar{M}</u>	<u>Computed</u> <u>Residual</u>
.00	1.000	.000
.37	.959	.008
.75	.927	.011
1.50	.869	.013
2.25	.818	.001
3.13	.769	.007
3.75	.738	.008
4.50	.705	.012
5.25	.671	.010
5.62	.657	.012
7.74	.579	.011
8.50	.553	.009
9.24	.531	.011
10.00	.509	.011
17.25	.314	-.002
18.00	.297	-.003
18.75	.279	-.005
19.50	.263	-.006
20.62	.241	-.005
21.75	.219	-.004
23.62	.199	.010

Test number: 14	Fiber orientation: perpendicular
Air temperature: -2.8°C	Sample half-thickness: .461 cm
System pressure: .58 atm	Initial moisture content: 1.62

<u>Dimensionless Time</u> $\theta \times 10^{-4}$	<u>Experimental Dimensionless</u> <u>Mean Moisture Content, \bar{M}</u>	<u>Computed</u> <u>Residual</u>
.00	1.000	.000
.47	.936	.006
2.04	.811	-.010
2.67	.775	-.014
3.30	.745	-.009
3.93	.714	-.010
10.06	.498	-.010
10.68	.481	-.010
11.37	.464	-.009
12.10	.445	-.009
12.73	.425	-.014
13.36	.410	-.013
14.14	.392	-.013
15.02	.374	-.012
17.13	.331	-.010
17.75	.317	-.008
18.38	.306	-.006
19.01	.295	-.005
25.26	.190	.005
26.14	.178	.008
27.02	.165	.010
27.90	.153	.013
28.90	.140	.016

Test number: 15
 Air temperature: -2.8°C
 System pressure: .97 atm

Fiber orientation: parallel
 Sample half-thickness: .425 cm
 Initial moisture content: 1.575

<u>Dimensionless Time</u> <u>$\theta \times 10^{-4}$</u>	<u>Experimental Dimensionless</u> <u>Mean Moisture Content, \bar{M}</u>	<u>Computed</u> <u>Residual</u>
.00	1.000	.000
.44	.956	.007
.89	.918	.001
1.33	.884	.004
1.78	.853	.006
6.22	.635	.025
6.67	.615	.025
7.11	.586	.017
7.60	.570	.022
8.00	.546	.022
8.44	.512	.000
8.89	.494	.000
9.33	.478	.000
10.44	.437	.000
11.11	.415	.001
11.55	.400	.001
12.00	.386	.001
12.44	.372	.002
16.67	.257	.011
17.56	.233	.011
18.00	.222	.012
18.49	.210	.012
19.29	.195	.017
20.07	.176	.017

Test number: 16
 Air temperature: -2.8°C
 System pressure: .97 atm

Fiber orientation: parallel
 Sample half-thickness: .460 cm
 Initial moisture content: 1.25

<u>Dimensionless Time</u> <u>$\times 10^{-4}$</u>	<u>Experimental Dimensionless</u> <u>Mean Moisture Content, \bar{M}</u>	<u>Computed</u> <u>Residual</u>
.00	1.000	.000
.38	.942	.014
.76	.897	.006
4.36	.653	-.008
4.74	.637	-.006
5.12	.617	-.007
5.50	.600	-.007
5.88	.589	-.001
6.73	.557	.002
7.11	.542	.002
7.49	.530	.004
8.38	.497	.003
9.11	.474	.005
9.48	.464	.007
9.86	.450	.006
13.66	.330	-.003
14.04	.317	-.006
14.61	.300	-.008
15.18	.284	-.010
15.65	.272	-.009
17.74	.219	-.012

Test number: 17
 Air temperature: -8.2°C
 System pressure: .97 atm

Fiber orientation: parallel
 Sample half-thickness: .465 cm
 Initial moisture content: 1.479

<u>Dimensionless Time</u> <u>$\theta \times 10^{-4}$</u>	<u>Experimental Dimensionless</u> <u>Mean Moisture Content, M</u>	<u>Computed</u> <u>Residual</u>
.00	1.000	.000
.36	.958	.008
.72	.924	-.001
1.07	.898	-.003
1.43	.870	-.007
2.51	.809	-.014
2.86	.789	-.023
3.22	.773	-.019
3.49	.760	-.019
6.80	.642	-.007
7.16	.627	-.010
7.70	.611	-.009
8.23	.598	-.006
8.83	.578	-.009
9.31	.567	-.007
10.02	.549	-.006
10.74	.528	-.009
11.01	.523	-.007
11.28	.517	-.006
12.17	.497	-.005
16.23	.405	-.009
16.65	.400	-.005
17.18	.387	-.008
17.72	.377	-.007
18.26	.366	-.008
19.57	.343	-.007
20.22	.332	-.006
20.76	.322	-.006
24.16	.264	-.007
24.88	.255	-.004
25.59	.242	-.006

Test number: 18
 Air temperature: -8.2°C
 System pressure: .97 atm

Fiber orientation: perpendicular
 Sample half-thickness: .425 cm
 Initial moisture content: 1.442

<u>Dimensionless Time</u> <u>$\times 10^{-4}$</u>	<u>Experimental Dimensionless</u> <u>Mean Moisture Content, \bar{M}</u>	<u>Computed</u> <u>Residual</u>
.00	1.000	.000
.43	.955	.005
.86	.920	-.005
2.71	.828	-.005
3.43	.796	-.011
8.03	.669	-.007
8.57	.657	-.007
9.21	.642	-.009
9.42	.629	-.017
10.07	.600	-.020
12.29	.572	-.018
12.86	.563	-.016
13.33	.553	-.018
13.80	.548	-.015
18.68	.478	-.007
19.28	.469	-.007
20.00	.461	-.005
20.57	.452	-.006
21.25	.443	-.005
21.85	.435	-.005
29.90	.339	-.004
30.85	.325	-.003

MICHIGAN STATE UNIVERSITY LIBRARIES



3 1293 03065 4222